BIFURCATION IN CAVITY QUANTUM ELECTRODYNAMICS AND ITS APPLICATIONS

A DISSERTATION
SUBMITTED TO THE DEPARTMENT OF APPLIED PHYSICS
AND THE COMMITTEE ON GRADUATE STUDIES
OF STANFORD UNIVERSITY
IN PARTIAL FULFILLMENT OF THE REQUIREMENTS
FOR THE DEGREE OF
DOCTOR OF PHILOSOPHY

Jie Wu
June 2014

I certify that I have read this dissertation and that, in my opinion, it is fully adequate in scope and quality as a dissertation for the degree of Doctor of Philosophy.

Hideo Mabuchi, Primary Adviser

I certify that I have read this dissertation and that, in my opinion, it is fully adequate in scope and quality as a dissertation for the degree of Doctor of Philosophy.

Benjamin Lev

I certify that I have read this dissertation and that, in my opinion, it is fully adequate in scope and quality as a dissertation for the degree of Doctor of Philosophy.

David Reis

Approved for the Stanford University Committee on Graduate Studies.

Patricia J. Gumport, Vice Provost for Graduate Education

I certify that I have read this dissertation and that, in my opinion, it is fully adequate in scope and quality as a dissertation for the degree of Doctor of Philosophy.

(Hideo Mabuchi) Principal Adviser

I certify that I have read this dissertation and that, in my opinion, it is fully adequate in scope and quality as a dissertation for the degree of Doctor of Philosophy.

(David Reis)

I certify that I have read this dissertation and that, in my opinion, it is fully adequate in scope and quality as a dissertation for the degree of Doctor of Philosophy.

(Benjamin Lev)

Approved for the University Committee on Graduate Studies

Abstract

Cavity quantum electrodynamics (cQED) has received much attention as an ideal platform for theoretical modeling and proof-of-concept experiments on ultra-low energy all-optical information processing. Cavities provide an effective means of reducing the energy scale of nonlinear-optical effects down to the level of ten or fewer energy quanta, deep into the quantum-mechanical regime. On the other hand, bifurcation theory, which analyzes changes in the number and properties of equilibrium states upon some system parameter crossing a critical value, has been used in practice not only to ensure safe operation in a stable parameter range but also to realize robust devices with signal processing functionalities. In this dissertation I present theoretical results and numerical simulations that demonstrate how these two theories can combine to help not only interpret nonlinear dynamics from the perspective of the first-principle physics, but also suggest designs of useful devices for optical signal processing networks.

Under appropriate conditions the collective interaction of two-level atoms with a cavity field can give rise to interesting dynamical behaviors such as bistability and self-oscillation. Both of these phenomena can provide a physical basis for designing useful devices with signal processing functionalities. After introducing the necessary theoretical background I first discuss the cQED analog of absorptive bistability. I explain how transitions between the two metastable states—the quantum counterparts of the absorptive bistable states—can result from spontaneous emission and based on the understanding of this switching mechanism how we can implement an optical flip-flop using the Purcell effect. This is followed by the discussion of how the interaction between a two-level atom and a quantized cavity field in the semi-classical

limit can give rise to self-oscillation in the cavity field intensity and how we can make use of the system's sensitivity to this instability for small-signal amplification.

In addition to the potential applications, the present study of bifurcation-like phenomena in the context of cavity quantum electrodynamics is also motivated by the theoretical interest in investigating quantum-classical correspondence. The equations in the semi-classical limit have been found to be surprisingly accurate in predicting bifurcation-like phenomena for the full quantum model even in the strong coupling regime in which the semi-classical approximation necessarily breaks down. Therefore bifurcation has become a new subject for studying the correspondence. Nonetheless traits of quantum mechanical nature are omnipresent in these bifurcation-like phenomena such as the automatic switching in the quantum analog of classical absorptive bistability, which can be considered as the quantum-classical discrepancy in the context of absorptive bistability. In this dissertation I present the quantum-classical discrepancy in the context of Hopf bifurcation, which is demonstrated by the breakdown of the pre-Hopf small-signal amplification scheme. Moreover, previous study on the quantum-classical correspondence manifested in the prediction of bifurcation-like phenomena has focused on the single-atom cavity quantum electrodynamics. In the last part of this dissertation I extend the study to multi-atom cases, asking questions such as: would there be any new bifurcation-like phenomenon in a multi-atom cavity quantum electrodynamic system; if yes could it lead to new device application; in addition how would it depend on the number of atoms. This latter question in fact suggests a new perspective towards studying the quantum-classical transition.

Acknowledgment

First of all I would like to extend my sincere gratitude towards my research adviser Hideo Mabuchi, without his support I would never be able to whether through all the drawbacks and mistakes that I had to cope with in order to reach this point. Hideo is very hands-off yet has very high standard on research and graduate apprenticeship. I would say his training is more like that for a post-doc, that you should try to think on your own, come up with your own idea, and make your own judgment on his and/or your idea. Despite relatively fewer publications I am confident that (also based on my own interaction with the other professors and students) we who graduated from MabuchiLab are on average better at carrying out independent research. This one-leap-ahead training strategy would be invaluable for those who aim at landing a research-related job, albeit it would be a great challenge for a fresh graduate student without extensive undergraduate research experience. I am never a fast learner like Dr Mikey so it really took me quite some time to pick up the right intuition and effective research methodology (perhaps only a few months before ending my PhD studies by writing this dissertation). Although Hideo himself believes more in the born-to-be-researcher philosophy I do feel he has instilled on me some traits of a good researcher or at least showed me what I can imitate. Perhaps he would in an unexpected way disprove his own philosophy in the future! In addition, Hideo has been very open-minded in accommodating my perhaps too much interest in mathematics (or maybe stubbornness in proving myself). Without his support I would never be able to earn an additional master degree in mathematics here at Stanford. As CN Yang put it, modern mathematics have gone so remote from concreteness and intuitiveness, it is never trivial for even a sophisticated theoretical physicist to put his/her feet into a

mathematician's shoes. I would have never survived the master program were there no Hideo's encouragement: "Jie, graduate school is the last chance in your lifetime to conduct a systematic study on a subject. You will immediately be judged by your performance once you get out of graduate school". Although I have not had a chance to directly apply what I learned from the mathematics courses to my research, I feel my way of thinking has greatly improved and become much clearer and more effective. I therefore believe that this mathematical training would go a long way to benefit my future career. I still remember Hideo's enlightening comment that "Jie, it would take many years to blend physical intuition and mathematical maturity into a productive harmony so you should not expect to finish it in your graduate studies". That is certainly true but I feel I have started and am heading towards that fruitful direction, thanks to Hideo's open-mindedness and encouragements! In a word I am deeply indebted to Hideo and the chance of paying back in full is slim even if I spend my lifelong career effort on it.

I would also like to thank Dr Mikey, perhaps the best quantum optics experimentalist in the world. I am very grateful that Dr Mikey has always been very patient when explaining to me the experimental details that are not necessary for a theorist but just because I aspire to be a theorist well aware of the non-idealness and limitation of experiments, which seems to be a unique tradition of MabuchiLab because Hideo is both a good theorist and a good experimentalist, well-known for the comment that wherever he goes the experimental breakdown is fixed, opposite to the famous Pauli effect. Dr Mikey inherited this and is the first-stop for problems related to experiments and I found beneficial to approach him for theoretical questions as well.

Thanks to Tony too. I still remember how Tony encouraged me upon the failure of my first project. He was also very helpful when I ran into him for his comments on my group meeting presentations and they were very valuable for a fresh graduate student starting to learn how to present scientific work in a succinct and comprehensible way. Thanks to Tony I am now much more comfortable with giving presentations. I also remember Tony's saying during our trip to Oregon for conference that "We should wait for Jie. He is a member of our lab!" when I was stopped by the guards for lack of identification (I didn't have a driver's license and my passport was away for a visa). That was really heart-warming for a new member of the lab!

My gratitude towards Joe is mixed with apologies. I feel very sorry for monopolizing the servers' CPUs without being aware of it but it certainly affected the progress of Joe's simulation. I am very grateful for Joe's sincerity in suggesting me to learn how to adopt an optimization work attitude after our "fight" for the CPUs. I am also thankful for his honest comments on my group meeting presentations. I wish him every success in his endeavor to land in a faculty job at a research institute.

I was very much impressed by Orion's benevolent personality and warm-heartedness. To me he seems to be an all-purpose glue that can bind every team together. My path towards the PhD is filled with his wishes and encouragements.

I also enjoyed very much the camaraderie of the "Five Stars"—little Mikey, Dmitri, Gopal, Yeong-dae and Charles and me. I am a little bit introverted, feeling not very comfortable with mingling with people. It was little Mikey who discovered this and encouraged me to participate in lab activities as much as possible. Dmitri is really good at probability and statistics and I learned a lot from asking him questions related to his expertise. Dmitri is also an expert in MATLAB coding knowing so many fancy built-in functions of the program. Starting learning MATLAB programming by mimicking his codes I almost formed the habit of asking him for codes to modify instead of writing my own codes from scratch. Gopal is a mathematician-turned physicist so we have a lot in common to talk about, especially after I took the mathematics courses and I was amazed at how he managed to be so friendly to so many friends. Yeong-dae is a really good experimental partner and I enjoyed a lot discussing with him and was very keen at it because the different ways of thinking between theorists and experimentalists made the discussion very interesting. Before Hardeep joining the lab Charles and I were the only international students (Yeong-dae attended Princeton so he was already adapted) so we had a lot in common to discuss, one of which is that we both love to go to dining halls! We had a lot of happy hours in dining halls discussing not only academics but also sports and cultures. Besides Charles has always been a perfect technical support to my simulation thanks to his outstanding skills at linux programming and computer hardware and admirable patience with my

disturbing requests all the time!

Last but not least, Ryan, I find it very helpful to discuss with you about the reduced order model derivation, and the difference in our philosophy towards it, that I always look for as ad-hoc as possible model whereas you wish your model to be as general as possible made the discussion so interesting! Dodd, I really like your manner of asking questions, so attractive that I cannot help inundating you with my answers and many more related details that you might not wish to listen to! Hardeep, I appreciate very much your effort on preparing delicious pizzas for our group meeting, taking charge of the coffee machine and organizing various social activities to boost our team spirit and make MabuchiLab a beloved family. And Paula and Claire, you have completely overthrown my impression of secretaries and bureaucracy. I feel I am very well taken care of like at home even being thousands of miles away from it. I am very much moved by your attentiveness to every single bit of our academic life.

And finally to my parents, being the only child yet so far away from home for so long a time, I must have been missed by you so much. You are always my strongest support and greatest inspiration and my appreciation and indebtedness is beyond words.

Contents

List of Tables

List of Figures

Outline

This dissertation consists of four chapters. Chapter 1 introduces the theoretical model of the quantum system and three equations that are used throughout the dissertation to provide quantitative description of the system dynamics. After the introduction of the theoretical tools Chapter 2 is devoted to the elucidation of the mechanism of the automatic switching in the quantum analog of absorptive bistability. Based on the understanding of the mechanism a flip-flop is proposed which could serve as the basic logic operation unit in future ultra-low energy optical information processing network. In addition a reduced order model involving only three variables is derived to approximate the dynamics, which is computationally much simpler than the quantum model based on wave function. Chapter 3 further illustrates the possibility of exploring bifurcation in cavity quantum electrodynamics for providing physical basis for device application. In this chapter the mechanism of Hopf bifurcation in the semi-classical equations is explained based on which an all-optical amplifier that preserves phase information is proposed. Moreover the amplification proposal is examined in the full quantum model and the discrepancy from the semi-classical prediction is found and discussed. Chapter 4 presents the effort in exploring bifurcation-like phenomena in cavity quantum electrodynamic systems involving more than one atom. A new bifurcation that is dependent upon the number of atoms is provided. Furthermore, two algebraic properties of the multi-atom models are given as an example illustrating the possibility of searching for analytical insights about the dynamics.

Chapter 1

Theoretical Modeling

In this chapter I present three models for describing the open quantum system built on a two-level atom interacting with a quantized cavity mode which also take into account of the atomic spontaneous emission and photon leakage out of cavity end mirrors. They are (1) the master equation (2) the stochastic Schrödinger equation and (3) the Maxwell-Bloch equations. The master equation is an equation of motion for the system density matrix thus it describes the ensemble averaged behavior of the system dynamics. The stochastic Schrödinger equation is useful for tracing out individual system state evolution trajectory (apparently analogous to the path integral but in fact is of different nature thus the word "trajectory" is used to distinguish from it) and considering explicitly the system state collapse due to the atomic spontaneous emission and photon leakage through cavity end mirrors. The Maxwell-Bloch equations are equations of motion for the expectation values of the atomic Pauli matrices and the real and imaginary part of the annihilation operator of the cavity field. The solution to the master equation can be approximated by averaging over sufficiently many trajectory solutions to the stochastic Schrödiner equation. The Maxwell-Bloch equations represent the so-called "semiclassical limit" of the master equation when the correlations between the observables of the atom and those of the cavity field can be safely ignored.

1.1 The Master Equation

The exact quantum model that I will use is built upon the driven Jaynes-Cummings Hamiltonian [2] which models the interaction of a single mode of an optical cavity having a resonant frequency ω_c, with a two-level atom comprised of a ground state $|g\rangle$ and an excited state $|e\rangle$ separated by a frequency ω_a. For an atom-field coupling constant g and an external coherent driving field with frequency ω_l and amplitude $\mathcal{E}$ coupled to the cavity mode, the Hamiltonian for a reference frame rotating at the driving frequency ω_l adopting rotating wave approximation (RWA) that discards high frequency coupling terms is given by ($\hbar = 1$)

$$H = \Delta_c a^\dagger a + \Delta_a \sigma_+ \sigma_- + ig(a^\dagger \sigma_- - a\sigma_+) + i\mathcal{E}(a^\dagger - a) \tag{1.1}$$

where $\Delta_a = \omega_a - \omega_l$ and $\Delta_c = \omega_c - \omega_l$. In equation (1.1), a is the annihilation operator for the chosen cavity mode (I will refer to it as "cavity field" below) and $\sigma_- = |g\rangle\langle e| = (\sigma_x - i\sigma_y)/2$ is the atomic lowering operator. In addition to the coherent dynamics governed by (1.1) there are two dissipative channels for the system: the atom may spontaneously emit into modes other than the preferred cavity mode at a rate $\gamma_\perp$, and photons may leak out of the cavity mirror at a rate 2κ. Fig.1.1 below provides a conceptual picture of the open quantum system with the two lossy channels. Assuming only these two incoherent processes the overall dynamics can be

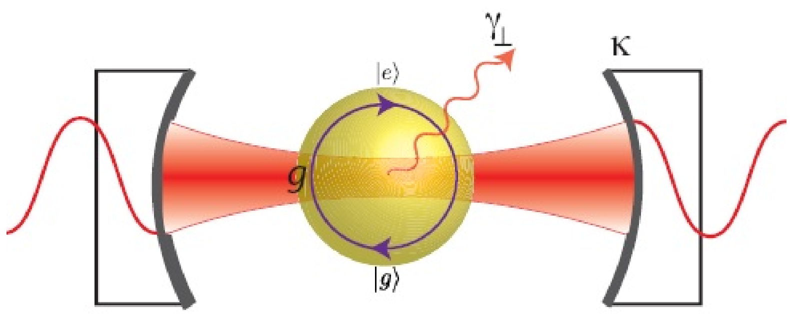

Figure 1.1: A conceptual picture of the open quantum system

described by the following unconditional master equation [2]

$$\frac{d}{dt}\rho = -i[H,\rho] + \kappa(2a\rho a^\dagger - a^\dagger a\rho - \rho a^\dagger a) + \gamma_\perp(2\sigma_-\rho\sigma_+ - \sigma_+\sigma_-\rho - \rho\sigma_+\sigma_-) \quad (1.2)$$

where ρ denotes the system (atom + field) density matrix.

1.2 The Stochastic Schrödinger Equation

Apart from the master equation there is also a stochastic process perspective towards the quantum dynamics, which is described by the following stochastic Schrödinger equation [2]

$$i\frac{d}{dt}|\psi\rangle = H_{eff}|\psi\rangle \quad (1.3)$$

with the collapse operators

$$C_1 = \sqrt{2\kappa}a \quad C_2 = \sqrt{2\gamma_\perp}\sigma_- \quad (1.4)$$

and the effective non-Hermitian Hamiltonian

$$H_{eff} = H - \frac{i}{2}\sum_k C_k^\dagger C_k = \Delta_c a^\dagger a + \Delta_a\sigma_+\sigma_- + ig(a^\dagger\sigma_- - a\sigma_+) + i\mathcal{E}(a^\dagger - a) - i\kappa a^\dagger a - i\gamma_\perp\sigma_+\sigma_- \quad (1.5)$$

The continuous evolution of the stochastic Schrödinger equation (1.3) is punctured by "quantum jumps" at which the state vector $|\psi\rangle$ collapses to

$$|\psi\rangle \mapsto \frac{C_k|\psi\rangle}{\|C_k|\psi\rangle\|} \quad (1.6)$$

the probability of the collapse in an interval dt being given by $\|C_k|\psi\rangle\|^2 dt$. This makes the time evolution of $|\psi(t)\rangle$ a multi-dimensional stochastic process. Such a time series of $|\psi(t)\rangle$ is known as a **quantum trajectory** of the system evolution. Its relation with the master equation is that, the ensemble average of all possible quantum trajectories is the steady state solution to the master equation.

The time series of $|\psi(t)\rangle$ may be used to find the trajectory of the expectation of any operator O acting on the system Hilbert space using the following formula

$$\langle O\rangle = \frac{\langle\psi(t)|O|\psi(t)\rangle}{\langle\psi(t)|\psi(t)\rangle} \tag{1.7}$$

1.3 The Maxwell-Bloch Equations

The master equation (1.2) can be used to find the time evolution for any operator O acting on the system Hilbert space using the formula $\langle\dot{O}\rangle = \mathrm{Tr}[O\dot{\rho}]$. The simplest set of operators that can approximately describe the dynamics is $\{a, \sigma_-, \sigma_z\}$. Applying the above formula I obtain the following three equations

$$\begin{aligned}
\dot{\langle a\rangle} &= -(\kappa + i\Delta_c)\langle a\rangle + g\langle\sigma_-\rangle + \mathcal{E} \\
\dot{\langle\sigma_-\rangle} &= -(\gamma_\perp + i\Delta_a)\langle\sigma_-\rangle + g\langle a\sigma_z\rangle \\
\dot{\langle\sigma_z\rangle} &= -2\gamma_\perp(1 + \langle\sigma_z\rangle) - 2g(\langle a^\dagger\sigma_-\rangle + \langle a\sigma_+\rangle)
\end{aligned} \tag{1.8}$$

Note that the above operator expectation equations (1.8) also apply to the case of N non-interacting atoms each coupled to the same cavity mode with the same coupling constant g. In this case the atomic operators are the sums of those of the individual atoms [3]

$$\sigma_- = \sum_{j=1}^{N}\sigma_-^j, \quad \sigma_z = \sum_{j=1}^{N}\sigma_z^j \tag{1.9}$$

Notice that equations (1.8) are not closed as they contain expectations of operator products. The common practice in the quantum optics community to close the equations is to simply factorize the operator products, e.g. $\langle a^\dagger\sigma_-\rangle \approx \langle a^\dagger\rangle\langle\sigma_-\rangle$ which corresponds to taking the thermodynamic limit of many weakly excited atoms hence the correlations between the atomic operators and the field operator averaging to zero [4]. The closed equations after factorization are the well-known Maxwell-Bloch equations (MBE)

$$\begin{aligned}
\dot{\langle a\rangle} &= -(\kappa + i\Delta_c)\langle a\rangle + g\langle\sigma_-\rangle + \mathcal{E} \\
\dot{\langle\sigma_-\rangle} &= -(\gamma_\perp + i\Delta_a)\langle\sigma_-\rangle + g\langle a\rangle\langle\sigma_z\rangle \\
\dot{\langle\sigma_z\rangle} &= -2\gamma_\perp(1 + \langle\sigma_z\rangle) - 2g(\langle a^\dagger\rangle\langle\sigma_-\rangle + \langle a\rangle\langle\sigma_+\rangle)
\end{aligned} \tag{1.10}$$

which can be rewritten using physical observables $x = (a+a^\dagger)/2, y = (a-a^\dagger)/2i, \sigma_x = \sigma_+ + \sigma_-, \sigma_y = -i(\sigma_+ - \sigma_-), \sigma_z$ as

$$\begin{aligned}
\frac{d}{dt}\langle x\rangle &= -\kappa\langle x\rangle + \Delta_c\langle y\rangle + \frac{g}{2}\langle\sigma_x\rangle + \mathrm{Re}[\mathcal{E}] \\
\frac{d}{dt}\langle y\rangle &= -\kappa\langle y\rangle - \Delta_c\langle x\rangle - \frac{g}{2}\langle\sigma_y\rangle + \mathrm{Im}[\mathcal{E}] \\
\frac{d}{dt}\langle\sigma_x\rangle &= -\gamma_\perp\langle\sigma_x\rangle - \Delta_a\langle\sigma_y\rangle + 2g\langle x\rangle\langle\sigma_z\rangle \\
\frac{d}{dt}\langle\sigma_y\rangle &= -\gamma_\perp\langle\sigma_y\rangle + \Delta_a\langle\sigma_x\rangle - 2g\langle y\rangle\langle\sigma_z\rangle \\
\frac{d}{dt}\langle\sigma_z\rangle &= -2\gamma_\perp - 2\gamma_\perp\langle\sigma_z\rangle - 2g\langle x\rangle\langle\sigma_x\rangle + 2g\langle y\rangle\langle\sigma_y\rangle
\end{aligned} \tag{1.11}$$

The above Maxwell-Bloch equations (1.10) describing the evolution of the operator expectations for any number of atoms (i.e. any value of N) can be put into a dimensionless form which facilitates the comparison between cases with different number of non-interacting atoms [3]

$$\begin{aligned}
x' &= -k[(1 + i\Theta)x + 2Cp - y] \\
p' &= -(1 + i\Delta)p + xD \\
D' &= -\gamma[D - 1 + (x^*p + p^*x)/2]
\end{aligned} \tag{1.12}$$

using the following scaling factors

$$x = \frac{\sqrt{2}g}{\gamma_\perp}\langle a\rangle, \quad p = -\frac{\sqrt{2}}{N}\langle\sigma_-\rangle, \quad D = -\frac{1}{N}\langle\sigma_z\rangle \tag{1.13}$$

$$\gamma = \frac{2\gamma_\perp}{\gamma_\perp}, \quad k = \frac{\kappa}{\gamma_\perp}, \quad C = \frac{Ng^2}{2\kappa\gamma_\perp}, \quad y = \frac{\sqrt{2}g}{\kappa\gamma_\perp}\mathcal{E}, \quad t' = \gamma_\perp t \tag{1.14}$$

where C termed "cooperativity" is a measure of the strength of the collective interaction of the atoms with the field. Thus to vary the number of atoms while keeping the overall interaction constant I need to keep C constant by making g inversely proportional to $\sqrt{N}$. Hence as N increases g would go from the strong coupling regime ($g \gg \kappa, \gamma_\perp$) to the weak coupling regime ($g \ll \kappa, \gamma_\perp$) therefore making a transition from the quantum realm to the semi-classical limit.

Under the resonance condition $\Delta_c = \Delta_a = 0$, $\langle a \rangle$ and $\langle \sigma_- \rangle$ are real thus the above Maxwell-Bloch equations (1.10) can be re-written using only three physical observables $x = (a + a^\dagger)/2$, $\sigma_x = (\sigma_+ + \sigma_-)$ and σ_z as

$$\begin{aligned} \dot{\langle x \rangle} &= -\kappa \langle x \rangle + \frac{g}{2} \langle \sigma_x \rangle + \mathcal{E} \\ \dot{\langle \sigma_x \rangle} &= -\gamma_\perp \langle \sigma_x \rangle + g \langle x \rangle \langle \sigma_z \rangle \\ \dot{\langle \sigma_z \rangle} &= -2\gamma_\perp (1 + \langle \sigma_z \rangle) - 2g \langle x \rangle \langle \sigma_x \rangle \end{aligned} \tag{1.15}$$

In this case it turns out that the atom-field interaction fits into a spin precession picture—I can rewrite the driving terms of the atomic operator expectation equations in the form of the classical equation of motion for a magnetic moment in a static magnetic field

$$\frac{d}{dt} \begin{pmatrix} \langle \sigma_x \rangle \\ 0 \\ \langle \sigma_z \rangle \end{pmatrix} = \frac{d}{dt} \vec{S} = 2g \vec{S} \times \vec{B} = 2g \begin{pmatrix} \langle \sigma_x \rangle \\ 0 \\ \langle \sigma_z \rangle \end{pmatrix} \times \begin{pmatrix} 0 \\ -\langle x \rangle \\ 0 \end{pmatrix} \tag{1.16}$$

where $\vec{S} = \begin{pmatrix} \langle \sigma_x \rangle & 0 & \langle \sigma_z \rangle \end{pmatrix}^T$, $\vec{B} = \begin{pmatrix} 0 & -\langle x \rangle & 0 \end{pmatrix}^T$. It shows that the atomic spin undergoes precession in xz-plane driven by the cavity field acting as a pseudo-magnetic field (out of phase with the dipole moment $\langle \sigma_x \rangle$ though because of the minus sign in front of $\langle x \rangle$). This spin precession representation of the atomic dynamics turns out to be crucial to deciphering the mechanism of automatic switching between the metastable states in the quantum analog of absorptive bistability.

Chapter 2

The Mechanism of Automatic Switching in the Quantum Analog of Absorptive Bistability

The mechanism of automatic switching between the two metastable states in the quantum analog of absorptive bistability is elucidated, based on which an optical implementation of flip-flop control in the context of single-atom cavity quantum electrodynamics is proposed.

2.1 Introduction

Cavity quantum electrodynamics has received much attention as the ideal platform for theoretical modeling and concept-proving experiments on ultra-low energy all-optical information processing devices [5]. One of the physical bases for the proposed logic devices is absorptive bistability. It has been extensively studied in the classical context [4] and its analog found in the single-atom strong-coupling quantum regime [3]. As the operating energy of a device is reduced to only dozens of quanta the physical process inevitably bears the footprint of quantum mechanics. One such example is the automatic switching between the two metastable states in the quantum analog of absorptive bistability due to quantum fluctuation [6]. There has already been a proposal on how to suppress the automatic switching in the context of dispersive bistability which certainly regards it as something unwanted [7]. However the understanding of the mechanism suggests a way to engineer the switching for implementing flip-flop logic operation thus convert something undesirable into something useful, as I will discuss later in this chapter.

For a simple physical picture, in this chapter the resonance condition $\Delta_c = \Delta_a = 0$ is always assumed so as to eliminate the effect of detuning.

2.2 The Switching Mechanism via Spontaneous Emission

The automatic switching refers to the following phenomenon: for an absorptive bistable parameter set identified by the Maxwell-Bloch equations the quantum trajectory simulation would show that the system has two preferred states with low and high field amplitude respectively resembling absorptive bistability; however unlike in the limiting case described by the Maxwell-Bloch equations the system does not stay in one of the two states forever; instead it frequently jumps between them as is illustrated in Fig.2.1 below. This observation has been confirmed by our recent experiment [6].

Since the automatic switching is a stochastic process, to search for the underlying physical mechanism one should obviously focus on the stochastic processes contained in our theoretical model, which are the atomic spontaneous emission and photon leakage out of the cavity mirror. It is intuitive that intrinsic field fluctuation due to photon leakage could induce transitions between the two metastable states as is suggested by the dispersive bistability in a Kerr-nonlinear cavity [7]. However it is not clear whether the atomic spontaneous emission also contributes to the automatic switching and if yes how it results in the switching.

The numerical evidence for the active role of the atomic spontaneous emission in inducing the switching is based on the Monte Carlo simulation of the quantum trajectory defined in the chapter of theoretical modeling. In particular I used the

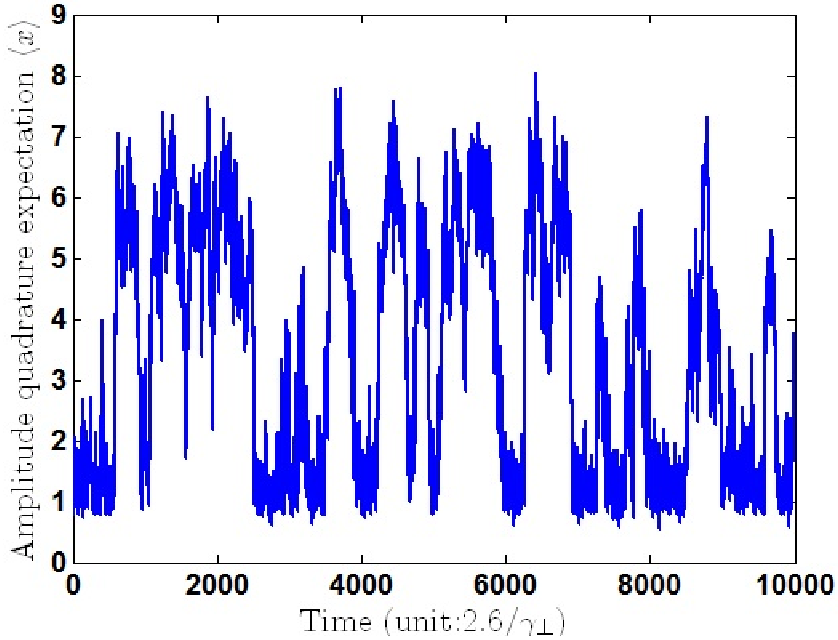

Figure 2.1: A typical quantum trajectory simulation result for the evolution of the field amplitude quadrature expectation $\langle x\rangle$ for an absorptive bistable parameter set identified by the Maxwell-Bloch equations

quantum optics toolbox [8] to generate quantum trajectories. I then used 3-state hidden Markov model (HMM) to classify all the data points of the trajectory into 3 groups: (1) low-state (weak cavity field but strong dipole moment) points (2) in-transit points and (3) high-state (weak dipole moment but strong cavity field) points based on the corresponding observable expectation triplet $(\langle x\rangle, \langle\sigma_x\rangle, \langle\sigma_z\rangle)$ and defined the occurrence of switching as the moment at which the system goes from low/high-state to in-transit state followed by the system going from in-transit state to high/low-state. With this I collected the statistics of spontaneous emission, photon leakage and the observable expectation triplet conditioned upon the occurrence of switching using a counting window with a suitable width. Moreover I slid the counting window from the occurrence of switching backward in time just like rewinding the film to see what happened that precedes the switching. The conditioned statistics versus the time the counting window is positioned for low-to-high transitions are plotted in Fig.2.2 below. As one can see from the plot, there is excessive spontaneous emission preceding the onset of low-to-high transitions.

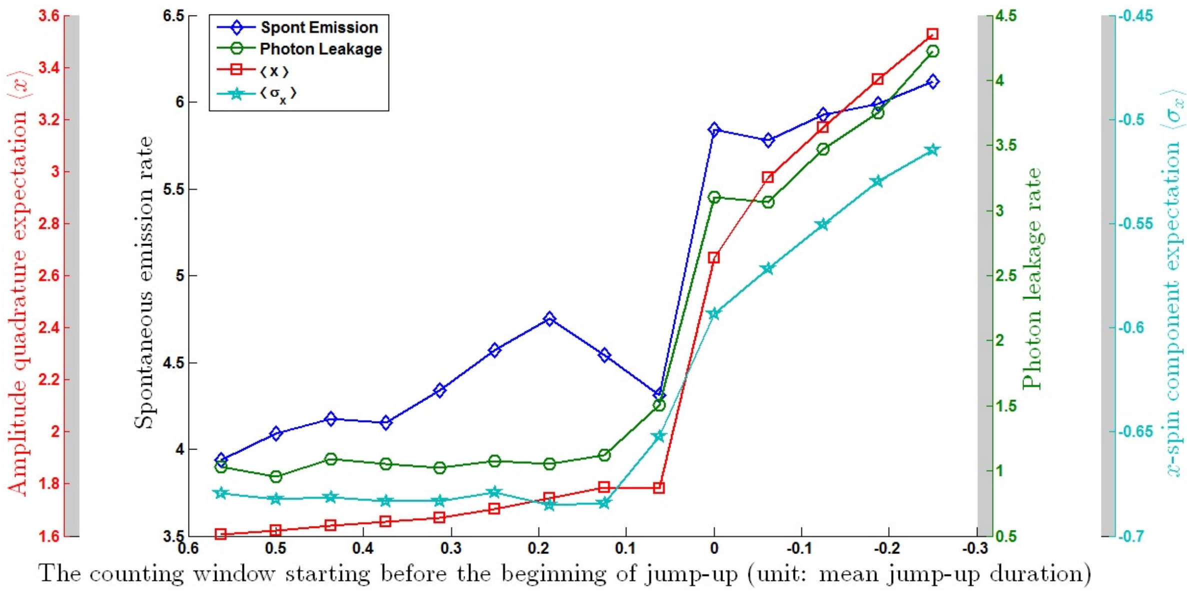

Figure 2.2: The statistics of spontaneous emission, photon leakage and $\langle x \rangle, \langle \sigma_x \rangle$ conditioned upon low-to-high state transitions, where the origin of the x-axis is defined as the moment the system goes from low- to in-transit state and the position of the counting window is defined as the moment one starts counting; the time unit of the x-axis is chosen to be the mean time the system takes to complete the low-to-high state transitions (termed "mean jump-up duration" in the plot) and the counting window width is set to be 1/16 of the time unit

This excessive spontaneous emission is also observed in the statistics conditioned upon high-to-low transitions as is shown in Fig.2.2 below.

It seems like excessive spontaneous emission is a precursor to the automatic switching. More careful examination of the effect of spontaneous emission on the spin precession representation of the atomic-field interaction (refer to the chapter of theoretical modeling) reveals that excessive spontaneous emission is not just a precursor

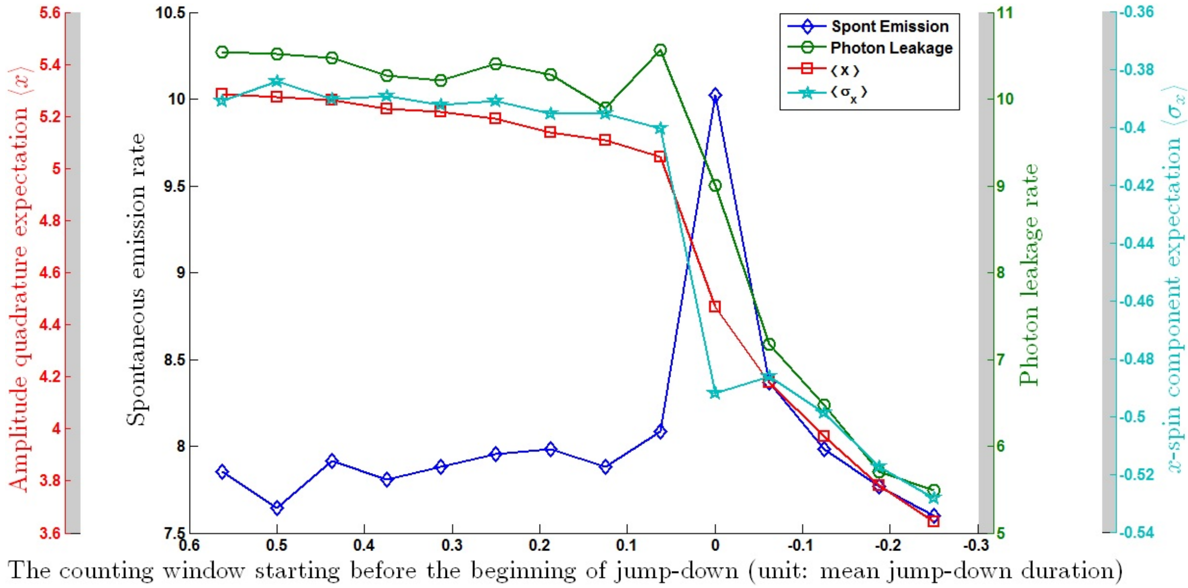

Figure 2.3: The statistics of spontaneous emission, photon leakage and $\langle x\rangle, \langle\sigma_x\rangle$ conditioned upon high-to-low state transitions, where the origin of the x-axis is defined as the moment the system goes from high- to in-transit state and the position of the counting window is defined as the moment one starts counting; the time unit of the x-axis is chosen to be the mean time the system takes to complete the high-to-low state transitions (termed "mean jump-down duration" in the plot) and the counting window width is set to be 1/16 of the time unit

to the automatic switching but actually responsible for inducing the switching by weakening or strengthening, depending on whether the speed of precession is slow or fast, the dipole moment hence the dipole radiation that destructively interferes with the external field coupled into the cavity.

Whenever a spontaneous emission occurs the atomic spin is reset to pointing vertically downward in the unit sphere ($\langle\sigma_z\rangle = -1$) and the dipole moment is reset to zero ($\langle\sigma_x\rangle = 0$ and recall that the resonant case is being considered thus $\langle\sigma_y\rangle \equiv 0$). After the emission, the atomic spin continues precessing and because of the out of phase relation between the cavity field and the dipole moment/radiation (refer to the chapter of theoretical modeling), the cavity field drives the spin back towards its position before spontaneous emission i.e. the dipole moment recovers. Fig.2.4

below helps to visualize the consequence of spontaneous emission on the atomic spin precession.

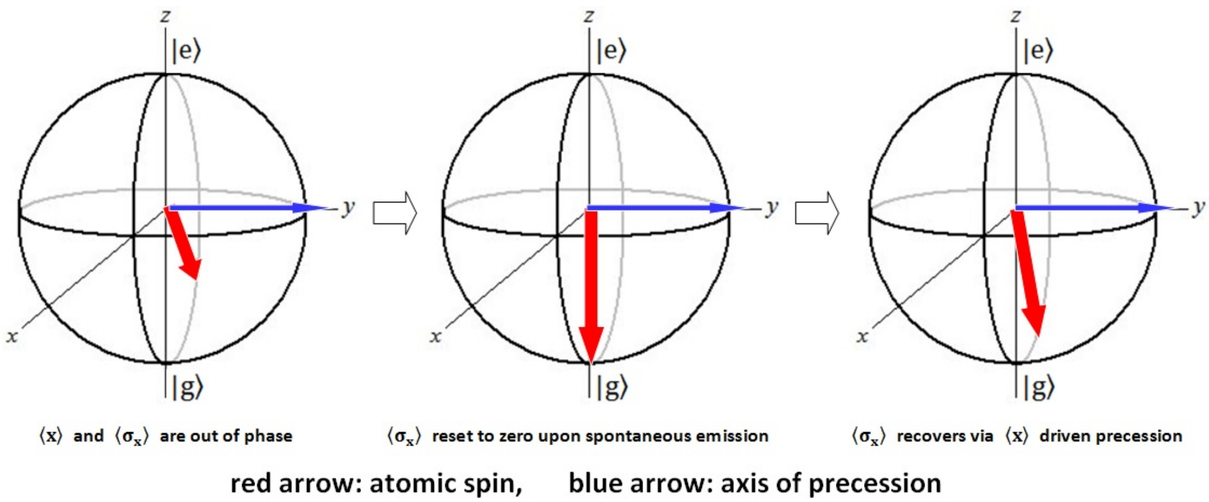

Figure 2.4: Graphical representation of spontaneous emission interrupting the atomic spin precession in which the red arrow represents the atomic spin whereas the blue arrow represents the cavity field acting as a pseudo-magnetic field

Therefore at low-state the cavity field is weak thus the speed of precession is slow hence the recovery is slow. But once the dipole moment is recovered it will remain strong for a long time because of its slow precession. As a result excessive spontaneous emission leads to weaker dipole moment and dipole radiation as is illustrated by Fig.2.5 below.

In contrast, at high-state the cavity field is strong thus the speed of precession is fast therefore the recovery is immediate. But once the dipole moment is recovered it will quickly precess to the opposite sign and complete many revolutions if there is no spontaneous emission to interrupt the cycling. As a consequence the dipole moment averages to almost zero when there are few emissions. This is illustrated in Fig.2.6 below.

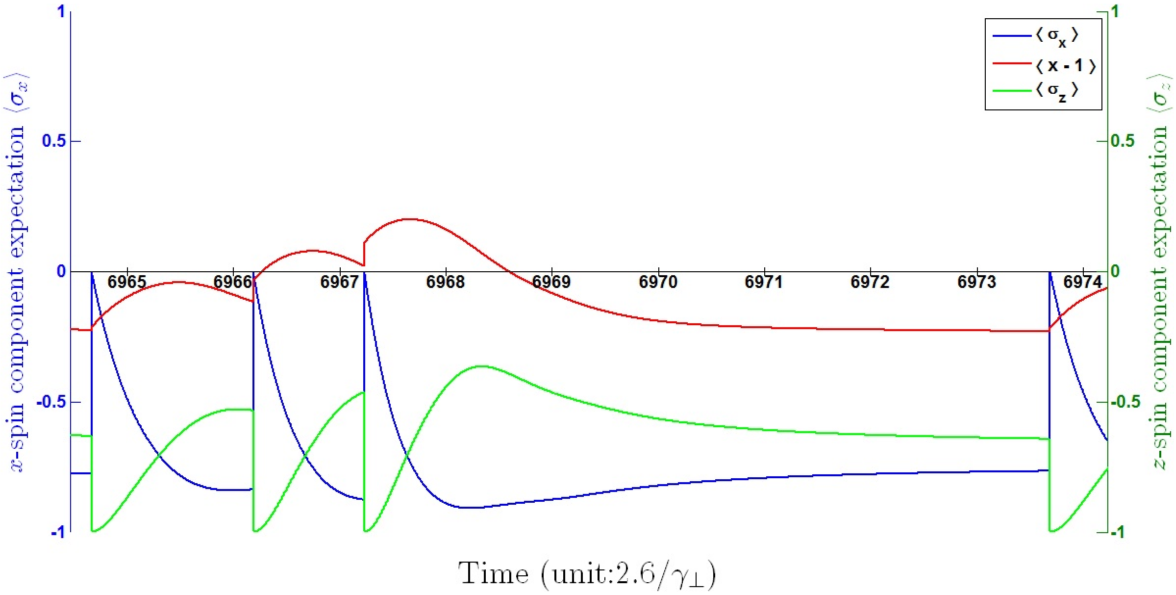

Figure 2.5: Illustration of excessive spontaneous emission weakening the dipole moment when the speed of the atomic spin precession is slow

As a verification for the above hypothesis I randomly chose a trajectory and divided it into time segments of equal length and for each segment I counted the number of spontaneous emissions. After that I evaluated for each segment the time average of $\langle x\rangle$ and classified a segment as low-intensity segment if its $\langle x\rangle$ average is smaller than a chosen limit or high-intensity segment if its $\langle x\rangle$ average is greater than a chosen limit. The final step consists of making a histogram for both the set of low-intensity segments and that of high-intensity segments based on the number of spontaneous emissions occurred within the segment, and evaluating for each of the histogram bins the average of $\langle\sigma_x\rangle$. The resulted histogram on the bin average of $\langle\sigma_x\rangle$ versus the number of spontaneous emissions for both the low-intensity segments and the high-intensity segments are plotted in Fig.2.7 and Fig.2.8 below, which show clearly the dipole moment weakening/strengthening by excessive spontaneous emission.

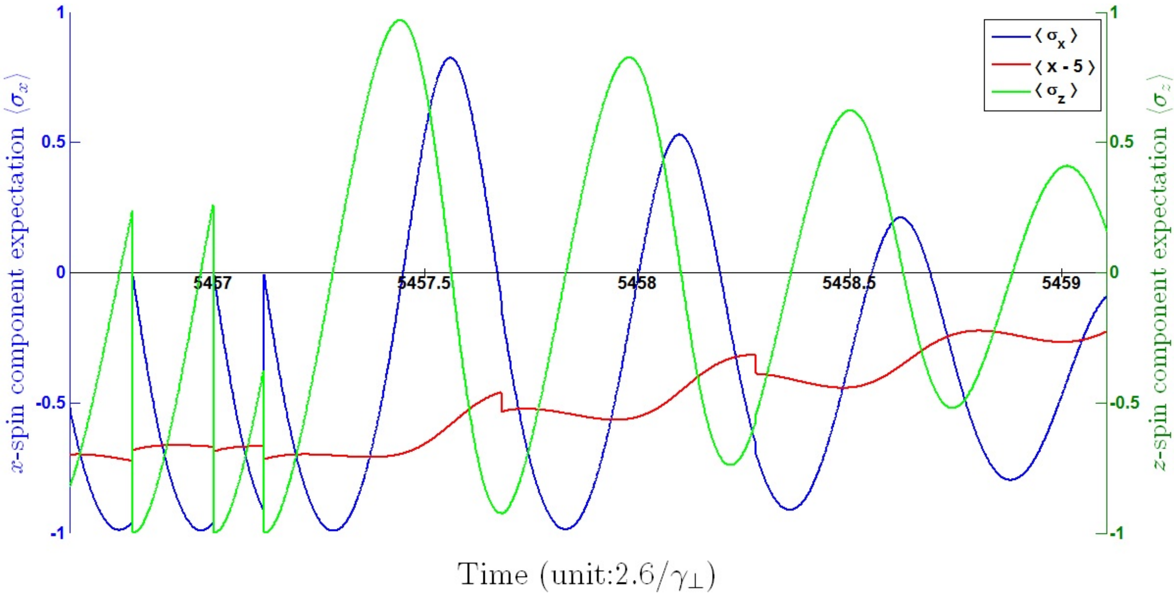

Figure 2.6: Illustration of excessive spontaneous emission strengthening the dipole moment when the speed of the atomic spin precession is fast

2.3 Flip-Flop Control via Spontaneous Emission Enhancement

With the above understanding of the switching mechanism via spontaneous emission, I proposed an implementation of flip-flop control in the context of single-atom cavity quantum electrodynamics via spontaneous emission enhancement, which provides further corroboration to the above hypothesized mechanism. The idea is straightforward: if excessive spontaneous emission can lead to state transition then when state transition is desired what needs to be done is just to artificially introduce excessive spontaneous emission, and there is a well-known method to enhance spontaneous emission—the Purcell effect, which promotes more spontaneous emissions by increasing the local oscillation mode density via an optical cavity [9]. Thus suppose there is some means to alter the cavity detuning (w.r.t. the atomic resonance frequency)—either by some kind of electro-optic mechanism or by Kerr effect with a control beam—then one can realize state transition in the first cavity, the absorptive bistable cavity, by reducing to zero the detuning of the second cavity, the cavity

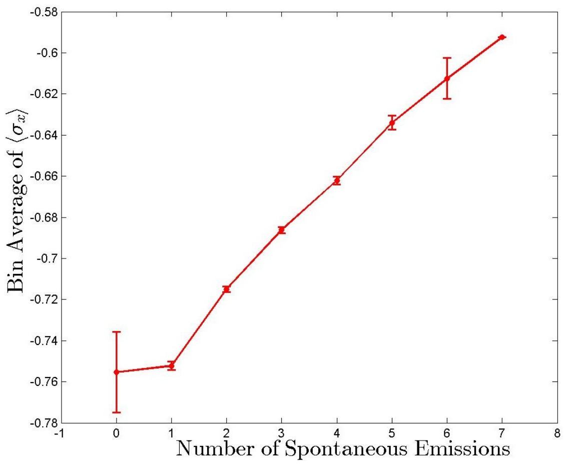

Figure 2.7: Bin average of $\langle\sigma_x\rangle$ vs. the number of spontaneous emissions histogram for the low-intensity segments

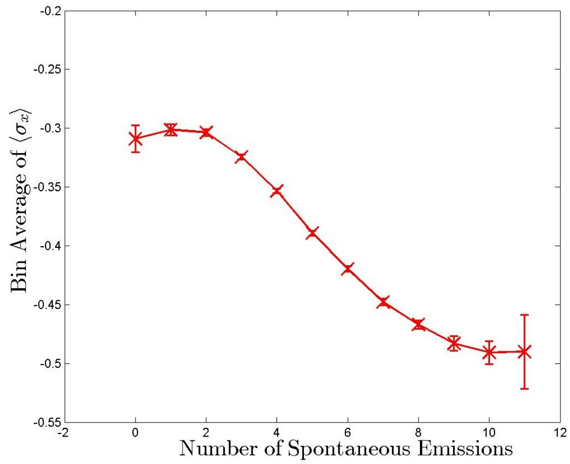

Figure 2.8: Bin average of $\langle\sigma_x\rangle$ vs. the number of spontaneous emissions histogram for the high-intensity segments

for spontaneous emission enhancement. Fig. 2.9 and Fig. 2.10 below illustrate the flip-flop control via turning the detuning off.

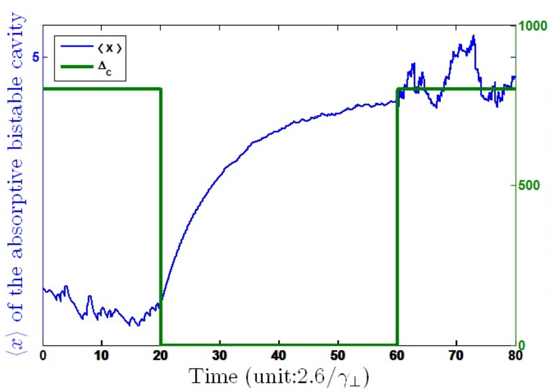

Figure 2.9: Cavity enhanced spontaneous emission induces low-to-high transition

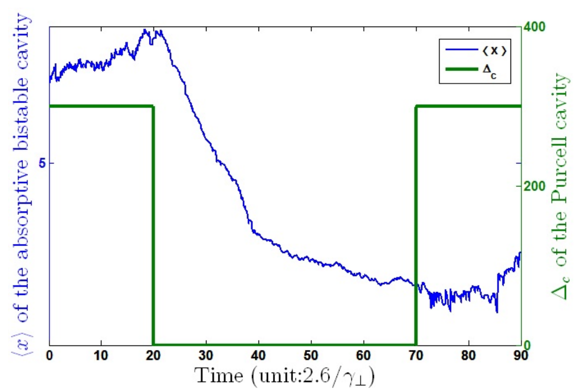

Figure 2.10: Cavity enhanced spontaneous emission induces high-to-low transition

An added advantage of this flip-flop control is that, for conventional flip-flops the required input to trigger bit flip from "0" to "1" is different from that to trigger bit flip from "1" to "0"; however for our proposal, the same input, which is turning off the detuning of the Purcell cavity, can be used to trigger both "0" to "1" and "1" to

"0" bit flips.

2.4 A Reduced Order Model for the Dynamics

In view of the accuracy of the mean-field Maxwell-Bloch equations in predicting various parameter regimes with bifurcation-like phenomena for the full quantum model [3], having understood the mechanism of the automatic switching I attempted to derive a reduced order model that can approximately describe the switching dynamics (which the Maxwell-Bloch equations can not). The approach I took is to derive trajectories of operator expectations from the standard quantum trajectory formulation. The continuous evolution of the standard quantum trajectory formulation is given by the following effective Schrödinger equation

$$\frac{d}{dt}|\psi\rangle = -iH_{eff}|\psi\rangle \tag{2.1}$$

where the effective non-Hermitian Hamiltonian is given by

$$H_{eff} = H - \frac{i}{2}\sum_k C_k^\dagger C_k \quad \Longrightarrow H_{eff}^\dagger = H + \frac{i}{2}\sum_k C_k^\dagger C_k \tag{2.2}$$

in which $\{C_k\}$ are a family of collapse operators. For any operator O its expectation is given by

$$\frac{\langle\psi|O|\psi\rangle}{\langle\psi|\psi\rangle} \tag{2.3}$$

thus its equation of motion is given by

$$\begin{aligned} \frac{d}{dt}\frac{\langle\psi|O|\psi\rangle}{\langle\psi|\psi\rangle} &= \frac{1}{\langle\psi|\psi\rangle}\left[\frac{d}{dt}\langle\psi|O|\psi\rangle\right] - \frac{\langle\psi|O|\psi\rangle}{\langle\psi|\psi\rangle^2}\left[\frac{d}{dt}\langle\psi|\psi\rangle\right] \\ &= \frac{1}{\langle\psi|\psi\rangle}\left[\left(\frac{d}{dt}\langle\psi|\right)O|\psi\rangle + \langle\psi|O\left(\frac{d}{dt}|\psi\rangle\right)\right] - \frac{\langle\psi|O|\psi\rangle}{\langle\psi|\psi\rangle^2}\left[\left(\frac{d}{dt}\langle\psi|\right)|\psi\rangle + \langle\psi|\left(\frac{d}{dt}|\psi\rangle\right)\right] \end{aligned} \tag{2.4}$$

Substitute in

$$\frac{d}{dt}|\psi\rangle = -iH_{eff}|\psi\rangle \qquad \frac{d}{dt}\langle\psi| = +i\langle\psi|H_{eff}^\dagger \tag{2.5}$$

and notice that $H_{eff}^{\dagger} \neq H_{eff}$ I have

$$\begin{aligned}\frac{d}{dt}\frac{\langle\psi|O|\psi\rangle}{\langle\psi|\psi\rangle} &= \frac{1}{\langle\psi|\psi\rangle}\left[+i\langle\psi|H_{eff}^{\dagger}O|\psi\rangle - i\langle\psi|OH_{eff}|\psi\rangle\right] - \frac{\langle\psi|O|\psi\rangle}{\langle\psi|\psi\rangle^2}\left[+i\langle\psi|H_{eff}^{\dagger}|\psi\rangle - i\langle\psi|H_{eff}|\psi\rangle\right] \\ &= +i\frac{1}{\langle\psi|\psi\rangle}\langle\psi|(H_{eff}^{\dagger}O - OH_{eff})|\psi\rangle - i\frac{\langle\psi|O|\psi\rangle}{\langle\psi|\psi\rangle^2}\langle\psi|(H_{eff}^{\dagger} - H_{eff})|\psi\rangle\end{aligned} \tag{2.6}$$

where ([,] represents commutator and { , } represents anti-commutator)

$$\begin{aligned}H_{eff}^{\dagger}O - OH_{eff} &= (HO + \frac{i}{2}\sum_k C_k^{\dagger}C_k O) - (OH - \frac{i}{2}\sum_k OC_k^{\dagger}C_k) \\ &= [H, O] + \frac{i}{2}\sum_k \{C_k^{\dagger}C_k, O\}\end{aligned} \tag{2.7}$$

and

$$H_{eff}^{\dagger} - H_{eff} = (H + \frac{i}{2}\sum_k C_k^{\dagger}C_k) - (H - \frac{i}{2}\sum_k C_k^{\dagger}C_k) = i\sum_k C_k^{\dagger}C_k \tag{2.8}$$

the expectations of which may need to be approximated in order to close the equations.

For absorptive bistability at resonance the Hamiltonian is $H = +ig(a^{\dagger}\sigma_- - a\sigma_+) + i(\mathcal{E}a^{\dagger} - \mathcal{E}^* a)$ and the basic set of operator expectations is $\{\langle x\rangle, \langle\sigma_x\rangle, \langle\sigma_z\rangle\}$ and the family of collapse operators is $\{C_1 = \sqrt{2\kappa}a, C_2 = \sqrt{2\gamma_\perp}\sigma_-\}$ hence $\{C_1^{\dagger}C_1 = +2\kappa a^{\dagger}a, C_2^{\dagger}C_2 = +2\gamma_\perp\sigma_+\sigma_-\}$ for which I have

$$\begin{aligned}[H, x] &= -i\frac{g}{2}\sigma_x - i\mathrm{Re}[\mathcal{E}] \\ \{C_1^{\dagger}C_1 + C_2^{\dagger}C_2, x\} &= +2\gamma_\perp + 2\gamma_\perp x\sigma_z + 2\kappa(xa^{\dagger}a + a^{\dagger}ax) \\ [H, \sigma_x] &= -i2gx\sigma_z \\ \{C_1^{\dagger}C_1 + C_2^{\dagger}C_2, \sigma_x\} &= +2\gamma_\perp\sigma_x + 4\kappa\sigma_x a^{\dagger}a \\ [H, \sigma_z] &= +i2g(x\sigma_x - y\sigma_y) \\ \{C_1^{\dagger}C_1 + C_2^{\dagger}C_2, \sigma_z\} &= +2\gamma_\perp + 2\gamma_\perp\sigma_z + 4\kappa\sigma_z a^{\dagger}a\end{aligned} \tag{2.9}$$

therefore the equations of motion for $\langle x\rangle, \langle\sigma_x\rangle, \langle\sigma_z\rangle$ are

$$\begin{aligned}
\frac{d}{dt}\langle x\rangle &= \frac{d}{dt}\frac{\langle\psi|x|\psi\rangle}{\langle\psi|\psi\rangle} = \frac{1}{\langle\psi|\psi\rangle}\langle\psi|\frac{g}{2}\sigma_x + \mathrm{Re}[\mathcal{E}] - \gamma_\perp x - \gamma_\perp x\sigma_z - \kappa(xa^\dagger a + a^\dagger a x)|\psi\rangle \\
&+ \frac{\langle\psi|x|\psi\rangle}{\langle\psi|\psi\rangle}\frac{1}{\langle\psi|\psi\rangle}\langle\psi|2\kappa a^\dagger a + 2\gamma_\perp\sigma_+\sigma_-|\psi\rangle \\
&= +\frac{g}{2}\langle\sigma_x\rangle + \mathrm{Re}[\mathcal{E}] - \gamma_\perp\langle x\rangle - \gamma_\perp\langle x\sigma_z\rangle - \kappa\langle xa^\dagger a + a^\dagger a x\rangle + \langle x\rangle(2\kappa\langle a^\dagger a\rangle + \gamma_\perp\langle\sigma_z + I\rangle) \\
\frac{d}{dt}\langle\sigma_x\rangle &= \frac{d}{dt}\frac{\langle\psi|\sigma_x|\psi\rangle}{\langle\psi|\psi\rangle} = \frac{1}{\langle\psi|\psi\rangle}\langle\psi|2gx\sigma_z - \gamma_\perp\sigma_x - 2\kappa\sigma_x a^\dagger a|\psi\rangle \\
&+ \frac{\langle\psi|\sigma_x|\psi\rangle}{\langle\psi|\psi\rangle}\frac{1}{\langle\psi|\psi\rangle}\langle\psi|2\kappa a^\dagger a + 2\gamma_\perp\sigma_+\sigma_-|\psi\rangle \\
&= +2g\langle x\sigma_z\rangle - \gamma_\perp\langle\sigma_x\rangle - 2\kappa\langle\sigma_x a^\dagger a\rangle + \langle\sigma_x\rangle(2\kappa\langle a^\dagger a\rangle + 2\gamma_\perp\langle\sigma_+\sigma_-\rangle) \\
\frac{d}{dt}\langle\sigma_z\rangle &= \frac{d}{dt}\frac{\langle\psi|\sigma_z|\psi\rangle}{\langle\psi|\psi\rangle} = \frac{1}{\langle\psi|\psi\rangle}\langle\psi|2gy\sigma_y - 2gx\sigma_x - \gamma_\perp - \gamma_\perp\sigma_z - 2\kappa\sigma_z a^\dagger a|\psi\rangle \\
&+ \frac{\langle\psi|\sigma_z|\psi\rangle}{\langle\psi|\psi\rangle}\frac{1}{\langle\psi|\psi\rangle}\langle\psi|2\kappa a^\dagger a + 2\gamma_\perp\sigma_+\sigma_-|\psi\rangle \\
&= +2g\langle y\sigma_y\rangle - 2g\langle x\sigma_x\rangle - \gamma_\perp - \gamma_\perp\langle\sigma_z\rangle - 2\kappa\langle\sigma_z a^\dagger a\rangle + \langle\sigma_z\rangle(2\kappa\langle a^\dagger a\rangle + 2\gamma_\perp\langle\sigma_+\sigma_-\rangle)
\end{aligned} \tag{2.10}$$

The above equations are obviously not closed therefore approximation needs to be made. The prudent choice, in view of the basis set of operator expectations that one wants to confine to, is the following

1. factorize the field and atomic wave function and hence the field and atomic operator expectations e.g. $\langle x\sigma_z\rangle \approx \langle x\rangle\langle\sigma_z\rangle, \langle x\sigma_x\rangle \approx \langle x\rangle\langle\sigma_x\rangle$ (the numerical solution to the stochastic master equation [10] shows that this is a fairly good approximation)

2. assume coherent state (with amplitude α) for the field, and as the resonant condition is assumed $\alpha = \alpha^* = \mathrm{Re}[\alpha] = \langle x\rangle$ and $\langle y\rangle \equiv 0$

with which one have the following closed equations of motion for $\langle\sigma_x\rangle$ and $\langle\sigma_z\rangle$

$$\begin{aligned}
\frac{d}{dt}\langle\sigma_x\rangle &\approx +2g\langle x\rangle\langle\sigma_z\rangle - \gamma_\perp\langle\sigma_x\rangle - 2\kappa\langle\sigma_x\rangle\langle x\rangle^2 + 2\kappa\langle\sigma_x\rangle\langle x\rangle^2 + \gamma_\perp\langle\sigma_x\rangle(\langle\sigma_z\rangle + 1) \\
&= +2g\langle x\rangle\langle\sigma_z\rangle + \gamma_\perp\langle\sigma_x\rangle\langle\sigma_z\rangle
\end{aligned} \tag{2.11}$$

$$\begin{aligned}\frac{d}{dt}\langle\sigma_z\rangle &\approx -2g\langle x\rangle\langle\sigma_x\rangle - \gamma_\perp - \gamma_\perp\langle\sigma_z\rangle - 2\kappa\langle\sigma_z\rangle\langle x\rangle^2 + 2\kappa\langle\sigma_z\rangle\langle x\rangle^2 + \gamma_\perp\langle\sigma_z\rangle(\langle\sigma_z\rangle+1)\\ &= -2g\langle x\rangle\langle\sigma_x\rangle - \gamma_\perp + \gamma_\perp\langle\sigma_z\rangle^2\end{aligned} \tag{2.12}$$

whereas the equation of motion for $\langle x\rangle$ is reduced to

$$\begin{aligned}\frac{d}{dt}\langle x\rangle &\approx +\frac{g}{2}\langle\sigma_x\rangle + \mathrm{Re}[\mathcal{E}] - \gamma_\perp\langle x\rangle - \gamma_\perp\langle x\rangle\langle\sigma_z\rangle - \kappa\langle xa^\dagger a + a^\dagger a x\rangle + 2\kappa\langle x\rangle\langle a^\dagger a\rangle + \gamma_\perp\langle x\rangle(\langle\sigma_z\rangle+1)\\ &= +\frac{g}{2}\langle\sigma_x\rangle + \mathrm{Re}[\mathcal{E}] - \kappa\langle xa^\dagger a + a^\dagger a x\rangle + 2\kappa\langle x\rangle\langle a^\dagger a\rangle\end{aligned} \tag{2.13}$$

To close the equation of motion for $\langle x\rangle$ some approximation needs to be adopted for the higher order operator expectation $xa^\dagger a + a^\dagger a x$. One has two choices of approximation

normal order approximation:

$$\begin{aligned}\langle xa^\dagger a + a^\dagger a x\rangle &= \left\langle \frac{a+a^\dagger}{2}a^\dagger a + a^\dagger a\frac{a+a^\dagger}{2}\right\rangle = \left\langle\frac{aa^\dagger a + a^\dagger a^\dagger a + a^\dagger aa + a^\dagger a a^\dagger}{2}\right\rangle\\ &= \left\langle\frac{(a^\dagger a+1)a + a^\dagger a^\dagger a + a^\dagger aa + a^\dagger(a^\dagger a+1)}{2}\right\rangle = \left\langle\frac{a^\dagger aa + a + a^\dagger a^\dagger a + a^\dagger aa + a^\dagger a^\dagger a + a^\dagger}{2}\right\rangle\\ &= \langle a^\dagger aa + a^\dagger a^\dagger a\rangle + \langle\frac{a+a^\dagger}{2}\rangle = \langle a^\dagger aa\rangle + \langle a^\dagger a^\dagger a\rangle + \langle x\rangle\end{aligned} \tag{2.14}$$

with which I have $-\kappa\langle xa^\dagger a + a^\dagger a x\rangle = -\kappa\langle x\rangle\langle x\rangle\langle x\rangle - \kappa\langle x\rangle\langle x\rangle\langle x\rangle - \kappa\langle x\rangle = -2\kappa\langle x\rangle\langle x\rangle\langle x\rangle - \kappa\langle x\rangle$ resulting in the following equation of motion for $\langle x\rangle$ (adopt normal order approximation to $\langle a^\dagger a\rangle$ as well i.e. $\langle a^\dagger a\rangle \approx \langle x\rangle\langle x\rangle$)

$$\frac{d}{dt}\langle x\rangle \approx +\frac{g}{2}\langle\sigma_x\rangle + \mathrm{Re}[\mathcal{E}] - 2\kappa\langle x\rangle\langle x\rangle\langle x\rangle - \kappa\langle x\rangle + 2\kappa\langle x\rangle\langle x\rangle\langle x\rangle = -\kappa\langle x\rangle + \frac{g}{2}\langle\sigma_x\rangle + \mathrm{Re}[\mathcal{E}] \tag{2.15}$$

number operator factorization approximation:

$$
\begin{aligned}
a^\dagger a x &= a^\dagger a \frac{a+a^\dagger}{2} = \frac{a^\dagger a a + a^\dagger a a^\dagger}{2} = \frac{(aa^\dagger - 1)a + a^\dagger(a^\dagger a + 1)}{2} \\
&= \frac{aa^\dagger a + a^\dagger a^\dagger a}{2} - \frac{a - a^\dagger}{2} = \frac{a+a^\dagger}{2} a^\dagger a - i\frac{a-a^\dagger}{2i} = x a^\dagger a - iy \\
&\Rightarrow x a^\dagger a + a^\dagger a x = 2 x a^\dagger a - iy
\end{aligned} \tag{2.16}
$$

with which I have $-\kappa\langle x a^\dagger a + a^\dagger a x\rangle = -\kappa\langle 2 x a^\dagger a - iy\rangle = -2\kappa\langle x a^\dagger a\rangle + i\kappa\langle y\rangle \approx -2\kappa\langle x\rangle\langle a^\dagger a\rangle$ (recall that the resonance condition is assumed thus $\langle y\rangle \equiv 0$) resulting in the following equation of motion for $\langle x\rangle$

$$
\frac{d}{dt}\langle x\rangle \approx +\frac{g}{2}\langle \sigma_x\rangle + \mathrm{Re}[\mathcal{E}] - 2\kappa\langle x\rangle\langle a^\dagger a\rangle + 2\kappa\langle x\rangle\langle a^\dagger a\rangle = +\frac{g}{2}\langle \sigma_x\rangle + \mathrm{Re}[\mathcal{E}] \tag{2.17}
$$

One can see that the only difference between these two approximations is the presence or absence of a mean field decay term $-\kappa\langle x\rangle$. However as can be seen in the following, the field amplitude decay due to photon leaking out of cavity end mirror is already taken into account in the collapse operation. Thus one should not incorporate another decay in the equation of motion governing the continuous evolution.

The effects of the two collapse operations are the following: with the collapse $|\psi\rangle \to \sqrt{2\gamma_\perp}\sigma_-|\psi\rangle$ I have

$$
\begin{aligned}
\frac{\langle\psi|x|\psi\rangle}{\langle\psi|\psi\rangle} &\to \frac{2\gamma_\perp\langle\psi|\sigma_+ x \sigma_-|\psi\rangle}{2\gamma_\perp\langle\psi|\sigma_+\sigma_-|\psi\rangle} = \frac{\langle\psi|x 2\sigma_+\sigma_-|\psi\rangle}{\langle\psi|2\sigma_+\sigma_-|\psi\rangle} = \frac{\langle\psi|x(\sigma_z + I)|\psi\rangle/\langle\psi|\psi\rangle}{\langle\psi|\sigma_z + I|\psi\rangle/\langle\psi|\psi\rangle} \\
&= \frac{\langle x\sigma_z\rangle + \langle x\rangle}{\langle\sigma_z\rangle + 1} \approx \frac{\langle x\rangle\langle\sigma_z\rangle + \langle x\rangle}{\langle\sigma_z\rangle + 1} = \langle x\rangle \\
\frac{\langle\psi|\sigma_x|\psi\rangle}{\langle\psi|\psi\rangle} &\to \frac{2\gamma_\perp\langle\psi|\sigma_+\sigma_x\sigma_-|\psi\rangle}{2\gamma_\perp\langle\psi|\sigma_+\sigma_-|\psi\rangle} = \frac{\langle\psi|\sigma_+\sigma_x\sigma_-|\psi\rangle}{\langle\psi|\sigma_+\sigma_-|\psi\rangle} = \frac{\langle\psi|0|\psi\rangle}{\langle\psi|\sigma_+\sigma_-|\psi\rangle} = 0 \\
\frac{\langle\psi|\sigma_z|\psi\rangle}{\langle\psi|\psi\rangle} &\to \frac{2\gamma_\perp\langle\psi|\sigma_+\sigma_z\sigma_-|\psi\rangle}{2\gamma_\perp\langle\psi|\sigma_+\sigma_-|\psi\rangle} = \frac{\langle\psi|\sigma_+\sigma_z\sigma_-|\psi\rangle}{\langle\psi|\sigma_+\sigma_-|\psi\rangle} = \frac{-\langle\psi|\sigma_+\sigma_-|\psi\rangle}{\langle\psi|\sigma_+\sigma_-|\psi\rangle} = -1
\end{aligned} \tag{2.18}
$$

and the collapse probability given by $2\gamma_\perp dt\langle\sigma_+\sigma_-\rangle = \gamma_\perp dt(\langle\sigma_z\rangle + 1)$ [2].

With the collapse $|\psi\rangle \to \sqrt{2\kappa}a|\psi\rangle$ I have

$$\begin{aligned}
\frac{\langle\psi|x|\psi\rangle}{\langle\psi|\psi\rangle} &\to \frac{2\kappa\langle\psi|a^\dagger x a|\psi\rangle}{2\kappa\langle\psi|a^\dagger a|\psi\rangle} = \frac{\langle\psi|a^\dagger x a|\psi\rangle/\langle\psi|\psi\rangle}{\langle\psi|a^\dagger a|\psi\rangle/\langle\psi|\psi\rangle} = \frac{\langle a^\dagger x a\rangle}{\langle a^\dagger a\rangle} \\
\frac{\langle\psi|\sigma_x|\psi\rangle}{\langle\psi|\psi\rangle} &\to \frac{2\kappa\langle\psi|a^\dagger \sigma_x a|\psi\rangle}{2\kappa\langle\psi|a^\dagger a|\psi\rangle} = \frac{\langle\psi|\sigma_x a^\dagger a|\psi\rangle/\langle\psi|\psi\rangle}{\langle\psi|a^\dagger a|\psi\rangle/\langle\psi|\psi\rangle} = \frac{\langle\sigma_x a^\dagger a\rangle}{\langle a^\dagger a\rangle} \approx \frac{\langle\sigma_x\rangle\langle a^\dagger a\rangle}{\langle a^\dagger a\rangle} = \langle\sigma_x\rangle \\
\frac{\langle\psi|\sigma_z|\psi\rangle}{\langle\psi|\psi\rangle} &\to \frac{2\kappa\langle\psi|a^\dagger \sigma_z a|\psi\rangle}{2\kappa\langle\psi|a^\dagger a|\psi\rangle} = \frac{\langle\psi|\sigma_z a^\dagger a|\psi\rangle/\langle\psi|\psi\rangle}{\langle\psi|a^\dagger a|\psi\rangle/\langle\psi|\psi\rangle} = \frac{\langle\sigma_z a^\dagger a\rangle}{\langle a^\dagger a\rangle} \approx \frac{\langle\sigma_z\rangle\langle a^\dagger a\rangle}{\langle a^\dagger a\rangle} = \langle\sigma_z\rangle
\end{aligned} \tag{2.19}$$

and the collapse probability given by $2\kappa dt\langle a^\dagger a\rangle \approx 2\kappa dt\langle x\rangle^2$. Again some approximation needs to be adopted, this time for $\langle a^\dagger x a\rangle/\langle a^\dagger a\rangle$. However the effect of one photon leaking out of cavity end mirror is obvious: the intracavity photon number is reduced by one. If one adopts coherent state approximation then the reduction in the intracavity photon number can be translated into the reduction in the squared norm of the coherent state amplitude: $\langle\alpha|a^\dagger a|\alpha\rangle = \alpha^*\alpha = |\alpha|^2 \mapsto |\alpha|^2 - 1 = \beta^*\beta = \langle\beta|a^\dagger a|\beta\rangle$. The mapping that can generate the desired reduction in the squared norm of the coherent state amplitude is the following

$$\begin{aligned}
\langle x\rangle &\mapsto \langle x\rangle - \frac{\langle x\rangle}{2(\langle x\rangle^2 + \langle y\rangle^2)} \\
\langle x\rangle^2 &\mapsto \left(\langle x\rangle - \frac{\langle x\rangle}{2(\langle x\rangle^2 + \langle y\rangle^2)}\right)^2 = \langle x\rangle^2 - \frac{\langle x\rangle^2}{\langle x\rangle^2 + \langle y\rangle^2} + o(1) \\
\langle y\rangle &\mapsto \langle y\rangle - \frac{\langle y\rangle}{2(\langle x\rangle^2 + \langle y\rangle^2)} \\
\langle y\rangle^2 &\mapsto \left(\langle y\rangle - \frac{\langle y\rangle}{2(\langle x\rangle^2 + \langle y\rangle^2)}\right)^2 = \langle y\rangle^2 - \frac{\langle y\rangle^2}{\langle x\rangle^2 + \langle y\rangle^2} + o(1)
\end{aligned} \tag{2.20}$$

which with coherent state approximation $\langle\alpha|a^\dagger a|\alpha\rangle = \alpha^*\alpha = |\alpha|^2$ leads to

$$\begin{aligned}
|\alpha|^2 = |\langle x\rangle + i\langle y\rangle|^2 = \langle x\rangle^2 + \langle y\rangle^2 &\mapsto \left(\langle x\rangle - \frac{\langle x\rangle}{2(\langle x\rangle^2 + \langle y\rangle^2)}\right)^2 + \left(\langle y\rangle - \frac{\langle y\rangle}{2(\langle x\rangle^2 + \langle y\rangle^2)}\right)^2 \\
&= \langle x\rangle^2 + \langle y\rangle^2 - \frac{\langle x\rangle^2}{\langle x\rangle^2 + \langle y\rangle^2} - \frac{\langle y\rangle^2}{\langle x\rangle^2 + \langle y\rangle^2} + o(1) = \langle x\rangle^2 + \langle y\rangle^2 - 1 = |\alpha|^2 - 1
\end{aligned} \tag{2.21}$$

Under resonance $\langle y\rangle \equiv 0$ thus with the collapse $|\psi\rangle \to \sqrt{2\kappa}a|\psi\rangle$ one should have

$\langle x \rangle \mapsto \langle x \rangle - \langle x \rangle / 2\langle x \rangle^2 = \langle x \rangle - 1/(2\langle x \rangle)$.

With all the above derivation and approximations a reduced order model in terms of the basic set of 3 operator expectations $\langle x \rangle, \langle \sigma_x \rangle, \langle \sigma_z \rangle$ is finally arrived:

continuous evolution: governed by

$$\begin{aligned} \frac{d}{dt}\langle x \rangle &= +\frac{g}{2}\langle \sigma_x \rangle + \mathrm{Re}[\mathcal{E}] \\ \frac{d}{dt}\langle \sigma_x \rangle &= +2g\langle x \rangle\langle \sigma_z \rangle + \gamma_\perp \langle \sigma_x \rangle\langle \sigma_z \rangle \\ \frac{d}{dt}\langle \sigma_z \rangle &= -2g\langle x \rangle\langle \sigma_x \rangle - \gamma_\perp + \gamma_\perp \langle \sigma_z \rangle^2 \end{aligned} \tag{2.22}$$

discrete collapses: two collapse channels

first collapse probability: $p_{c1} = 2\kappa dt\langle x \rangle\langle x \rangle$

first collapse criterion: a random number r_n drawn from a $[0, 1]$ uniform distribution $< p_{c1}$

first collapse operation: $\langle x \rangle \mapsto \langle x \rangle - 1/(2\langle x \rangle)$, no change to $\langle \sigma_x \rangle, \langle \sigma_z \rangle$

second collapse probability: $p_{c2} = \gamma_\perp dt(\langle \sigma_z \rangle + 1)$

second collapse criterion: $p_{c1} \leq$ the random number r_n drawn $< p_{c1} + p_{c2}$

second collapse operation: $\langle \sigma_z \rangle \mapsto -1$ and $\langle \sigma_x \rangle \mapsto 0$, no change to $\langle x \rangle$

This reduced order model manages to reproduce the automatic switching as can been seen from Fig. 2.11 and Fig. 2.12 below.

Not only does the model exhibit bistable state switching but also it yields low-/high-state statistical distributions similar to those produced by the quantum trajectory simulation as can be seen from Fig. 2.13 and Fig. 2.14 below.

As a quantitative measure of the goodness of approximation, the $\langle x \rangle$ autocorrelation of the model at $\mathcal{E} = 0.515, 0.520$ and 0.525 averaged over 10, 20 and 40 trials respectively is compared with that of master equation and plotted in Fig. 2.15 below.

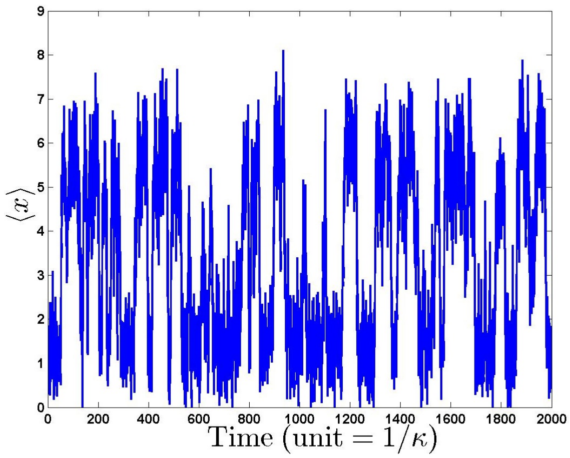

Figure 2.11: The 3D reduced order model at $\mathcal{E} = 0.525$ starting from low-state showing both low-to-high and high-to-low transitions

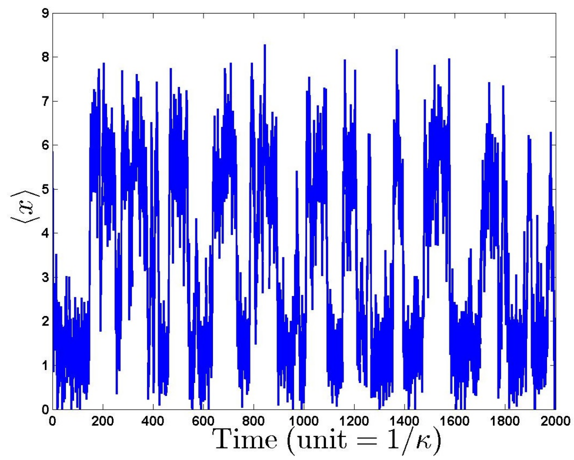

Figure 2.12: The 3D reduced order model at $\mathcal{E} = 0.525$ starting from high-state showing both high-to-low and low-to-high transitions

For comparison the external driving dependence of the $\langle x \rangle$ autocorrelation of the master equation is shown in Fig. 2.16 where $\mathcal{E} = 0.5354 \sim 0.540$ corresponds to the case with approximately equal probability of the system staying in low- and high-state and $\mathcal{E} = 0.525 \sim 0.555$ is roughly the range of bistability. As can be seen in the plot, the autocorrelation remains almost the same as the external driving is slightly varied from $\mathcal{E} = 0.5354$ to $\mathcal{E} = 0.540$, indicating its relative insensitivity to the external driving when the bistability is most manifested. This same insensitivity is also observed in the autocorrelation plot for the reduced order model at $\mathcal{E} = 0.520 \sim 0.525$ as can be seen in Fig. 2.15 and the time evolution plots of $\langle x \rangle$ at $\mathcal{E} = 0.525$ (Fig. 2.13 and Fig. 2.14) for the reduced order model show roughly equal time split between low- and high-state thus the condition at $\mathcal{E} = 0.525$ for the reduced order model roughly corresponds to the condition at $\mathcal{E} = 0.540$ for the master equation. Therefore the $\langle x \rangle$ autocorrelation comparison between them at these two driving levels is reasonable and the plot suggests that the autocorrelations are pretty close to each other.

As another quantitative measure of the goodness of approximation, hidden Markov model is used to identify (reasonable) transitions for both the reduced order model and the quantum trajectory simulation and then the number of transitions compared.

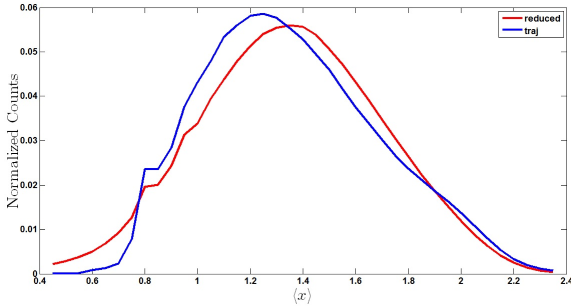

Figure 2.13: The low-state statistical distribution of the reduced order model (red) and that of the quantum trajectory simulation (blue)

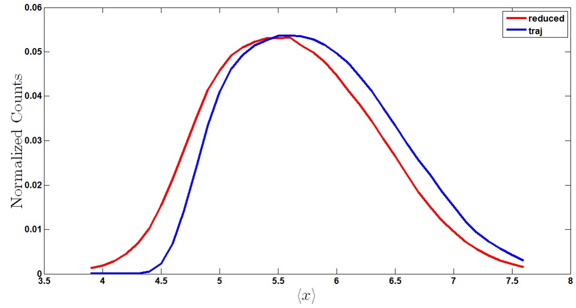

Figure 2.14: The high-state statistical distribution of the reduced order model (red) and that of the quantum trajectory simulation (blue)

For the sake of generality the coupling constant g and the field decay rate κ are varied to change the critical photon number $n_0 = \gamma_\perp^2/2g^2$ while keeping the cooperativity C fixed to examine different separations/distances between low- and high-state. In the following the cooperativity C is fixed at 6 and the external driving is tweaked towards 50-50 time split between low- and high-state. A stay duration requirement (that the system should stay in the destination state for a sufficiently long time) is imposed to distinguish true low-to-high/high-to-low transitions from mere field fluctuations.

Critical photon number = 3

The steady state solution to the master equation produces the Q-function plotted in Fig. 2.17 and Fig. 2.18.

The transition counts of 7 trajectories for both the reduced order model at $E = 0.434$ and the quantum trajectory simulation at $E = 0.433$ with 130 Fock bases are as follows

reduced order model: with a stay duration cutoff of 125 in 7 trajectories

the number of jump-ups identified by 3-state HMM = 279

the number of good jump-ups selected by the cutoff criterion = 209

the number of jump-downs identified by 3-state HMM = 278

the number of good jump-downs selected by the cutoff criterion = 209

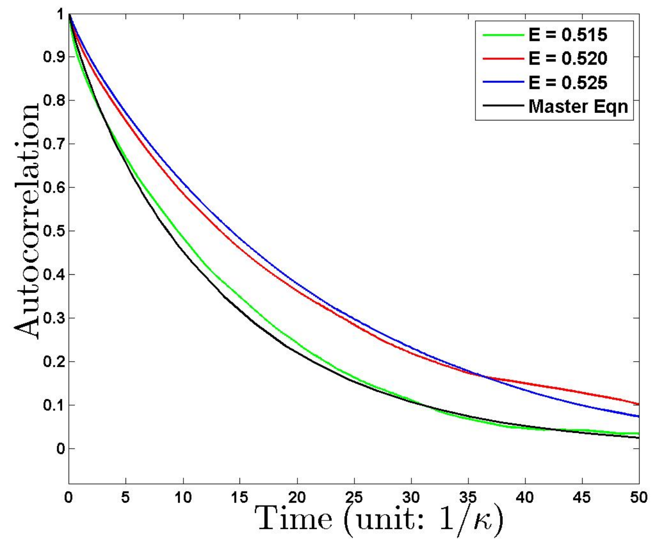

Figure 2.15: Autocorrelation of $\langle x \rangle$ for the 3D reduced order model with number operator factorization approximation at $\mathcal{E} = 0.515, 0.520, 0.525$ averaged over 10, 20 and 40 trials respectively and the master equation at $\mathcal{E} = 0.540$

quantum trajectory simulation: with a stay duration cutoff of 125 in 7 trajectories

the number of jump-ups identified by 3-state HMM = 248

the number of good jump-ups selected by the cutoff criterion = 175

the number of jump-downs identified by 3-state HMM = 245

the number of good jump-downs selected by the cutoff criterion = 176

The transition counts of 10 trajectories for both the reduced order model at $E = 0.434$ and the quantum trajectory simulation at $E = 0.433$ with 130 Fock bases are as follows

reduced order model: with a stay duration cutoff of 125 in 10 trajectories

the number of jump-ups identified by 3-state HMM = 432

the number of good jump-ups selected by the cutoff criterion = 292

the number of jump-downs identified by 3-state HMM = 433

the number of good jump-downs selected by the cutoff criterion = 295

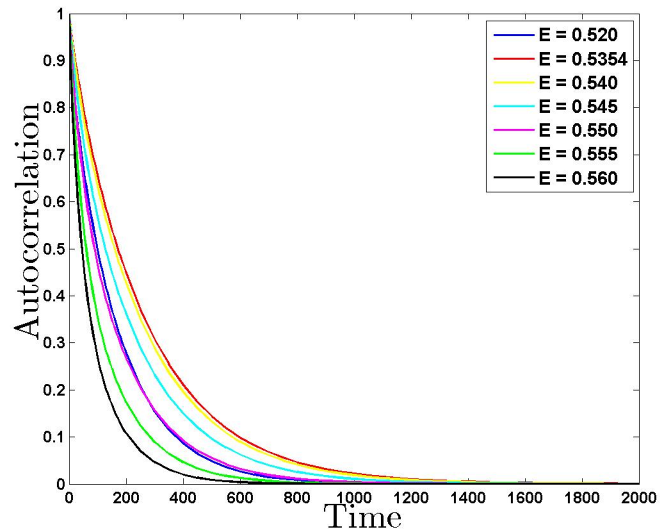

Figure 2.16: Autocorrelation of $\langle x \rangle$ for the master equation at various external driving

quantum trajectory simulation: with a stay duration cutoff of 125 in 10 trajectories

the number of jump-ups identified by 3-state HMM = 344

the number of good jump-ups selected by the cutoff criterion = 243

the number of jump-downs identified by 3-state HMM = 340

the number of good jump-downs selected by the cutoff criterion = 243

Critical photon number = 4

The steady state solution to the master equation produces the Q-function plotted in Fig. 2.19 and Fig. 2.20.

The transition counts of 7 trajectories for both the reduced order model at $E = 0.376$ and the quantum trajectory simulation at $E = 0.373$ with 170 Fock bases are as follows

reduced order model: with a stay duration cutoff of 125 in 7 trajectories

the number of jump-ups identified by 3-state HMM = 142

the number of good jump-ups selected by the cutoff criterion = 111

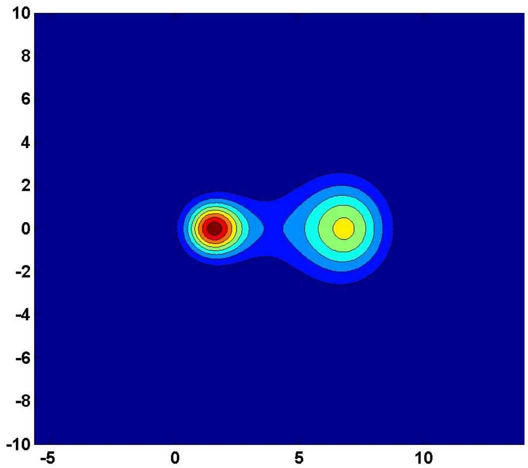

Figure 2.17: Q-function contour plot for $C = 6, n_0 = 3, E = 0.433$ with 130 Fock bases

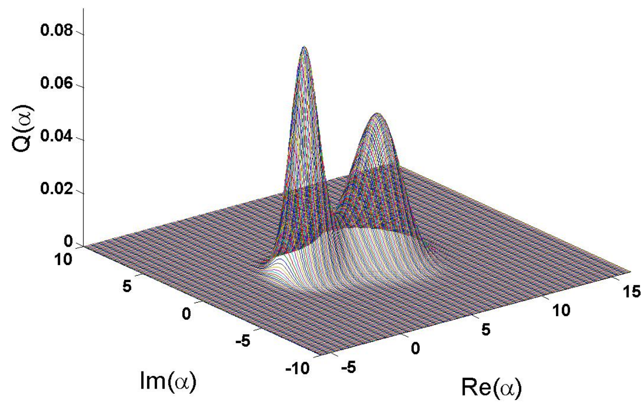

Figure 2.18: Q-function 3D plot for $C = 6, n_0 = 3, E = 0.433$ with 130 Fock bases

the number of jump-downs identified by 3-state HMM = 145

the number of good jump-downs selected by the cutoff criterion = 112

quantum trajectory simulation: with a stay duration cutoff of 125 in 7 trajectories

the number of jump-ups identified by 3-state HMM = 145

the number of good jump-ups selected by the cutoff criterion = 102

the number of jump-downs identified by 3-state HMM = 139

the number of good jump-downs selected by the cutoff criterion = 95

The transition counts of 10 trajectories for both the reduced order model at $E = 0.376$ and the quantum trajectory simulation at $E = 0.373$ with 170 Fock bases are as follows

reduced order model: with a stay duration cutoff of 125 in 10 trajectories

the number of jump-ups identified by 3-state HMM = 193

the number of good jump-ups selected by the cutoff criterion = 155

the number of jump-downs identified by 3-state HMM = 195

the number of good jump-downs selected by the cutoff criterion = 155

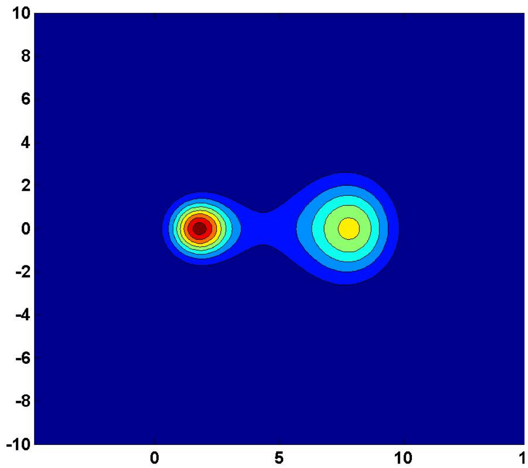

Figure 2.19: Q-function contour plot for $C = 6, n_0 = 4, E = 0.373$ with 160 Fock bases

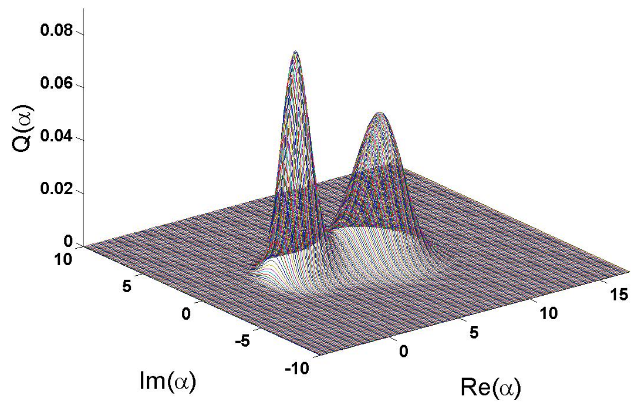

Figure 2.20: Q-function 3D plot for $C = 6, n_0 = 4, E = 0.373$ with 160 Fock bases

quantum trajectory simulation: with a stay duration cutoff of 125 in 10 trajectories

the number of jump-ups identified by 3-state HMM = 202

the number of good jump-ups selected by the cutoff criterion = 145

the number of jump-downs identified by 3-state HMM = 194

the number of good jump-downs selected by the cutoff criterion = 137

Critical photon number = 5

The steady state solution to the master equation produces the Q-function plotted in Fig. 2.21 and Fig. 2.22.

The transition counts of 7 trajectories for both the reduced order model at $E = 0.337$ and the quantum trajectory simulation at $E = 0.3325$ with 210 Fock bases are as follows

reduced order model: with a stay duration cutoff of 125 in 7 trajectories

the number of jump-ups identified by 3-state HMM = 70

the number of good jump-ups selected by the cutoff criterion = 56

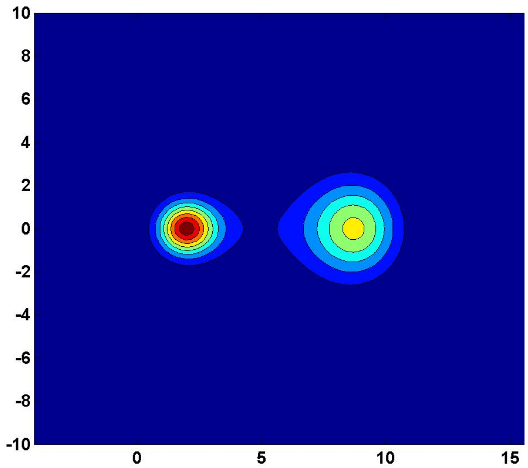

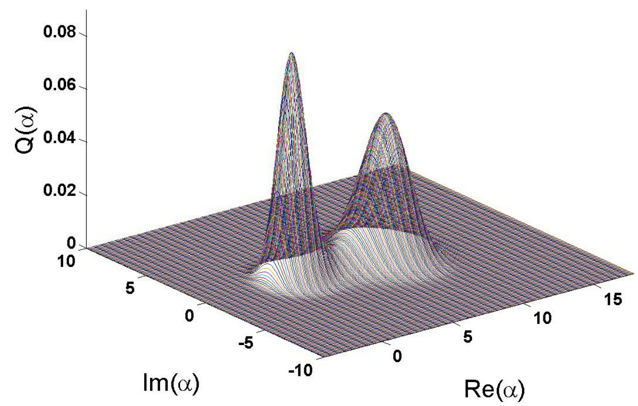

Figure 2.21: Q-function contour plot for $C = 6, n_0 = 5, E = 0.3325$ with 200 Fock bases

Figure 2.22: Q-function 3D plot for $C = 6, n_0 = 5, E = 0.3325$ with 200 Fock bases

the number of jump-downs identified by 3-state HMM = 70

the number of good jump-downs selected by the cutoff criterion = 55

quantum trajectory simulation: with a stay duration cutoff of 125 in 7 trajectories

the number of jump-ups identified by 3-state HMM = 64

the number of good jump-ups selected by the cutoff criterion = 57

the number of jump-downs identified by 3-state HMM = 59

the number of good jump-downs selected by the cutoff criterion = 54

The transition counts of 10 trajectories for both the reduced order model at $E = 0.337$ and the quantum trajectory simulation at $E = 0.3325$ with 210 Fock bases are as follows

reduced order model: with a stay duration cutoff of 125 in 10 trajectories

the number of jump-ups identified by 3-state HMM = 100

the number of good jump-ups selected by the cutoff criterion = 80

the number of jump-downs identified by 3-state HMM = 99

the number of good jump-downs selected by the cutoff criterion = 77

quantum trajectory simulation: with a stay duration cutoff of 125 in 10 trajectories

the number of jump-ups identified by 3-state HMM = 131

the number of good jump-ups selected by the cutoff criterion = 78

the number of jump-downs identified by 3-state HMM = 125

the number of good jump-downs selected by the cutoff criterion = 74

From the above transition count comparison one can see that the reduced order model is at least as capable of inducing state transition as the standard quantum trajectory formulation. Thus the goodness of approximation of the reduced order model is finally established.

2.5 Conclusion and Discussion

I have elucidated the contribution of excessive spontaneous emission to the automatic switching between the two metastable states in the quantum analog of absorptive bistability, which weakens/strengthens the dipole moment thus dipole radiation under weak/strong cavity field. The difference in the consequence of excessive spontaneous emission is resulted from the difference in the speed of the atomic spin precession driven by the cavity field. Even though the modeling and analysis is carried out under the resonance assumption, the underlying mechanism is present under non-resonance condition as well. Based on this understanding I proposed a flip-flop control of an absorptive bistable cavity via cavity enhanced spontaneous emission using a second cavity with tunable detuning, which provides a physical basis for designing ultra-low energy information processing logic devices.

Regarding the merit of having a reduced order model, facilitating faster numerical solution thereby enabling design of real-time feedback control is beyond question. But to physicists the most attractive merit is the reduced order model being able to reveal the underlying physics. However it is doubtful whether a reduced order model can become such a useful tool or not, even in our special case—recall how I selected the approach for deriving the reduced order model: I choose deriving trajectories of operator expectations exactly because I understand the switching mechanism based on the atomic spontaneous emission collapse and the natural way of incorporating this collapse operation into a reduced order model is to start from the standard quantum trajectory formulation. If deriving a reduced order model is a useful tool for unraveling the underlying physics then the derivation process should be in the opposite order, i.e. based on some very general principle one derives a reduced order model which contains the collapse operations capable of inducing the switching and the model shows the switching as a necessary consequence of the collapse operations, perhaps in the manner that if one replaces the collapse(s) by mean field decay one would then not be able to observe the switching. Nonetheless such a general principle for deriving the "right" reduced order model does not seem to exist because one really needs to make a decision as to what kind of quantum dynamics unraveling i.e. what type of measurement to take [2]. There is in fact another reduced order model that can produce the switching yet is based on homodyne measurement of the field amplitude quadrature: consider the stochastic master equation with homodyne measurement on the amplitude quadrature $x = (a + a^\dagger)/2$ of the cavity field which reads [10]

$$\begin{aligned}\dot{\rho} &= -i[H,\rho] + \kappa(2a\rho a^\dagger - a^\dagger a\rho - \rho a^\dagger a) + \gamma_\perp(2\sigma_-\rho\sigma_+ - \sigma_+\sigma_-\rho - \rho\sigma_+\sigma_-) \\ &\quad + \sqrt{2\kappa}(a\rho + \rho a^\dagger - \mathrm{Tr}[(a+a^\dagger)\rho])dW\end{aligned} \tag{2.23}$$

The stochastic term involving the Wiener process dW accounts for the update of our information about the system based on how much the actual measurement result differs from the expected value (the trace term). With this stochastic master equation one can use the trace formula for deriving the Maxwell-Bloch equations to derive stochastic differential equations (SDE) for a suitable set of observables and then close the equations by making appropriate approximations of the expectations of observable products exactly as what I did before. The simplest example is to apply the formula to the same set of physical observables $\{x, \sigma_x, \sigma_z\}$ to obtain a stochastic version of the Maxwell-Bloch equations. After applying the trace formula I have

$$\begin{aligned} d\langle x\rangle &= -\kappa\langle x\rangle dt + \frac{g}{2}\langle\sigma_x\rangle dt + \mathcal{E}dt + \sqrt{2\kappa}(2\langle xx\rangle - \frac{1}{2} - 2\langle x\rangle\langle x\rangle)dW \\ d\langle\sigma_x\rangle &= -\gamma_\perp\langle\sigma_x\rangle dt + 2g\langle x\sigma_z\rangle dt + 2\sqrt{2\kappa}(\langle x\sigma_x\rangle - \langle x\rangle\langle\sigma_x\rangle)dW \\ d\langle\sigma_z\rangle &= -2\gamma_\perp(1+\langle\sigma_z\rangle)dt - 2g\langle x\sigma_x\rangle dt + 2\sqrt{2\kappa}(\langle x\sigma_z\rangle - \langle x\rangle\langle\sigma_z\rangle)dW \end{aligned} \tag{2.24}$$

and then one can close the equations by approximating $\langle xx\rangle, \langle x\sigma_x\rangle, \langle x\sigma_z\rangle$ using suitable functions of $\langle x\rangle$, $\langle\sigma_x\rangle$ and $\langle\sigma_z\rangle$, for example $\langle xx\rangle \approx \langle x\rangle\langle x\rangle, \langle\sigma_x\rangle \approx \langle x\rangle\langle\sigma_x\rangle$ and $\langle x\sigma_z\rangle \approx \langle x\rangle\langle\sigma_z\rangle$.

To derive a reduced order model for describing the automatic switching, it turns out that one needs to add $\langle xx\rangle, \langle x\sigma_x\rangle, \langle xx\sigma_z\rangle$ to the set of expectation variables. Applying the trace formula to the set of six physical observables $\{x, \sigma_x, \sigma_z, xx, x\sigma_x, xx\sigma_z\}$ I have (where $y = (a - a^\dagger)/2i$)

$$\begin{aligned} d\langle x\rangle &= -\kappa\langle x\rangle dt + \frac{g}{2}\langle\sigma_x\rangle dt + \mathcal{E}dt + \sqrt{2\kappa}(2\langle xx\rangle - \frac{1}{2} - 2\langle x\rangle\langle x\rangle)dW \\ d\langle\sigma_x\rangle &= -\gamma_\perp\langle\sigma_x\rangle dt + 2g\langle x\sigma_z\rangle dt + 2\sqrt{2\kappa}(\langle x\sigma_x\rangle - \langle x\rangle\langle\sigma_x\rangle)dW \\ d\langle\sigma_z\rangle &= -2\gamma_\perp(1+\langle\sigma_z\rangle)dt - 2g\langle x\sigma_x\rangle dt + 2\sqrt{2\kappa}(\langle x\sigma_z\rangle - \langle x\rangle\langle\sigma_z\rangle)dW \\ d\langle xx\rangle &= -2\kappa\left(\langle xx\rangle - \frac{1}{4}\right)dt + g\langle x\sigma_x\rangle dt + 2\mathcal{E}\langle x\rangle dt \\ &\quad + \sqrt{2\kappa}(2\langle xxx\rangle + i\langle xxy - yxx\rangle - 2\langle x\rangle\langle xx\rangle)dW \\ d\langle x\sigma_x\rangle &= -(\gamma+\kappa)\langle x\sigma_x\rangle dt + \mathcal{E}\langle\sigma_x\rangle dt + 2g\left(\langle xx\sigma_z\rangle + \frac{1}{4}\right)dt \\ &\quad + \sqrt{2\kappa}(2\langle xx\sigma_x\rangle - \frac{1}{2}\langle\sigma_x\rangle - 2\langle x\rangle\langle x\sigma_x\rangle)dW \\ d\langle xx\sigma_z\rangle &= -2(\kappa+\gamma_\perp)\langle xx\sigma_z\rangle dt + \frac{1}{2}\kappa\langle\sigma_z\rangle dt - 2\gamma_\perp\langle xx\rangle dt + 2\mathcal{E}\langle x\sigma_z\rangle dt \\ &\quad - 2g\langle xxx\sigma_x\rangle dt + 2g\langle yxy\sigma_x\rangle dt - g\langle(yyx+xyy)\sigma_x\rangle dt + g\langle(yxx+xxy)\sigma_y\rangle dt \\ &\quad + \sqrt{2\kappa}(2\langle xxx\sigma_z\rangle - 2\langle yxy\sigma_z + \langle(xyy+yyx)\sigma_z - \langle x\sigma_z\rangle)dW \end{aligned}$$

I then make various approximations based on the numerical solution to the stochastic master equation to arrive at the following set of closed SDEs

$$
\begin{aligned}
d\langle x\rangle &= -\kappa\langle x\rangle dt + \frac{g}{2}\langle\sigma_x\rangle dt + \mathcal{E}dt + \sqrt{2\kappa}(2\langle xx\rangle - \frac{1}{2} - 2\langle x\rangle\langle x\rangle)dW \\
d\langle\sigma_x\rangle &= -\gamma_\perp\langle\sigma_x\rangle dt + 2g\langle x\rangle\langle\sigma_z\rangle dt + 2\sqrt{2\kappa}(\langle x\sigma_x\rangle - \langle x\rangle\langle\sigma_x\rangle)dW \\
d\langle\sigma_z\rangle &= -2\gamma_\perp(1+\langle\sigma_z\rangle)dt - 2g\langle x\sigma_x\rangle dt \\
d\langle xx\rangle &= -2\kappa\left(\langle xx\rangle - \frac{1}{4}\right)dt + g\langle x\sigma_x\rangle dt + 2\mathcal{E}\langle x\rangle dt \\
d\langle x\sigma_x\rangle &= -(\gamma+\kappa)\langle x\sigma_x\rangle dt + \mathcal{E}\langle\sigma_x\rangle dt + 2g\left(\langle xx\sigma_z\rangle + \frac{1}{4}\right)dt \\
d\langle xx\sigma_z\rangle &= -2(\kappa+\gamma_\perp)\langle xx\sigma_z\rangle dt + \frac{1}{2}\kappa\langle\sigma_z\rangle dt - 2\gamma_\perp\langle xx\rangle dt + 2\mathcal{E}\langle x\rangle\langle\sigma_z\rangle dt - 2g\langle xx\rangle\langle x\sigma_x\rangle dt
\end{aligned}
\tag{2.25}
$$

I now verify whether this 6D reduced order model is able to produce the automatic switching. Fig.2.23 and Fig.2.24 below depict the time evolution of $\langle x\rangle$ starting from low- and high-state respectively.

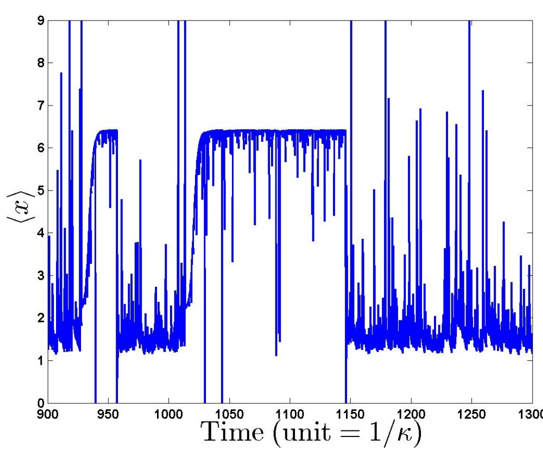

Figure 2.23: A 6D reduced order model based on stochastic master equation starting from low-state showing both low-to-high and high-to-low transitions

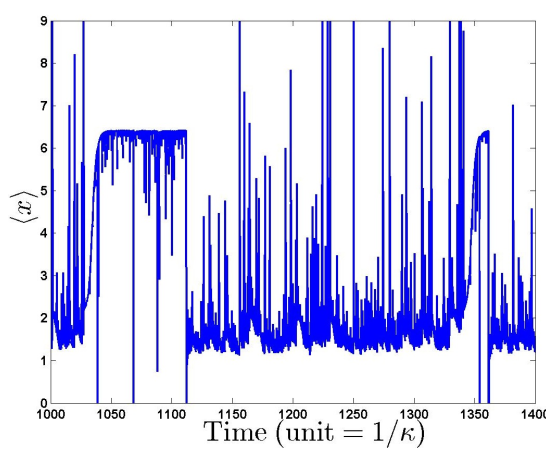

Figure 2.24: A 6D reduced order model based on stochastic master equation starting from high-state showing both low-to-high and high-to-low transitions

The plots show clearly that the SDEs are capable of producing low-to-high and high-to-low transitions albeit the evolution is not as smooth as that of the 3D reduced order model based on the quantum trajectory formulation. As a quantitative measure of the goodness of approximation let's also check the autocorrelation function of $\langle x \rangle$ and compare it with that of the master equation computed using the quantum regression theorem [2] which is plotted in Fig.2.25 below. As one can see in the plot that the $\langle x \rangle$ autocorrelation of the 6D reduced order model can also be close to that yielded by the master equation.

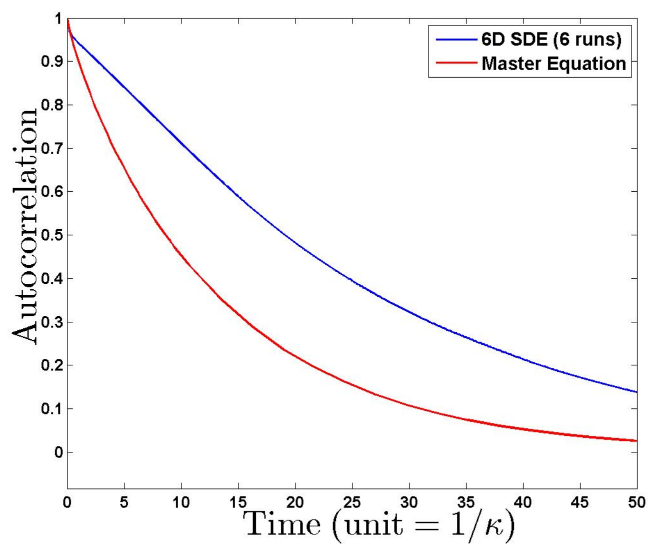

Figure 2.25: Autocorrelation function of $\langle x \rangle$ comparison between the reduced order model and the master equation, both at $\mathcal{E} = 0.540$

In fact it is this 6D reduced order model that was first derived because the homodyne measurement on the amplitude quadrature yields more direct and unambiguous information about the system state as low- and high-state are most distinguishable in terms of the cavity intensity.

As Carmichael puts it [2], a quantum trajectory is an unraveling of the master equation giving us a picture of what is going on in a visible form; different unravelings of the master equation "will give us different pictures, suited to help us understand different aspects of the physics. The complete picture is the complement of all the separate pictures, and by the very nature of quantum mechanics no single picture can substitute for them all." Understanding of a particular aspect of quantum dynamics requires choosing the right picture/unraveling. Therefore if deriving a reduced order model still has to rely on such a choice, then the derivation of a reduced order model would not be useful to elucidating what aspect of the dynamics is the right picture/unraveling not to mention the essential physics in that picture/unraveling. And up to now we do not have any clue as to finding a general guideline for selecting the right picture/unraveling. But my personal view is that, when no hint/intuition is available for guiding the selection, the very first one to try should perhaps be direct photon + fluorescence detection as it amounts to direct observation of what the atom and the photons are doing. This opinion is also backed by the recent work on the mechanism of automatic switching in phase bistability [11] in which spontaneous emission is shown to be the cause through a quantum trajectory unraveling based on it.

Chapter 3

Self-oscillation and Phase Insensitive Amplification in the Maxwell-Bloch Equations

The mechanism of supercritical Hopf bifurcation in the semi-classical Maxwell-Bloch equations for cavity quantum electrodynamics (QED) is elucidated by formulating the atom-field interaction as a feedback control loop. The generation of self-oscillation in the cavity field intensity upon the bifurcation turns out to be the consequence of loop instability. A computational study is conducted on the possibility of phase insensitive amplification of weak coherent light field by making use of the system's sensitivity to this loop instability and the simulation result confirms the feasibility.

3.1 Introduction

Bifurcation theory analyzing changes in the number and properties of possible equilibrium states upon variation of system parameters is a fundamental aspect of dynamical systems theory [12, 13]. In practice bifurcation theory has been used not only to ensure safe operation in a stable parameter range but also to realize robust devices with signal processing functionality. In the previous chapter I have proposed a flip-flip control based on absorptive bistability in the context of single-atom cavity quantum electrodynamics. In this chapter, I will elaborate on another proposal of making useful devices out of bifurcation theory—utilizing the sensitivity to periodic perturbation tuned to intrinsic frequency near supercritical Hopf bifurcation to amplify small signals. Here "Hopf bifurcation" refers to the phenomenon in which self-oscillatory state emerges upon system parameter crossing a critical value as is illustrated in Fig.3.1 below and "intrinsic frequency" refers to its oscillation frequency which is a characteristic of the system; "supercritical" refers to the fact that the generated self-oscillatory state is stable against perturbation [12].

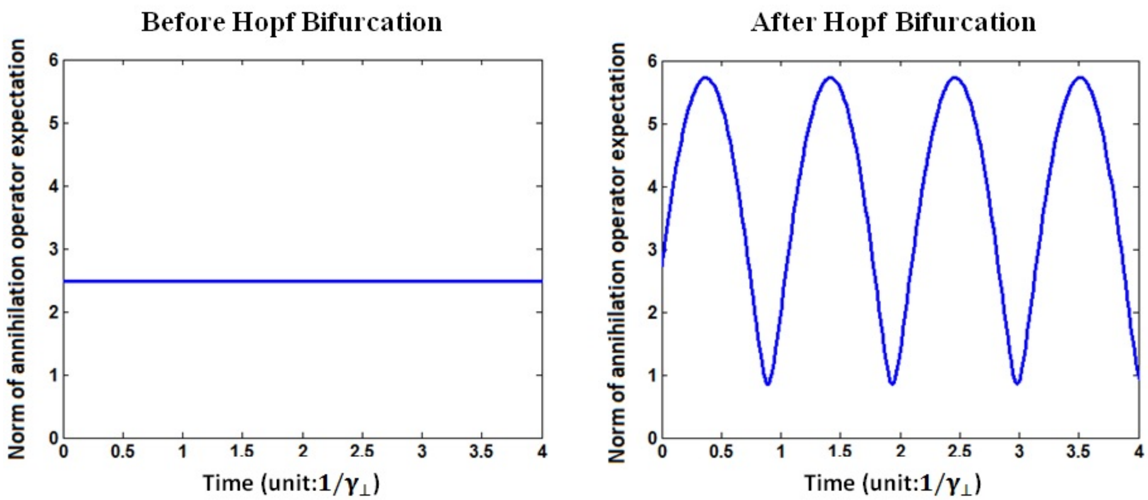

Figure 3.1: Illustration of Hopf bifurcation: the solution is stationary before the system parameter (in our model the amplitude of the external classical driving field) crossing a critical value, it becomes self-oscillatory after the crossing

The theoretical foundation of this amplifier proposal is Wiesenfeld and McNamara's analysis [14], which shows that a nonlinear dynamical system right before bifurcation becomes extremely sensitive to external perturbations—the response to a periodic perturbation will be greatly enhanced if its frequency is tuned to the intrinsic frequency. Since then this phenomenon has been confirmed in many physical systems, such as nano-mechanical resonators [15], single trapped-ion systems [16], as well as superconducting circuits [17]. However, as far as we know there has not been any study on systems operating in optical frequency range. In addition, Wiesenfeld and McNamara's analysis is based on Floquet theory which reveals the existence of instability as divergences in the computed power spectra but does not provide an explanation as to how the instability comes into being. In this chapter I will point out that the instability in question is in fact the very common loop instability found in control theory. Although the explanation does involve the details of our physical model the same perspective should be applicable to other physical systems to elucidate the origin of their instabilities.

The present study is also motivated by the current technological trend towards ultra-low power signal processing, which is exemplified by recent efforts on developing attojoule devices based on photonic crystals [5]. This raises the issue of detecting and propagating weak signals in the desired energy scale which often calls for the deployment of amplifiers. Although single photon detection combined with electronic processing is a viable solution, the coherence is lost. In contrast this bifurcation-based proposal has the potential to preserve it because its input-output phase relation is fixed [18]. This direct optical amplification also outshines degenerate parametric amplification by being insensitive to the phase of input signal and non-degenerate parametric amplification by avoiding waste of energy through generating idlers.

Moreover, physical processes involving only dozens of energy quanta inevitably bear the footprint of quantum mechanics and the study on quantum-classical transition comparing the prediction of semi-classical approximate equations of motion and that of exact quantum models has long been a theme of quantum physics. Even though the semi-classical Maxwell-Bloch equations have been found to be surprisingly accurate in predicting the existence of bifurcation-like phenomena for the quantum model even outside the applicable regime of the semi-classical approximation [3], the phenomena do exhibit characteristics of quantum nature different from their counterparts in dynamical systems theory [6]. It is therefore worth asking whether this bifurcation-based small signal amplification would carry over to the quantum regime or not and if yes to what extent the quantum nature is manifested.

3.2 The Mechanism of Supercritical Hopf Bifurcation

Previous study has shown that the semi-classical Maxwell-Bloch equations can produce supercritical Hopf bifurcation with properly chosen parameter values, for example those of Armen and Mabuchi's Fig.4 [3]. To elucidate the mechanism of the self-oscillation state generation, the system is modeled as a feedback control system, treating the cavity field as the "plant" controlled by the "controller" which is the atom. According to the Maxwell-Bloch equations the dynamical equations for the "plant" are

$$\begin{aligned} \frac{d}{dt}\langle x\rangle &= -\kappa\langle x\rangle + \Delta_c\langle y\rangle + \frac{g}{2}\langle\sigma_x\rangle + \mathrm{Re}[\mathcal{E}] \\ \frac{d}{dt}\langle y\rangle &= -\kappa\langle y\rangle - \Delta_c\langle x\rangle - \frac{g}{2}\langle\sigma_y\rangle + \mathrm{Im}[\mathcal{E}] \end{aligned} \tag{3.1}$$

and the dynamical equations for the "controller" are

$$\begin{aligned} \frac{d}{dt}\langle\sigma_x\rangle &= -\gamma_\perp\langle\sigma_x\rangle - \Delta_a\langle\sigma_y\rangle + 2g\langle x\rangle\langle\sigma_z\rangle \\ \frac{d}{dt}\langle\sigma_y\rangle &= -\gamma_\perp\langle\sigma_y\rangle + \Delta_a\langle\sigma_x\rangle - 2g\langle y\rangle\langle\sigma_z\rangle \\ \frac{d}{dt}\langle\sigma_z\rangle &= -2\gamma_\perp - 2\gamma_\perp\langle\sigma_z\rangle - 2g\langle x\rangle\langle\sigma_x\rangle + 2g\langle y\rangle\langle\sigma_y\rangle \end{aligned} \tag{3.2}$$

Following the common practice in control theory I linearize the dynamical equations for the "plant" and the "controller" to form a state space model, the canonical form of which is [19]

$$\begin{aligned} \frac{d}{dt}\vec{x} &= A\vec{x} + B\vec{u} \\ \vec{y} &= C\vec{x} + D\vec{u} \end{aligned} \tag{3.3}$$

where $\vec{x}(t)$ is the vector representing the system state at time t and $\vec{u}(t)$, $\vec{y}(t)$ are the input and output vectors respectively. Once I have the state space representation of our feedback system, I can then evaluate its transfer function which is defined as the ratio of the Laplace transformed output and input [19]

$$G(s) = \frac{\mathcal{L}[\vec{y}(t)]}{\mathcal{L}[\vec{u}(t)]} = \frac{\vec{Y}(s)}{\vec{U}(s)} = C(sI - A)^{-1}B + D \tag{3.4}$$

The poles of the transfer function are the solutions to the equation $\det(sI - A) = 0$ i.e. the eigenvalues of the matrix A in the state space model, which determine the stability of the feedback system. If all the poles have negative real parts then the system is stable otherwise it is unstable [19]. The reason is that these eigenvalues would appear, after inverse Laplace transform, in the exponents of the exponential terms of the output (e.g. $e^{p_i t}$) thus if any one of them has a positive real part then the corresponding exponential term would go to infinity and hence the output would be unbounded.

Using the notation $\delta\langle O\rangle = \langle O\rangle - \overline{\langle O\rangle}$ to denote small deviation from $\overline{\langle O\rangle}$, the stationary solution to the operator expectation equation of O, the state space representation of the "plant" is

$$\begin{aligned}
\frac{d}{dt}\begin{pmatrix} \delta\langle x\rangle \\ \delta\langle y\rangle \end{pmatrix} &= \begin{pmatrix} -\kappa & +\Delta_c \\ -\Delta_c & -\kappa \end{pmatrix}\begin{pmatrix} \delta\langle x\rangle \\ \delta\langle y\rangle \end{pmatrix} + \begin{pmatrix} +g/2 & 0 \\ 0 & -g/2 \end{pmatrix}\begin{pmatrix} \delta\langle \sigma_x\rangle \\ \delta\langle \sigma_y\rangle \end{pmatrix} \\
\begin{pmatrix} \delta\langle x\rangle \\ \delta\langle y\rangle \end{pmatrix} &= \begin{pmatrix} 1 & 0 \\ 0 & 1 \end{pmatrix}\begin{pmatrix} \delta\langle x\rangle \\ \delta\langle y\rangle \end{pmatrix} + \begin{pmatrix} 0 & 0 \\ 0 & 0 \end{pmatrix}\begin{pmatrix} \delta\langle \sigma_x\rangle \\ \delta\langle \sigma_y\rangle \end{pmatrix}
\end{aligned} \tag{3.5}$$

and the state space representation of the "controller" is

$$\begin{aligned}
\frac{d}{dt}\begin{pmatrix} \delta\langle \sigma_x\rangle \\ \delta\langle \sigma_y\rangle \\ \delta\langle \sigma_z\rangle \end{pmatrix} &= \begin{pmatrix} -\gamma_\perp & -\Delta_a & +2g\overline{\langle x\rangle} \\ +\Delta_a & -\gamma_\perp & -2g\overline{\langle y\rangle} \\ -2g\overline{\langle x\rangle} & +2g\overline{\langle y\rangle} & -2\gamma_\perp \end{pmatrix}\begin{pmatrix} \delta\langle \sigma_x\rangle \\ \delta\langle \sigma_y\rangle \\ \delta\langle \sigma_z\rangle \end{pmatrix} + \begin{pmatrix} +2g\overline{\langle \sigma_z\rangle} & 0 \\ 0 & -2g\overline{\langle \sigma_z\rangle} \\ -2g\overline{\langle \sigma_x\rangle} & +2g\overline{\langle \sigma_y\rangle} \end{pmatrix}\begin{pmatrix} \delta\langle x\rangle \\ \delta\langle y\rangle \end{pmatrix} \\
\begin{pmatrix} \delta\langle \sigma_x\rangle \\ \delta\langle \sigma_y\rangle \end{pmatrix} &= \begin{pmatrix} 1 & 0 & 0 \\ 0 & 1 & 0 \end{pmatrix}\begin{pmatrix} \delta\langle \sigma_x\rangle \\ \delta\langle \sigma_y\rangle \\ \delta\langle \sigma_z\rangle \end{pmatrix} + \begin{pmatrix} 0 & 0 \\ 0 & 0 \end{pmatrix}\begin{pmatrix} \delta\langle x\rangle \\ \delta\langle y\rangle \end{pmatrix}
\end{aligned} \tag{3.6}$$

One now can draw for our feedback system a block diagram—the graphical representation commonly used in control theory to emphasize the information/signal flow [19] which is depicted in Fig.3.2 below. The diagram is simple yet informative

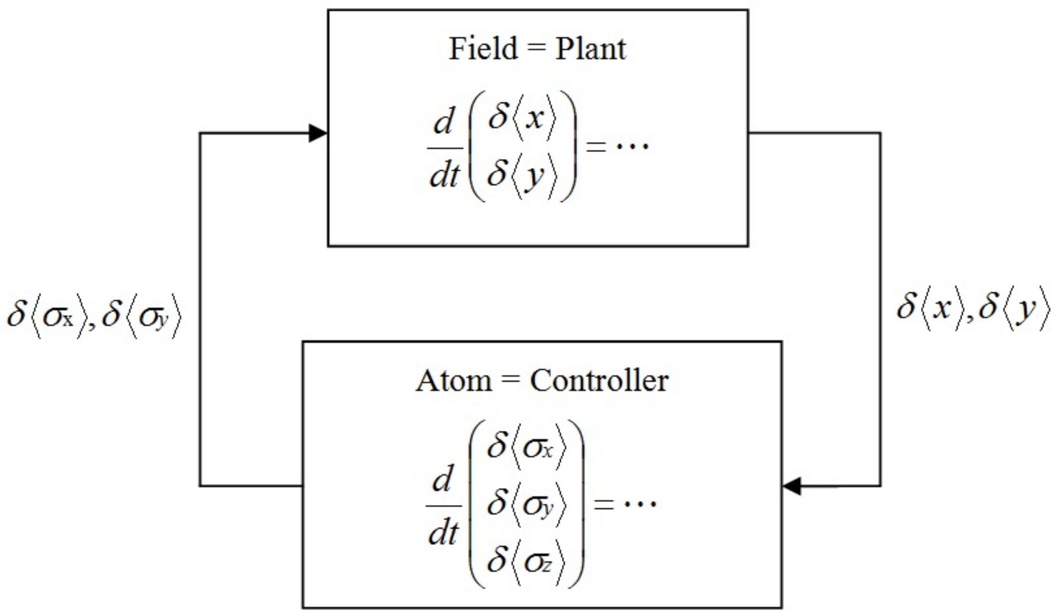

Figure 3.2: Block diagram for the linearized Maxwell-Bloch equations as the dynamical equations for a feedback control system

but to decipher the mechanism I need to look into the details that are omitted. In particular, although the block diagram seems to suggest one single feedback loop, rewriting the differential equations for the "controller" as follows

$$
\begin{aligned}
\frac{d}{dt}\begin{pmatrix}\delta\langle\sigma_x\rangle\\ \delta\langle\sigma_y\rangle\\ \delta\langle\sigma_z\rangle\end{pmatrix} &= \begin{pmatrix}-\gamma_\perp & -\Delta & +2g\overline{\langle x\rangle}\\ +\Delta & -\gamma_\perp & -2g\overline{\langle y\rangle}\\ -2g\overline{\langle x\rangle} & +2g\overline{\langle y\rangle} & -2\gamma_\perp\end{pmatrix}\begin{pmatrix}\delta\langle\sigma_x\rangle\\ \delta\langle\sigma_y\rangle\\ \delta\langle\sigma_z\rangle\end{pmatrix}\\
&+\underbrace{\begin{pmatrix}+2g\overline{\langle\sigma_z\rangle} & 0\\ 0 & -2g\overline{\langle\sigma_z\rangle}\\ 0 & 0\end{pmatrix}\begin{pmatrix}\delta\langle x\rangle\\ \delta\langle y\rangle\end{pmatrix}}_{\text{direct coupling}}+\underbrace{\begin{pmatrix}0 & 0\\ 0 & 0\\ -2g\overline{\langle\sigma_x\rangle} & +2g\overline{\langle\sigma_y\rangle}\end{pmatrix}\begin{pmatrix}\delta\langle x\rangle\\ \delta\langle y\rangle\end{pmatrix}}_{\text{indirect coupling}}
\end{aligned}
\tag{3.7}
$$

one can see that there actually exist two feedback loops, one that involves $\delta\langle\sigma_z\rangle$: $\delta\langle x\rangle, \delta\langle y\rangle \rightarrow \delta\langle\sigma_z\rangle \rightarrow \delta\langle\sigma_x\rangle, \delta\langle\sigma_y\rangle \rightarrow \delta\langle x\rangle, \delta\langle y\rangle$ and one that does not: $\delta\langle x\rangle, \delta\langle y\rangle \rightarrow \delta\langle\sigma_x\rangle, \delta\langle\sigma_y\rangle \rightarrow \delta\langle x\rangle, \delta\langle y\rangle$. For obvious reason one can call the former the indirect feedback loop and the latter the direct feedback loop. But what does this existence of two feedback loops have to do with the oscillation?

It is well-known in control theory that if the open loop phase lag of a closed loop system exceeds 180° or π radian before the open loop gain dropping below unity then a signal would be amplified even without sustained input, or equivalently the system output in response to an impulse would be unbounded. This is illustrated in Fig. 3.3 below where the signal is modeled as a unity-amplitude sine function $\sin(\omega_\phi t)$. In reality this signal can be supplied by any noise and it would grow in amplitude until it exhausts the energy supply and settles down into a stable oscillation. Thus oscillation is the consequence of a closed loop system going unstable due to excessive phase lag. With this in mind to explain the cavity field intensity self-oscillation one just needs to find out the source of phase lag in our feedback system and it turns out to be the indirect feedback loop.

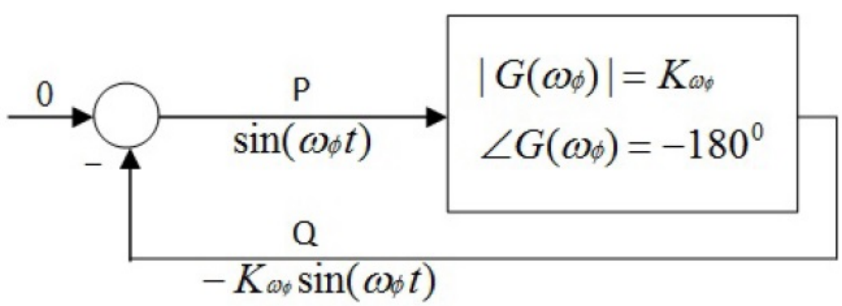

	1st round	2nd round	3rd round	$\cdots$	nth round
at P	$\sin(\omega_\phi t)$	$K_{\omega_\phi} \sin(\omega_\phi t)$	$K^2_{\omega_\phi} \sin(\omega_\phi t)$	$\cdots$	$K^n_{\omega_\phi} \sin(\omega_\phi t)$
at Q	$-K_{\omega_\phi} \sin(\omega_\phi t)$	$-K^2_{\omega_\phi} \sin(\omega_\phi t)$	$-K^3_{\omega_\phi} \sin(\omega_\phi t)$	$\cdots$	$-K^n_{\omega_\phi} \sin(\omega_\phi t)$

$K_{\omega_\phi} < 1$ at $\omega_\phi \Rightarrow$ loop is stable $\quad K_{\omega_\phi} > 1$ at $\omega_\phi \Rightarrow$ loop is unstable

Figure 3.3: Illustration of excessive phase lag leading to self-oscillation

However it is not convincing to conclude just based on the involvement of one extra variable that the indirect feedback loop would introduce excessive phase lag which is responsible for the oscillation. To understand why and how much lag there is associated with the indirect feedback loop one needs to take a close look at the coupling from $\delta\langle\sigma_z\rangle$ to $\delta\langle\sigma_x\rangle, \delta\langle\sigma_y\rangle$. To this end I decompose the matrix A in the state space model of the "controller" into the sum of a diagonal matrix representing decay due to dephasing and spontaneous emission and a skew-symmetric matrix which can be interpreted as the infinitesimal generator of a rotation

$$\frac{d}{dt}\begin{pmatrix}\delta\langle\sigma_x\rangle\\ \delta\langle\sigma_y\rangle\\ \delta\langle\sigma_z\rangle\end{pmatrix} = \underbrace{\begin{pmatrix}-\gamma_\perp & 0 & 0\\ 0 & -\gamma_\perp & 0\\ 0 & 0 & -2\gamma_\perp\end{pmatrix}\begin{pmatrix}\delta\langle\sigma_x\rangle\\ \delta\langle\sigma_y\rangle\\ \delta\langle\sigma_z\rangle\end{pmatrix}}_{\text{decay}}$$
$$+\underbrace{\begin{pmatrix}0 & -\Delta_a & +2g\overline{\langle x\rangle}\\ +\Delta_a & 0 & -2g\overline{\langle y\rangle}\\ -2g\overline{\langle x\rangle} & +2g\overline{\langle y\rangle} & 0\end{pmatrix}\begin{pmatrix}\delta\langle\sigma_x\rangle\\ \delta\langle\sigma_y\rangle\\ \delta\langle\sigma_z\rangle\end{pmatrix}}_{\text{rotation}} + \begin{pmatrix}+2g\overline{\langle\sigma_z\rangle} & 0\\ 0 & -2g\overline{\langle\sigma_z\rangle}\\ -2g\overline{\langle\sigma_x\rangle} & +2g\overline{\langle\sigma_y\rangle}\end{pmatrix}\begin{pmatrix}\delta\langle x\rangle\\ \delta\langle y\rangle\end{pmatrix} \tag{3.8}$$

The rotation turns out to be the precession of the change in the atomic spin driven by the cavity field plus the mixing between $\delta\langle\sigma_x\rangle$ and $\delta\langle\sigma_y\rangle$ due to the atomic detuning because one can write

$$\begin{aligned}&\begin{pmatrix}0 & -\Delta_a & +2g\overline{\langle x\rangle}\\ +\Delta_a & 0 & -2g\overline{\langle y\rangle}\\ -2g\overline{\langle x\rangle} & +2g\overline{\langle y\rangle} & 0\end{pmatrix}\begin{pmatrix}\delta\langle\sigma_x\rangle\\ \delta\langle\sigma_y\rangle\\ \delta\langle\sigma_z\rangle\end{pmatrix}\\ &= +2g\begin{pmatrix}\delta\langle\sigma_x\rangle\\ \delta\langle\sigma_y\rangle\\ \delta\langle\sigma_z\rangle\end{pmatrix}\times\begin{pmatrix}-\overline{\langle y\rangle}\\ -\overline{\langle x\rangle}\\ 0\end{pmatrix} + \begin{pmatrix}\delta\langle\sigma_x\rangle\\ \delta\langle\sigma_y\rangle\\ \delta\langle\sigma_z\rangle\end{pmatrix}\times\begin{pmatrix}0\\ 0\\ -\Delta_a\end{pmatrix}\end{aligned} \tag{3.9}$$

This atomic spin precession differs from the Larmor precession of magnetic moments in an magnetic field by the fact that the field playing the role of magnetic field in the Larmor precession as "felt" by the atom is in fact $\pi/2$ lagging behind the cavity field[1]. Therefore the rotation between $\delta\langle\sigma_x\rangle$ and $\delta\langle\sigma_z\rangle$ is induced by $\overline{\langle x\rangle}$ rather than $\overline{\langle y\rangle}$. Fig. 3.4 below helps to visualize the precession.

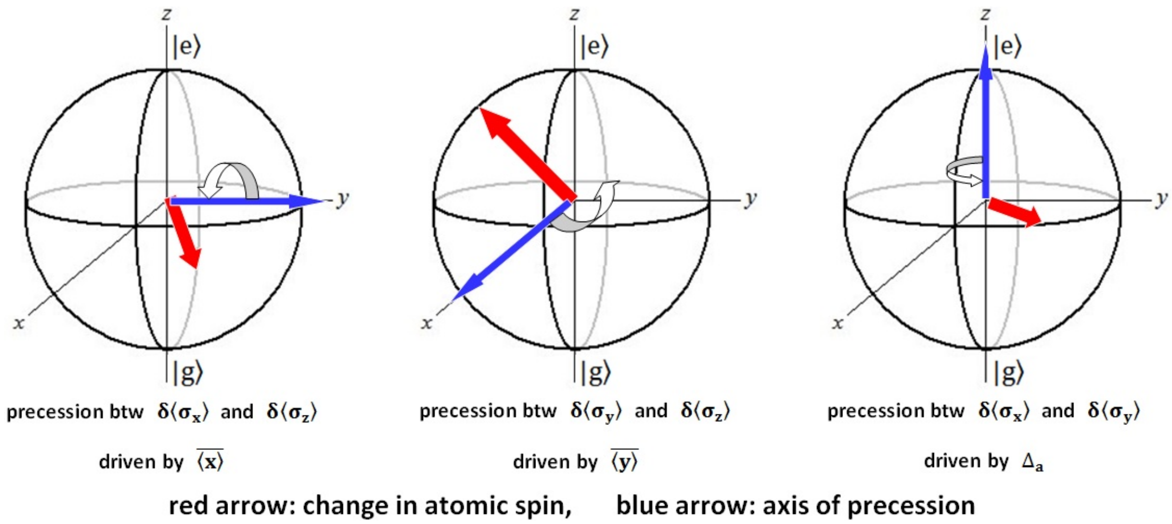

Figure 3.4: Illustration of the precession of the change in the atomic spin driven by the cavity field and the atomic detuning (red arrow: the atomic spin, blue arrow: the axis of rotation)

Now it should be clear why the indirect feedback loop can introduce excessive phase lag that gives rise to self-oscillation of the cavity field intensity. It is because the amplitude of the cavity field thus the speed of precession is finite hence it takes time for $\delta\langle\sigma_z\rangle$ to rotate into xy-plane to contribute to $\delta\langle\sigma_x\rangle$ and $\delta\langle\sigma_y\rangle$. Moreover one can imagine that as the cavity field becomes stronger the speed of rotation would become larger therefore the phase lag would be reduced thus the oscillation would eventually disappear if one continues increasing the external driving thus the cavity field intensity. Here one witnesses again the effectiveness of the spin precession picture as demonstrated in the previous chapter.

To demonstrate the validity of this oscillation mechanism hypothesis, the onset of instability of the above state space models determined by MATLAB control toolbox is compared with the onset of oscillation of the cavity field intensity identified by

[1] To see this one needs to use the imaginary part of the creation operator rather than that of the annihilation operator. This however does not affect the explanation or the overall picture.

numerically solving the Maxwell-Bloch equations. The system parameter set used is that of Armen and Mabuchi's Fig.4 [3] namely $\Delta_a = +1.25, \Delta_c = -6, g = 1, \kappa = 0.01, \gamma = 1$ and the external driving level $\mathcal{E}$ rescaled to a dimensionless parameter $y = \frac{\sqrt{2}g}{\kappa\gamma_\perp}\mathcal{E}$. The stabilities of the direct loop (discarding the indirect coupling term in equation (3.7)), the indirect loop (discarding the direct coupling term in equation (3.7)) and the combined feedback loop for various driving levels are determined using MATLAB's "*isstable*" function, which returns a Boolean value of 1 (true) if all system poles are in the open left-half complex plane and 0 (false) otherwise, and are plotted in Fig. 3.5 below. As can be seen from the plots, the direct loop is stable throughout the

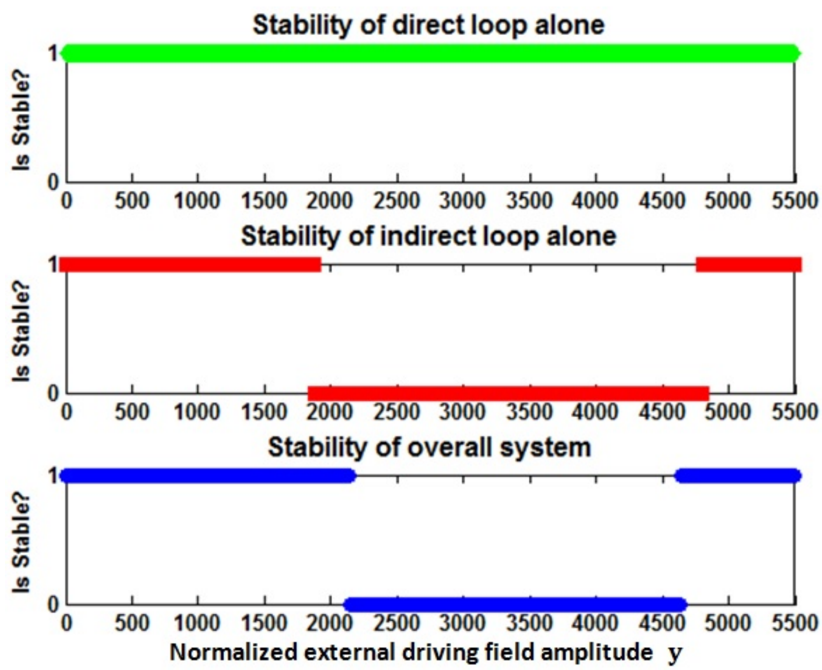

Figure 3.5: Stabilities of the feedback loops (top = direct loop, middle = indirect loop, bottom = combined loop) as functions of the external driving amplitude (rescaled to y values)

external driving amplitude sweeping range whereas the indirect loop goes unstable at as low as $y = 1871.90$ resulting in the combined loop going unstable at $y = 2140.22$. At high driving levels the excessive phase lag is reduced thus the combined loop becomes stable again at $y = 4631.95$ followed by the indirect loop becoming stable again at $y = 4799.57$. The instability range agrees very well with the oscillation range depicted in Armen and Mabuchi's Fig.4.

3.3 Small Signal Amplification near Super-critical Hopf Bifurcation

After understanding the origin of instability in the semi-classical Maxwell-Bloch equations one can then turn to confirming the small signal amplification based on the system's sensitivity to the instability proposed by Wiesenfeld and McNamara [14]. To numerically model the small signal input let the external driving field be consisting of two components: $\mathcal{E} = \mathcal{E}_0 + \mathcal{S}e^{-i\omega_s t}$ where $\mathcal{E}_0$ is the pumping field with frequency ω_l and $\mathcal{S}e^{-i\omega_s t}$ is the small signal with frequency $\omega_s + \omega_l$ (the frequency relative to the rotating frame is thus ω_s). The time origin is chosen such that $\mathcal{E}_0$ is a real number and since I am only interested in steady state solutions the initial phase of the signal would not matter one can choose it to be zero for convenience i.e. $\mathcal{S}$ is a real number too. I then numerically solved the semi-classical Maxwell-Bloch equations using MATLAB's ODE solver and quantified the output signal strength by comparing the oscillation amplitude of $|\langle a\rangle|$ with $\mathcal{S}$. Assuming one-ended cavity configuration i.e. the cavity has one fully reflected and one partially reflected end mirror the boundary condition at the partially reflected mirror is $\langle a_{IN}(\omega_s)\rangle + \langle a_{OUT}(\omega_s)\rangle = \sqrt{2\kappa}\langle a(\omega_s)\rangle$ where $\langle a_{IN}(\omega_s)\rangle$ is equal to $\mathcal{S}/\sqrt{2\kappa}$ thus the output signal is given by the oscillatory component of $\langle a\rangle$ transmitted through the mirror minus the input signal. If $\sqrt{2\kappa}|\langle a(\omega_s)\rangle| \gg |\langle a_{IN}(\omega_s)\rangle|$ then the amplitude gain $|\langle a_{OUT}(\omega_s)\rangle/\langle a_{IN}(\omega_s)\rangle|$ is approximately $\sqrt{2\kappa}|\langle a(\omega_s)\rangle|/|\langle a_{IN}(\omega_s)\rangle| - 1$. The parameter set used is again that of Armen and Mabuchi's Fig.4 [3] namely $\Delta_a = +1.25, \Delta_c = -6, g = 1, \kappa = 0.01, \gamma = 1$ for which supercritical Hopf bifurcation occurs at $\mathcal{E}_0$ rising beyond 15.13364. Four pumping levels were selected to investigate the effect of the distance to the bifurcation on the amplification and for each pumping level the relative frequency ω_s of the small signal was swept to trace out the spectrum of $|\langle a(\omega_s)\rangle|$ and identify the frequency that maximizes $|\langle a(\omega_s)\rangle|$ and hence the amplitude gain. Three small signal amplitudes were tested: $\mathcal{S} = 7.07107 \times 10^{-5}$, $\mathcal{S} = 7.07107 \times 10^{-4}$ and $\mathcal{S} = 7.07107 \times 10^{-3}$

the $\sqrt{2\kappa}|\langle a\rangle|$ spectra of which are plotted in Fig. 3.6, Fig. 3.7 and Fig. 3.8 respectively below.

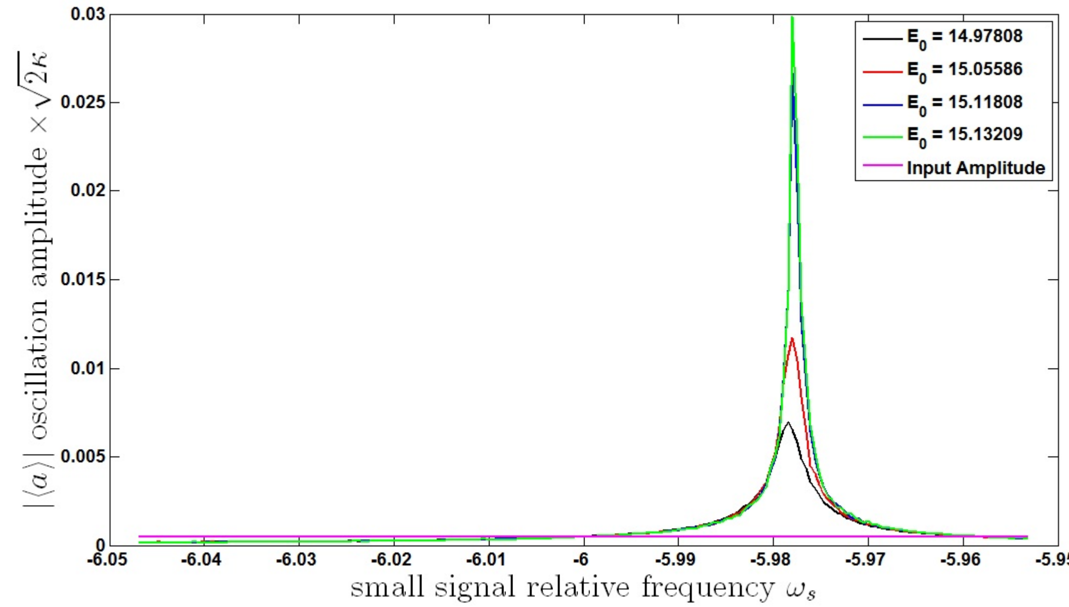

Figure 3.6: Oscillation amplitude of $\sqrt{2\kappa}|\langle a\rangle|$ vs. small signal relative frequency for an signal amplitude of $\mathcal{S} = 7.071 \times 10^{-5}$ by numerically solving the semi-classical Maxwell-Bloch equations

All three plots show clearly that the peak oscillation amplitudes of $\sqrt{2\kappa}|\langle a\rangle|$ are much greater than the input amplitudes, the highest ratio exceeding 30, which evidently demonstrate the existence of amplification. Moreover, all three plots show clearly that the closer $\mathcal{E}_0$ is to the critical pumping level 15.13364 the higher the amplitude ratio thus the amplitude gain, in accordance with Wiesenfeld and McNamara's theory [14]. In addition, the oscillation amplitude of $|\langle a\rangle|$ peaks at $-5.97 \sim -5.99$ which is in good agreement with the intrinsic frequency (about -5.978) calculated using the analytical method in Armen and Mabuchi's paper [3]. The three plots also show some differences that are characteristics of nonlinear amplification. First, as the signal amplitude is increased the frequency at which the oscillation amplitude peaks shifts slightly towards the cavity resonance frequency, from -5.978 for $\mathcal{S} = 7.07107 \times 10^{-5}$ to -5.993 for $\mathcal{S} = 7.07107 \times 10^{-3}$. Second, as the signal amplitude is increased the amplification bandwidth becomes broader but the maximum

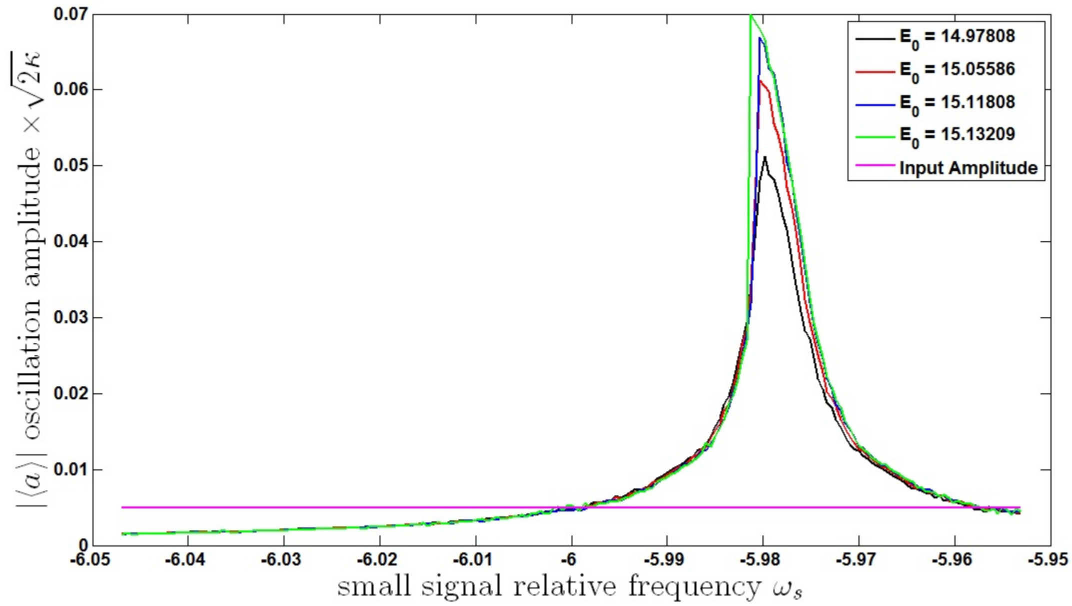

Figure 3.7: Oscillation amplitude of $\sqrt{2\kappa}|\langle a\rangle|$ vs. small signal relative frequency for an signal amplitude of $\mathcal{S} = 7.071 \times 10^{-4}$ by numerically solving the semi-classical Maxwell-Bloch equations

amplification drops, a clear sign of saturation; for $\mathcal{S} = 7.07107 \times 10^{-3}$ the maximum oscillation amplitude of $\sqrt{2\kappa}|\langle a\rangle|$ is limited to around 0.15, showing little difference between the four different pumping levels.

An added advantage of this bifurcation-based amplification is that the phase relation between the input and the output is fixed thus the phase information of the signal is preserved. Therefore it provides a promising physical basis for designing all-optical amplifiers for optical information processing networks.

3.4 Quantum-Classical Discrepancy

To investigate whether the small signal amplification carries over to the quantum regime I numerically solved the quantum master equation using the quantum optics toolbox written by Sze [8]. I recorded the density matrices of the system for a series of time moments which were then used to evaluate the expectation of the annihilation operator $\langle a(t)\rangle = \mathrm{Tr}[a\rho_t]$. The oscillation amplitude of its absolute value was then

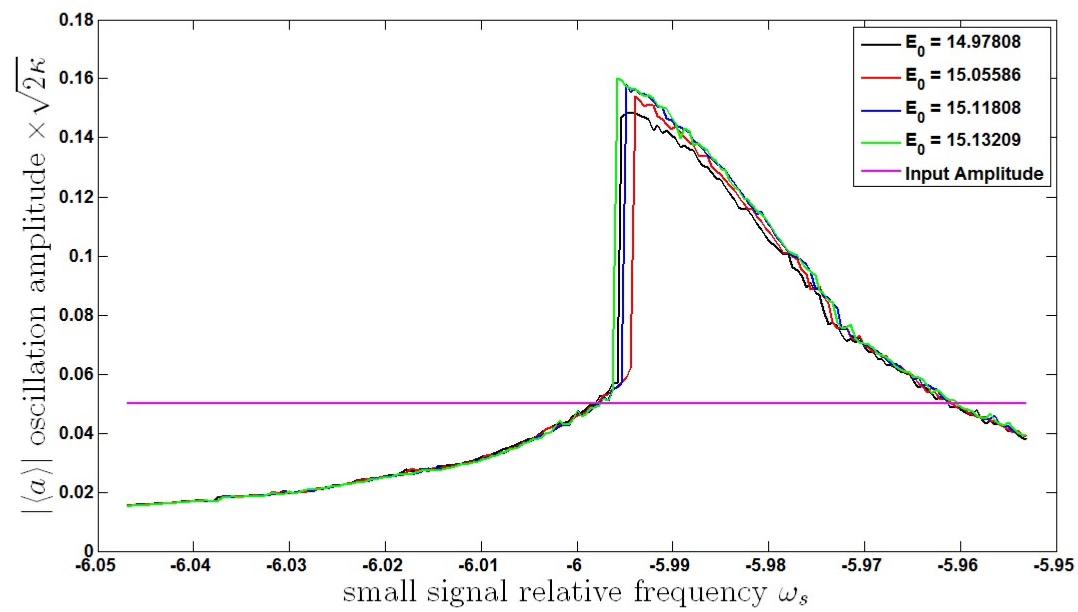

Figure 3.8: Oscillation amplitude of $\sqrt{2\kappa}|\langle a\rangle|$ vs. small signal relative frequency for an signal amplitude of $\mathcal{S} = 7.071 \times 10^{-3}$ by numerically solving the semi-classical Maxwell-Bloch equations

compared with that of the small signal input just as what has been done for the semi-classical Maxwell-Bloch equations. For comparison with the semi-classical result I used the same parameter set, the same signal amplitudes, and one of the four pumping levels $\mathcal{E}_0 = 15.11808$. The oscillation amplitude of $\sqrt{2\kappa}|\langle a\rangle|$ as a function of the small signal relative frequency ω_s for the three signal amplitudes are plotted in Fig. 3.9, Fig. 3.10 and Fig. 3.11 respectively below.

In contrast with the semi-classical case, the master equation yields an oscillation amplitude of $|\langle a\rangle|$ comparable to that of the small signal after taking into account the mirror coupling factor $\sqrt{2\kappa}$. In this case to compute the amplitude gain one needs to determine the relative phase of $\langle a(\omega_s)\rangle$ w.r.t. $\langle a_{IN}(\omega_s)\rangle$, which can be obtained by numerically fitting the time series of $\langle a(t)\rangle$ to a time-varying complex function $\mathcal{A}e^{-i(\omega_s t+\theta)}$, and then solving the boundary condition $\langle a_{IN}(\omega_s)\rangle + \langle a_{OUT}(\omega_s)\rangle = \sqrt{2\kappa}\langle a(\omega_s)\rangle$ exactly. The computed amplitude gain $|\langle a_{OUT}(\omega_s)\rangle/\langle a_{IN}(\omega_s)\rangle|$ as a function of the small signal relative frequency ω_s for the three signal amplitudes are plotted in Fig. 3.12 below.

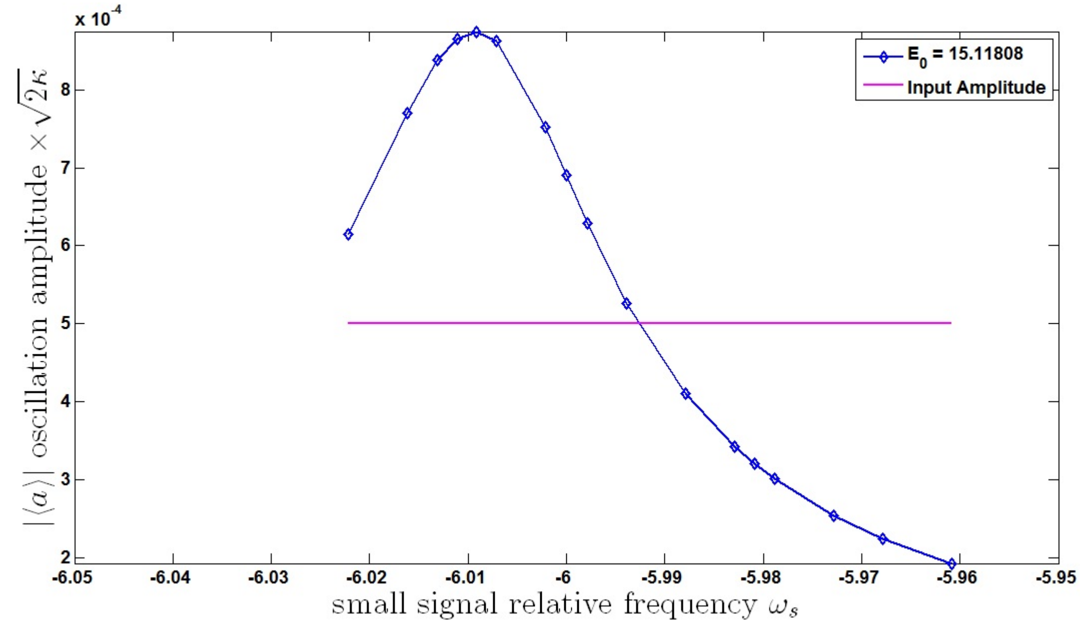

Figure 3.9: Oscillation amplitude of $\sqrt{2\kappa}|\langle a \rangle|$ vs. small signal relative frequency for an signal amplitude of $\mathcal{S} = 7.071 \times 10^{-5}$ by numerically solving the master equation

The plot indicates two differences from the semi-classical result. First, the amplitude gains are significantly smaller than those of the semi-classical cases, in fact there is virtually no gain because the maximum amplitude gain is only about 3%. Second, the amplitude gains at different signal amplitudes are almost identical for a given signal frequency, even though the oscillation amplitude of the intracavity photon number can be as high as 32% of its average indicating that the signal is no longer "small"; this implies a linear input-output relation for a fixed signal frequency which is in sharp contrast with the nonlinear characteristics of the amplification in the semi-classical case. These observations suggest that the gain available for signal amplification appears to be very scarce. This could be due to the fact that the quantitative agreement between the approximate semi-classical model and the exact quantum model is not as good as I initially thought, in the sense that the quantum analog of bifurcation requires a pumping level much higher than the semi-classical critical pumping level. Thus the chosen pumping level $\mathcal{E}_0 = 15.11808$, although being sufficient to supply substantial gain to the signal of the right frequency in the semi-classical case, is not

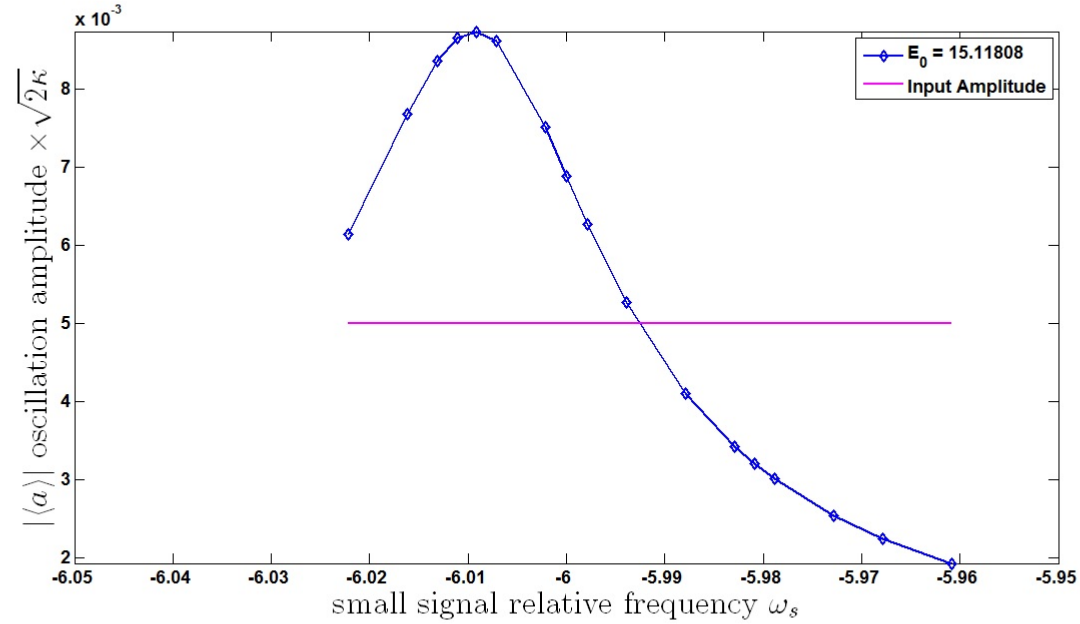

Figure 3.10: Oscillation amplitude of $\sqrt{2\kappa}|\langle a\rangle|$ vs. small signal relative frequency for an signal amplitude of $\mathcal{S} = 7.071 \times 10^{-4}$ by numerically solving the master equation

strong enough for the quantum case. I therefore increased the pumping level and tried various signal frequencies for the signal amplitude $S = 7.07107 \times 10^{-5}$ to look for significant gain. The computed amplitude gains are plotted in Fig. 3.13 below.

The plot seems to confirm what one would expect: the higher the pumping level the larger the amplitude gain. However the gains are still at most around 10%, much smaller than those of the semi-classical case. On the other hand, a quasi-probabilistic representation called Q-function of the partially traced field density matrix, which can be roughly interpreted as expanding the field density matrix over the coherent state basis $\{|\alpha\rangle\}$ because it is defined as $Q(\alpha) = \frac{1}{\pi}\langle\alpha|\rho|\alpha\rangle$ [20], is plotted in Fig. 3.14 below, which shows that for the highest pumping level used $\mathcal{E}_0 = 15.66242$ sign of oscillation is already present even without being periodically driven by the signal. This is manifested by the crater-like structure in the Q-function plot which can be formed by superposing coherent states rotating around a common center with uniformly distributed initial phases (the Q-function of a coherent state would be a bump due to its nonzero overlapping property $|\langle\alpha|\beta\rangle|^2 = \exp(-|\alpha - \beta|^2)$). This observation

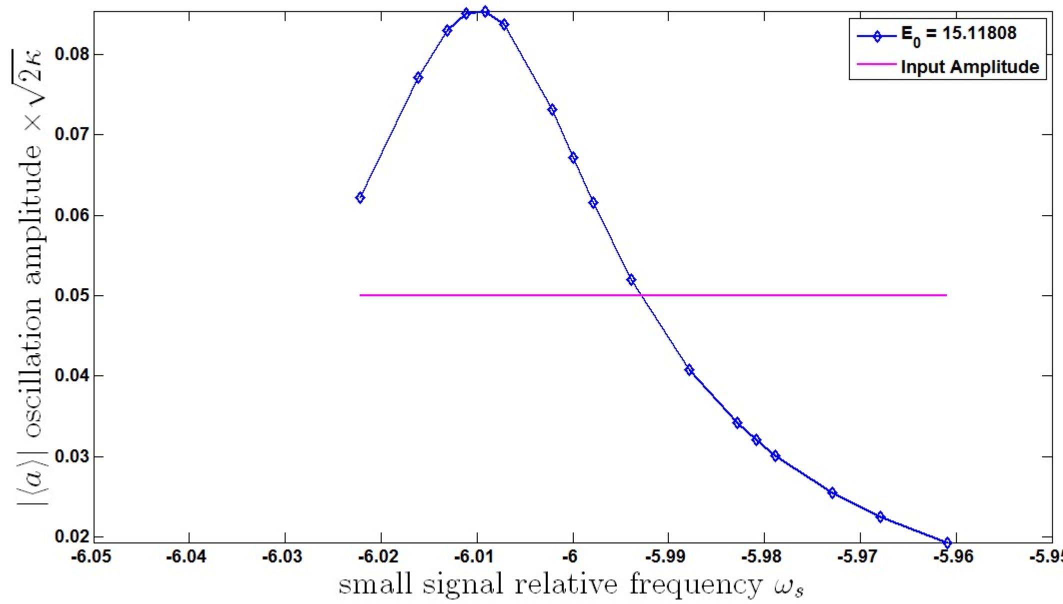

Figure 3.11: Oscillation amplitude of $\sqrt{2\kappa}|\langle a\rangle|$ vs. small signal relative frequency for an signal amplitude of $\mathcal{S} = 7.071 \times 10^{-3}$ by numerically solving the master equation

suggests that the observed increase in gain is probably not due to what I hoped for i.e. the sensitivity to loop instability.

It seems that instead of having used too low pumping levels I might have used too high pumping levels and the absence of significant gain could be due to the fact that I had passed the bifurcation and were already into the zone of self-oscillatory states i.e. the quantum critical pumping level might be even lower than $\mathcal{E}_0 = 15.11808$. A good guess for the quantum critical pumping level is $\mathcal{E}_0 = 7.07107$ because it is the pumping level at which the cavity field autocorrelation function starts oscillating as shown in Armen and Mabuchi's Fig.6 [3]. I therefore reduced the pumping level and tried various signal frequencies for the signal amplitude $S = 7.07107 \times 10^{-5}$ to look for significant increase in amplitude gain. The computed amplitude gains are plotted in Fig. 3.15 below.

We see in the plot that, at the lowest pumping level $\mathcal{E}_0 = 7.07107$ the amplitude gain is almost constant over the frequency range swept. This signifies that at this

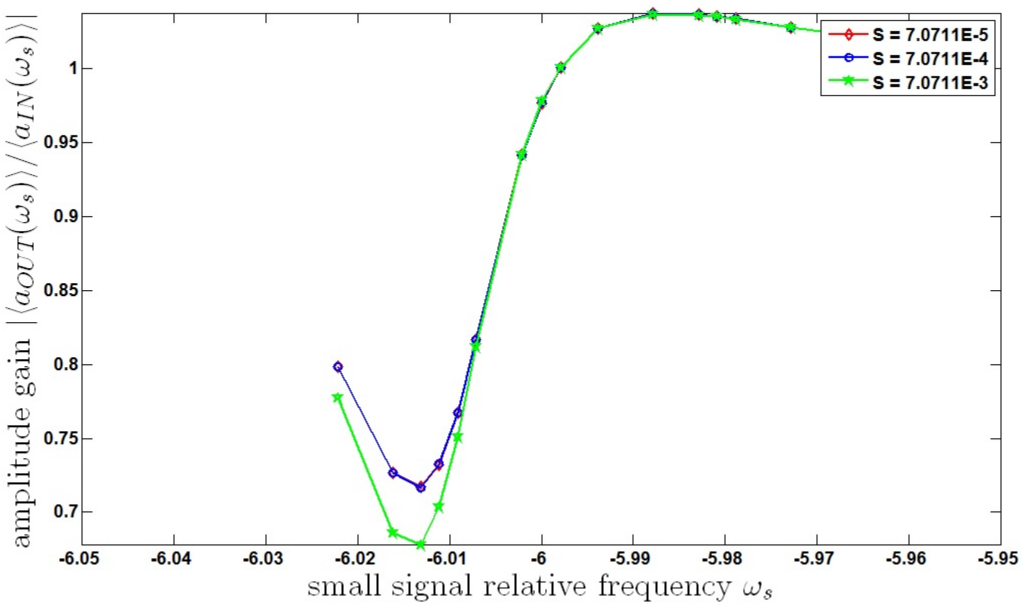

Figure 3.12: Amplitude gain $|\langle a_{OUT}(\omega_s)\rangle/\langle a_{IN}(\omega_s)\rangle|$ vs. small signal relative frequency for various signal amplitudes by numerically solving the master equation for a pumping level $\mathcal{E}_0 = 15.11808$

pumping level without signal input the cavity field contains almost no oscillatory component and the effect of the small signal driving is merely changing periodically the overall pumping strength and thus the observable expectations. The simulation result of the stochastic master equation with homodyne measurement on the observable $x = (a+a^\dagger)/2$ [10] plotted in Fig. 3.16 below supports this assertion, showing that the average oscillation amplitude of $|\langle a\rangle|$ is only about 2% of its mean value. Therefore if there were a quantum critical pumping level passing which would lead to abrupt change in amplitude gain it should lie between $\mathcal{E}_0 = 7.07107$ and $\mathcal{E}_0 = 15.66242$. Yet when the pumping level is varied in this range I do not see radical change in amplitude gain for the red-detuned range ($\omega_s > -6$). Note that the decline in amplitude gain in the blue-detuned range ($\omega_s < -6$), probably due to the burgeoning and growth of the oscillatory component, is rather gradual considering the amount of pumping level increment (from $\mathcal{E}_0 = 7.07107$ to $\mathcal{E}_0 = 10.6066$), unlike the semi-classical case in which the maximum amplitude gain skyrockets when the pumping level is increased from $\mathcal{E}_0 = 14.97808$ to $\mathcal{E}_0 = 15.13209$ (refer to Fig. 3.6). Furthermore, Fig. 3.17 below

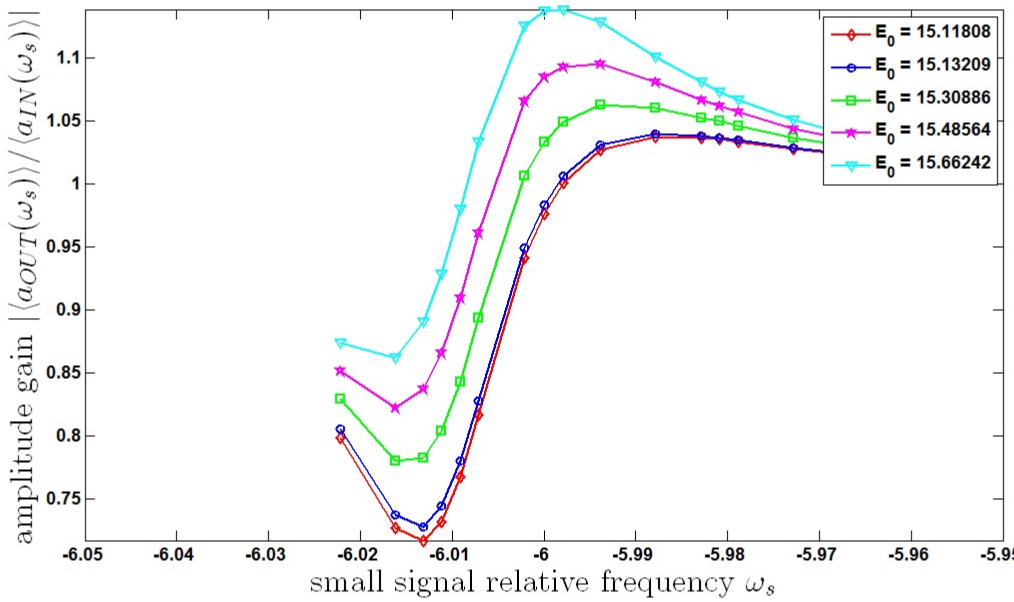

Figure 3.13: Amplitude gain $|\langle a_{OUT}(\omega_s)\rangle/\langle a_{IN}(\omega_s)\rangle|$ vs. small signal relative frequency for various pumping levels by numerically solving the master equation for an signal amplitude of $\mathcal{S} = 7.071 \times 10^{-5}$

shows that analogous to the amplitude gain spectrum at $\mathcal{E}_0 = 15.11808$ the amplitude loss/attenuation at $\mathcal{E}_0 = 10.6066$ also remains almost the same for a given signal frequency when the signal amplitude is increased by two orders of magnitude, even though the oscillation amplitude of the intracavity photon number can be as high as 25% of its average indicating that the signal is no longer "small". This again implies a linear input-output relation for a fixed signal frequency and contradicts with the nonlinear characteristics of the amplification in the semi-classical case.

3.5 Towards the Origin of the Quantum-Classical Discrepancy

To shed some light into the origin of the quantum-classical discrepancy, let's go one step from the most general quantum formulation by assuming a factorizable system density matrix $\rho = \rho_f \otimes \rho_a$ to see whether this intermediate case, on the one hand

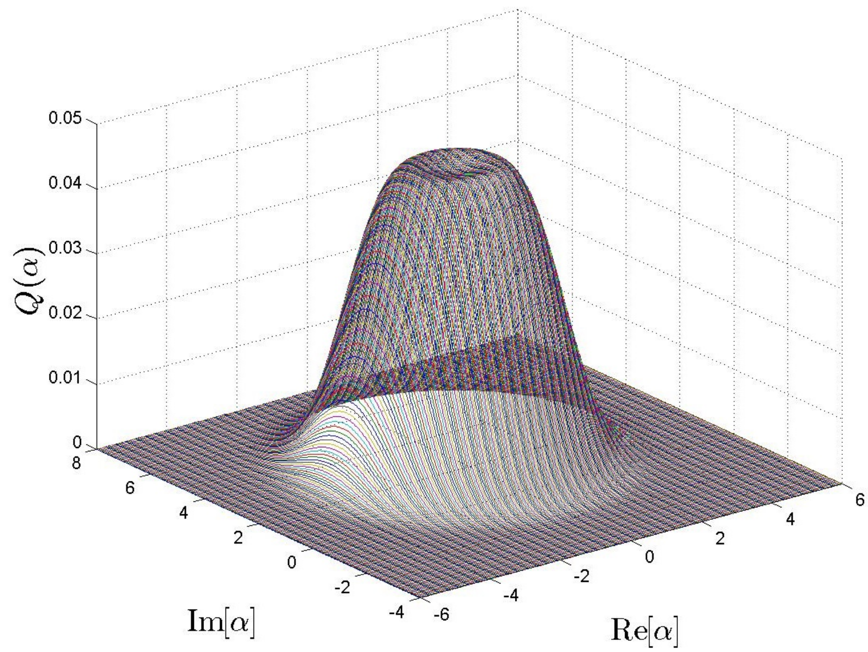

Figure 3.14: Q-function plot of the partially traced field density matrix of the solution to the master equation without signal input for a pumping level $\mathcal{E}_0 = 15.66242$

retaining the density matrix representation of the system state while on the other hand justifying the factorization of the expectations of operator products, would yield a result similar to that of the quantum master equation, or similar to that of the semi-classical Maxwell-Bloch equations, or distinct from both of the two limits. The master equation is reproduced below

$$\begin{aligned}\frac{d}{dt}\rho &= -i[H,\rho] + 2\kappa\left(a\rho a^\dagger - \frac{1}{2}a^\dagger a\rho - \frac{1}{2}\rho a^\dagger a\right) + 2\gamma_\perp\left(\sigma_-\rho\sigma_+ - \frac{1}{2}\sigma_+\sigma_-\rho - \frac{1}{2}\rho\sigma_+\sigma_-\right)\\ &= -iH\rho + i\rho H + 2\kappa\left(a\rho a^\dagger - \frac{1}{2}a^\dagger a\rho - \frac{1}{2}\rho a^\dagger a\right) + 2\gamma_\perp\left(\sigma_-\rho\sigma_+ - \frac{1}{2}\sigma_+\sigma_-\rho - \frac{1}{2}\rho\sigma_+\sigma_-\right)\end{aligned} \tag{3.10}$$

in which the Hamiltonian is

$$H = \Delta_c a^\dagger a + \Delta_a\sigma_+\sigma_- + ig(a^\dagger\sigma_- - a\sigma_+) + i(\mathcal{E}a^\dagger - \mathcal{E}^* a) \tag{3.11}$$

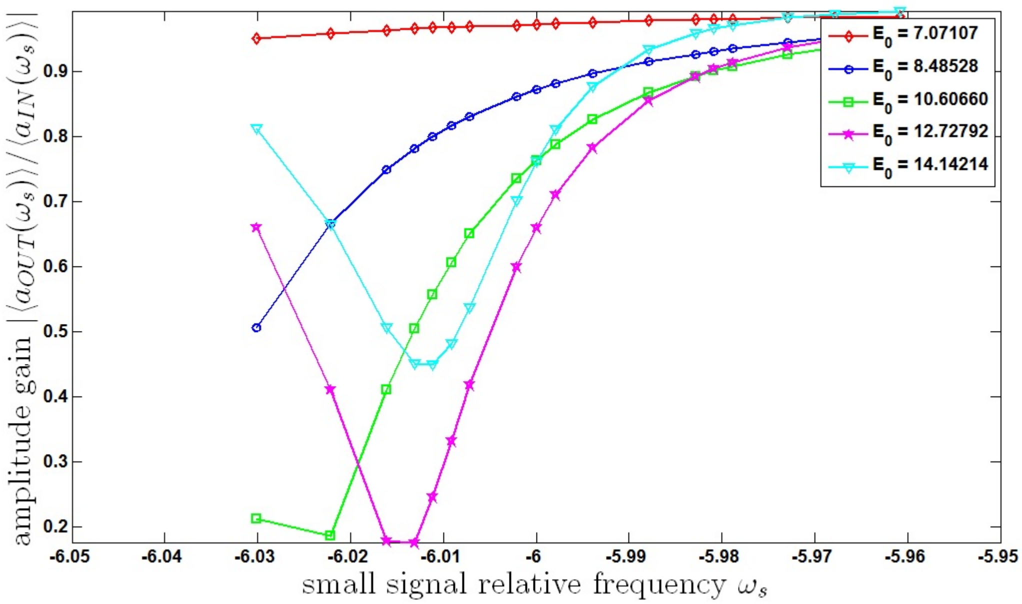

Figure 3.15: Amplitude gain $|\langle a_{OUT}(\omega_s)\rangle/\langle a_{IN}(\omega_s)\rangle|$ vs. small signal relative frequency for various pumping levels by numerically solving the master equation for an signal amplitude $\mathcal{S} = 7.071 \times 10^{-5}$

Substitute the factorizable template into the master equation I get

$$
\begin{aligned}
&\frac{d}{dt}\rho_f \otimes \rho_a = -i\Delta_c a^\dagger a \rho_f \otimes \rho_a - i\Delta_a \sigma_+\sigma_- \rho_f \otimes \rho_a + i\rho_f \otimes \rho_a \Delta_c a^\dagger a + i\rho_f \otimes \rho_a \Delta_a \sigma_+\sigma_- \\
&+ [g(a^\dagger \sigma_- - a\sigma_+) + (\mathcal{E}a^\dagger - \mathcal{E}^* a)]\rho_f \otimes \rho_a - \rho_f \otimes \rho_a [g(a^\dagger \sigma_- - a\sigma_+) + (\mathcal{E}a^\dagger - \mathcal{E}^* a)] \\
&+ 2\kappa \left(a(\rho_f \otimes \rho_a)a^\dagger - \frac{1}{2}a^\dagger a(\rho_f \otimes \rho_a) - \frac{1}{2}(\rho_f \otimes \rho_a)a^\dagger a \right) \\
&+ 2\gamma_\perp \left(\sigma_-(\rho_f \otimes \rho_a)\sigma_+ - \frac{1}{2}\sigma_+\sigma_-(\rho_f \otimes \rho_a) - \frac{1}{2}(\rho_f \otimes \rho_a)\sigma_+\sigma_- \right) \\
&= -i\Delta_c a^\dagger a \rho_f \otimes \rho_a - i\Delta_a \rho_f \otimes \sigma_+\sigma_- \rho_a + i\Delta_c \rho_f a^\dagger a \otimes \rho_a + i\Delta_a \rho_f \otimes \rho_a \sigma_+\sigma_- \\
&+ g(a^\dagger \rho_f \otimes \sigma_- \rho_a - a\rho_f \otimes \sigma_+ \rho_a) + (\mathcal{E}a^\dagger - \mathcal{E}^* a)\rho_f \otimes \rho_a \\
&- g(\rho_f a^\dagger \otimes \rho_a \sigma_- - \rho_f a \otimes \rho_a \sigma_+) - \rho_f(\mathcal{E}a^\dagger - \mathcal{E}^* a) \otimes \rho_a \\
&+ 2\kappa \left(a\rho_f a^\dagger \otimes \rho_a - \frac{1}{2}a^\dagger a \rho_f \otimes \rho_a - \frac{1}{2}\rho_f a^\dagger a \otimes \rho_a \right) \\
&+ 2\gamma_\perp \left(\rho_f \otimes \sigma_- \rho_a \sigma_+ - \frac{1}{2}\rho_f \otimes \sigma_+\sigma_- \rho_a - \frac{1}{2}\rho_f \otimes \rho_a \sigma_+\sigma_- \right)
\end{aligned}
\tag{3.12}
$$

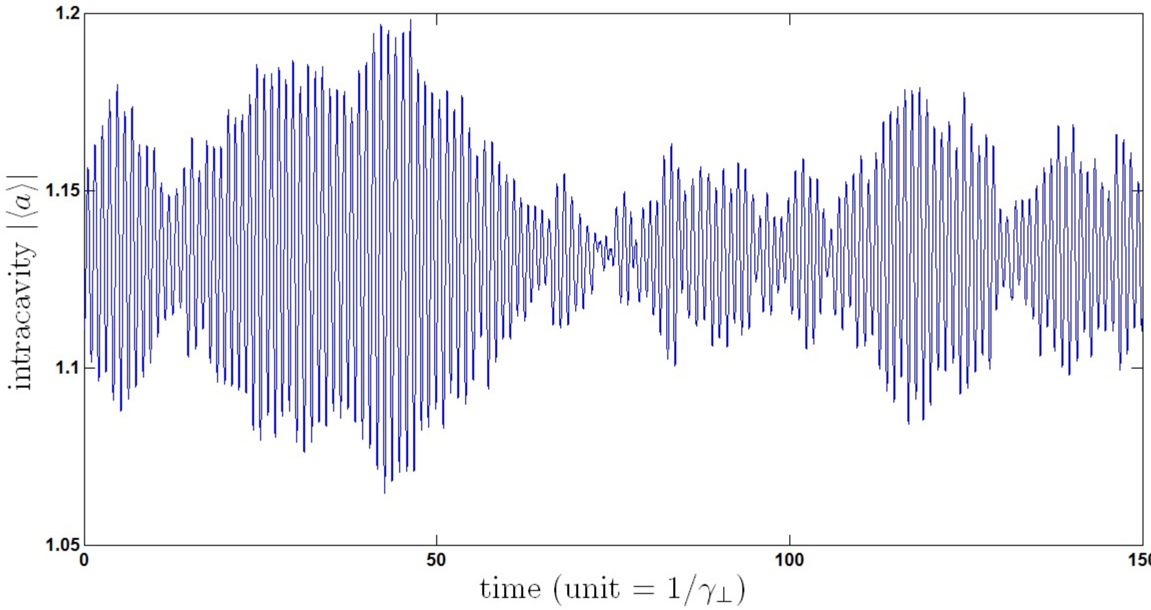

Figure 3.16: $|\langle a \rangle|$ yielded by the stochastic quantum master equation with homodyne measurement on the observable $x = (a + a^\dagger)/2$ and no signal input for a pumping level $\mathcal{E}_0 = 7.07107$

We now take the partial trace over the atomic degrees of freedom

$$
\begin{aligned}
&\mathrm{Tr}_a\left[\frac{d}{dt}\rho_f \otimes \rho_a\right] = \frac{d}{dt}\,\mathrm{Tr}_a\left[\rho_f \otimes \rho_a\right] = \frac{d}{dt}\rho_f \\
&= -i\Delta_c a^\dagger a \rho_f\,\mathrm{Tr}_a[\rho_a] - i\Delta_a \rho_f\,\mathrm{Tr}_a[\sigma_+\sigma_-\rho_a] + i\Delta_c \rho_f a^\dagger a\,\mathrm{Tr}_a[\rho_a] + i\Delta_a \rho_f\,\mathrm{Tr}_a[\rho_a\sigma_+\sigma_-] \\
&+ g(a^\dagger \rho_f\,\mathrm{Tr}_a[\sigma_-\rho_a] - a\rho_f\,\mathrm{Tr}_a[\sigma_+\rho_a]) + (\mathcal{E}a^\dagger - \mathcal{E}^* a)\rho_f\,\mathrm{Tr}_a[\rho_a] \\
&- g(\rho_f a^\dagger\,\mathrm{Tr}_a[\rho_a\sigma_-] - \rho_f a\,\mathrm{Tr}_a[\rho_a\sigma_+]) - \rho_f(\mathcal{E}a^\dagger - \mathcal{E}^* a)\,\mathrm{Tr}_a[\rho_a] \\
&+ 2\kappa\left(a\rho_f a^\dagger\,\mathrm{Tr}_a[\rho_a] - \frac{1}{2}a^\dagger a\rho_f\,\mathrm{Tr}_a[\rho_a] - \frac{1}{2}\rho_f a^\dagger a\,\mathrm{Tr}_a[\rho_a]\right) \\
&+ 2\gamma_\perp\left(\rho_f\,\mathrm{Tr}_a[\sigma_-\rho_a\sigma_+] - \frac{1}{2}\rho_f\,\mathrm{Tr}_a[\sigma_+\sigma_-\rho_a] - \frac{1}{2}\rho_f\,\mathrm{Tr}_a[\rho_a\sigma_+\sigma_-]\right) \\
&= -i\Delta_c a^\dagger a\rho_f + i\Delta_c\rho_f a^\dagger a - i\Delta_a\rho_f\,\mathrm{Tr}_a[\sigma_+\sigma_-\rho_a] + i\Delta_a\rho_f\,\mathrm{Tr}_a[\sigma_+\sigma_-\rho_a] - \rho_f(\mathcal{E}a^\dagger - \mathcal{E}^* a) \\
&+ g(a^\dagger\rho_f\,\mathrm{Tr}_a[\sigma_-\rho_a] - \rho_f a^\dagger\,\mathrm{Tr}_a[\sigma_-\rho_a] - a\rho_f\,\mathrm{Tr}_a[\sigma_+\rho_a] + \rho_f a\,\mathrm{Tr}_a[\sigma_+\rho_a]) + (\mathcal{E}a^\dagger - \mathcal{E}^* a)\rho_f \\
&+ 2\kappa\left(a\rho_f a^\dagger - \frac{1}{2}a^\dagger a\rho_f - \frac{1}{2}\rho_f a^\dagger a\right) + 2\gamma_\perp\left(\rho_f\,\mathrm{Tr}_a[\sigma_+\sigma_-\rho_a] - \frac{1}{2}\rho_f\,\mathrm{Tr}_a[\sigma_+\sigma_-\rho_a] - \frac{1}{2}\rho_f\,\mathrm{Tr}_a[\sigma_+\sigma_-\rho_a]\right) \\
&= -i[\Delta_c a^\dagger a, \rho_f] + g(\mathrm{Tr}_a[\sigma_-\rho_a][a^\dagger, \rho_f] - \mathrm{Tr}_a[\sigma_+\rho_a][a, \rho_f]) + [(\mathcal{E}a^\dagger - \mathcal{E}^* a), \rho_f] \\
&+ 2\kappa\left(a\rho_f a^\dagger - \frac{1}{2}a^\dagger a\rho_f - \frac{1}{2}\rho_f a^\dagger a\right)
\end{aligned}
\tag{3.13}
$$

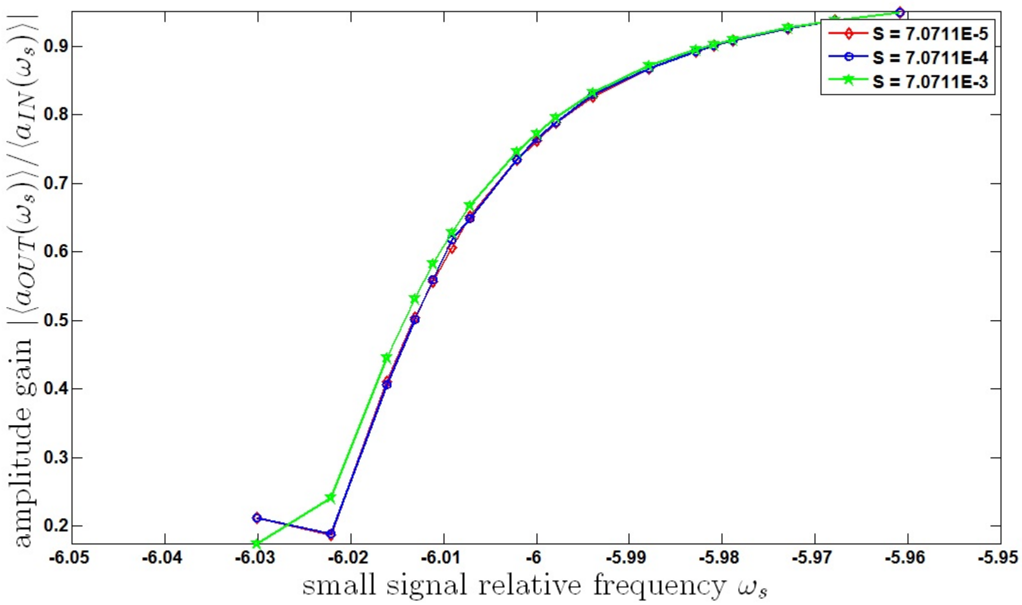

Figure 3.17: Amplitude gain $|\langle a_{OUT}(\omega_s)\rangle/\langle a_{IN}(\omega_s)\rangle|$ vs. small signal relative frequency for various signal amplitudes by numerically solving the master equation for a pumping level $\mathcal{E}_0 = 10.6066$

Since $\sigma_+ = (\sigma_x + i\sigma_y)/2$ and $\sigma_- = (\sigma_x - i\sigma_y)/2$ I have $\mathrm{Tr}_a[\sigma_+\rho_a] = \frac{1}{2}(\langle\sigma_x\rangle + i\langle\sigma_y\rangle)$ and $\mathrm{Tr}_a[\sigma_-\rho_a] = \frac{1}{2}(\langle\sigma_x\rangle - i\langle\sigma_y\rangle)$ the partially traced field master equation then reads

$$\begin{aligned}
&\mathrm{Tr}_a\left[\frac{d}{dt}\rho_f \otimes \rho_a\right] = \frac{d}{dt}\mathrm{Tr}_a\left[\rho_f \otimes \rho_a\right] = \frac{d}{dt}\rho_f \\
&= -i[\Delta_c a^\dagger a, \rho_f] + \frac{g}{2}(\langle\sigma_x\rangle[a^\dagger, \rho_f] - i\langle\sigma_y\rangle[a^\dagger, \rho_f] - \langle\sigma_x\rangle[a, \rho_f] - i\langle\sigma_y\rangle[a, \rho_f]) + [(\mathcal{E}a^\dagger - \mathcal{E}^* a), \rho_f] \\
&+ 2\kappa\left(a\rho_f a^\dagger - \frac{1}{2}a^\dagger a\rho_f - \frac{1}{2}\rho_f a^\dagger a\right) \\
&= -i[\Delta_c a^\dagger a, \rho_f] + \left[\frac{g}{2}\langle\sigma_x\rangle(a^\dagger - a) - \frac{g}{2}i\langle\sigma_y\rangle(a^\dagger + a), \rho_f\right] + [(\mathcal{E}a^\dagger - \mathcal{E}^* a), \rho_f] \\
&+ 2\kappa\left(a\rho_f a^\dagger - \frac{1}{2}a^\dagger a\rho_f - \frac{1}{2}\rho_f a^\dagger a\right) = -i[H_f, \rho_f] + 2\kappa\left(a\rho_f a^\dagger - \frac{1}{2}a^\dagger a\rho_f - \frac{1}{2}\rho_f a^\dagger a\right)
\end{aligned} \tag{3.14}$$

where

$$H_f = \Delta_c a^\dagger a + i\frac{g}{2}\langle\sigma_x\rangle(a^\dagger - a) + \frac{g}{2}\langle\sigma_y\rangle(a^\dagger + a) + i(\mathcal{E}a^\dagger - \mathcal{E}^* a) \tag{3.15}$$

We can also take the partial trace over the field degrees of freedom

$$
\begin{aligned}
&\mathrm{Tr}_f\left[\frac{d}{dt}\rho_f\otimes\rho_a\right]=\frac{d}{dt}\,\mathrm{Tr}_f\left[\rho_f\otimes\rho_a\right]=\frac{d}{dt}\rho_a\\
&=-i\Delta_c\,\mathrm{Tr}_f[a^\dagger a\rho_f]\rho_a-i\Delta_a\,\mathrm{Tr}_f[\rho_f]\sigma_+\sigma_-\rho_a+i\Delta_c\,\mathrm{Tr}_f[\rho_f a^\dagger a]\rho_a+i\Delta_a\,\mathrm{Tr}_f[\rho_f]\rho_a\sigma_+\sigma_-\\
&+g(\mathrm{Tr}_f[a^\dagger\rho_f]\sigma_-\rho_a-\mathrm{Tr}_f[a\rho_f]\sigma_+\rho_a)+\mathrm{Tr}_f[(\mathcal{E}a^\dagger-\mathcal{E}^*a)\rho_f]\rho_a\\
&-g(\mathrm{Tr}_f[\rho_f a^\dagger]\rho_a\sigma_--\mathrm{Tr}_f[\rho_f a]\rho_a\sigma_+)-\mathrm{Tr}_f[\rho_f(\mathcal{E}a^\dagger-\mathcal{E}^*a)]\rho_a\\
&+2\kappa\left(\mathrm{Tr}_f[a\rho_f a^\dagger]\rho_a-\frac{1}{2}\,\mathrm{Tr}_f[a^\dagger a\rho_f]\rho_a-\frac{1}{2}\,\mathrm{Tr}_f[\rho_f a^\dagger a]\rho_a\right)\\
&+2\gamma_\perp\left(\mathrm{Tr}_f[\rho_f]\sigma_-\rho_a\sigma_+-\frac{1}{2}\,\mathrm{Tr}_f[\rho_f]\sigma_+\sigma_-\rho_a-\frac{1}{2}\,\mathrm{Tr}_f[\rho_f]\rho_a\sigma_+\sigma_-\right)\\
&=-i\Delta_c\,\mathrm{Tr}_f[a^\dagger a\rho_f]\rho_a+i\Delta_c\,\mathrm{Tr}_f[a^\dagger a\rho_f]\rho_a-i\Delta_a\sigma_+\sigma_-\rho_a+i\Delta_a\rho_a\sigma_+\sigma_--\mathrm{Tr}_f[(\mathcal{E}a^\dagger-\mathcal{E}^*a)\rho_f]\rho_a\\
&+g(\mathrm{Tr}_f[a^\dagger\rho_f]\sigma_-\rho_a-\mathrm{Tr}_f[a^\dagger\rho_f]\rho_a\sigma_--\mathrm{Tr}_f[a\rho_f]\sigma_+\rho_a+\mathrm{Tr}_f[a\rho_f]\rho_a\sigma_+)+\mathrm{Tr}_f[(\mathcal{E}a^\dagger-\mathcal{E}^*a)\rho_f]\rho_a\\
&+2\kappa\left(\mathrm{Tr}_f[a^\dagger a\rho_f]\rho_a-\frac{1}{2}\,\mathrm{Tr}_f[a^\dagger a\rho_f]\rho_a-\frac{1}{2}\,\mathrm{Tr}_f[a^\dagger a\rho_f]\rho_a\right)+2\gamma_\perp\left(\sigma_-\rho_a\sigma_+-\frac{1}{2}\sigma_+\sigma_-\rho_a-\frac{1}{2}\rho_a\sigma_+\sigma_-\right)\\
&=-i[\Delta_a\sigma_+\sigma_-,\rho_a]+g(\mathrm{Tr}_f[a^\dagger\rho_f][\sigma_-,\rho_a]-\mathrm{Tr}_f[a\rho_f][\sigma_+,\rho_a])\\
&+2\gamma_\perp\left(\sigma_-\rho_a\sigma_+-\frac{1}{2}\sigma_+\sigma_-\rho_a-\frac{1}{2}\rho_a\sigma_+\sigma_-\right)
\end{aligned}
\tag{3.16}
$$

Since $a=x+iy$ and $a^\dagger=x-iy$ I have $\mathrm{Tr}_f[a^\dagger\rho_f]=\langle x\rangle-i\langle y\rangle$ and $\mathrm{Tr}_f[a\rho_f]=\langle x\rangle+i\langle y\rangle$ the partially traced atomic master equation then reads

$$
\begin{aligned}
&\mathrm{Tr}_f\left[\frac{d}{dt}\rho_f\otimes\rho_a\right]=\frac{d}{dt}\,\mathrm{Tr}_f\left[\rho_f\otimes\rho_a\right]=\frac{d}{dt}\rho_a=-i[\Delta_a\sigma_+\sigma_-,\rho_a]\\
&+g(\langle x\rangle[\sigma_-,\rho_a]-i\langle y\rangle[\sigma_-,\rho_a]-\langle x\rangle[\sigma_+,\rho_a]-i\langle y\rangle[\sigma_+,\rho_a])+2\gamma_\perp\left(\sigma_-\rho_a\sigma_+-\frac{1}{2}\sigma_+\sigma_-\rho_a-\frac{1}{2}\rho_a\sigma_+\sigma_-\right)\\
&=-i[\Delta_a\sigma_+\sigma_-,\rho_a]+[-ig\langle x\rangle\sigma_y-ig\langle y\rangle\sigma_x,\rho_a]+2\gamma_\perp\left(\sigma_-\rho_a\sigma_+-\frac{1}{2}\sigma_+\sigma_-\rho_a-\frac{1}{2}\rho_a\sigma_+\sigma_-\right)\\
&=-i[H_a,\rho_a]+2\gamma_\perp\left(\sigma_-\rho_a\sigma_+-\frac{1}{2}\sigma_+\sigma_-\rho_a-\frac{1}{2}\rho_a\sigma_+\sigma_-\right)
\end{aligned}
\tag{3.17}
$$

where

$$H_a=\Delta_a\sigma_+\sigma_-+g\langle x\rangle\sigma_y+g\langle y\rangle\sigma_x \tag{3.18}$$

We can derive equations of motion for the atomic operator expectations from the partially traced atomic master equation, just as how I derived the Maxwell-Bloch equations i.e. using the trace formula $d\langle O\rangle = \mathrm{Tr}[Od\rho]$.

With $O = \sigma_x$ I have

$$
\begin{aligned}
&\frac{d}{dt}\langle\sigma_x\rangle = \frac{d}{dt}\mathrm{Tr}_a[\sigma_x\rho_a] = \mathrm{Tr}_a\left[\sigma_x\frac{d}{dt}\rho_a\right] \\
&= \mathrm{Tr}_a\left[\sigma_x[-i\Delta_a\sigma_+\sigma_- - ig\langle x\rangle\sigma_y - ig\langle y\rangle\sigma_x, \rho_a] + 2\gamma_\perp\left(\sigma_x\sigma_-\rho_a\sigma_+ - \frac{1}{2}\sigma_x\sigma_+\sigma_-\rho_a - \frac{1}{2}\sigma_x\rho_a\sigma_+\sigma_-\right)\right] \\
&= \mathrm{Tr}_a\left[-i\Delta_a\sigma_x\sigma_+\sigma_-\rho_a + i\Delta_a\sigma_x\rho_a\sigma_+\sigma_- + 2\gamma_\perp\left(\sigma_+\sigma_x\sigma_-\rho_a - \frac{1}{2}\sigma_x\sigma_+\sigma_-\rho_a - \frac{1}{2}\sigma_+\sigma_-\sigma_x\rho_a\right)\right] \\
&+ \mathrm{Tr}_a\left[+g\langle x\rangle\sigma_z\rho_a - ig\langle y\rangle\rho_a + ig\langle x\rangle\sigma_x\rho_a\sigma_y + ig\langle y\rangle\sigma_x\rho_a\sigma_x\right] \\
&= \mathrm{Tr}_a\left[-i\Delta_a\sigma_x\sigma_+\sigma_-\rho_a + i\Delta_a\sigma_+\sigma_-\sigma_x\rho_a\right] \\
&+ \mathrm{Tr}_a\left[+g\langle x\rangle\sigma_z\rho_a - ig\langle y\rangle\rho_a + ig\langle x\rangle\sigma_y\sigma_x\rho_a + ig\langle y\rangle\sigma_x\sigma_x\rho_a - \gamma_\perp(\sigma_- + \sigma_+)\rho_a\right] \\
&= \mathrm{Tr}_a\left[-\Delta_a\sigma_y\rho_a + 2g\langle x\rangle\sigma_z\rho_a - \gamma_\perp\sigma_x\rho_a\right] \\
&= -\gamma_\perp\langle\sigma_x\rangle - \Delta_a\langle\sigma_y\rangle + 2g\langle x\rangle\langle\sigma_z\rangle
\end{aligned}
\tag{3.19}
$$

With $O = \sigma_y$ I have

$$
\begin{aligned}
&\frac{d}{dt}\langle\sigma_y\rangle = \frac{d}{dt}\mathrm{Tr}_a[\sigma_y\rho_a] = \mathrm{Tr}_a\left[\sigma_y\frac{d}{dt}\rho_a\right] \\
&= \mathrm{Tr}_a\left[\sigma_y[-i\Delta_a\sigma_+\sigma_- - ig\langle x\rangle\sigma_y - ig\langle y\rangle\sigma_x, \rho_a] + 2\gamma_\perp\left(\sigma_y\sigma_-\rho_a\sigma_+ - \frac{1}{2}\sigma_y\sigma_+\sigma_-\rho_a - \frac{1}{2}\sigma_y\rho_a\sigma_+\sigma_-\right)\right] \\
&= \mathrm{Tr}_a\left[-i\Delta_a\sigma_y\sigma_+\sigma_-\rho_a + i\Delta_a\sigma_y\rho_a\sigma_+\sigma_- + 2\gamma_\perp\left(\sigma_+\sigma_y\sigma_-\rho_a - \frac{1}{2}\sigma_y\sigma_+\sigma_-\rho_a - \frac{1}{2}\sigma_+\sigma_-\sigma_y\rho_a\right)\right] \\
&+ \mathrm{Tr}_a\left[-ig\langle x\rangle\rho_a - g\langle y\rangle\sigma_z\rho_a + ig\langle x\rangle\sigma_y\rho_a\sigma_y + ig\langle y\rangle\sigma_y\rho_a\sigma_x\right] \\
&= \mathrm{Tr}_a\left[-i\Delta_a\sigma_y\sigma_+\sigma_-\rho_a + i\Delta_a\sigma_+\sigma_-\sigma_y\rho_a\right] \\
&+ \mathrm{Tr}_a\left[-ig\langle x\rangle\rho_a - g\langle y\rangle\sigma_z\rho_a + ig\langle x\rangle\sigma_y\sigma_y\rho_a + ig\langle y\rangle\sigma_x\sigma_y\rho_a + i\gamma_\perp(\sigma_+ - \sigma_-)\rho_a\right] \\
&= \mathrm{Tr}_a\left[+\Delta_a\sigma_x\rho_a - 2g\langle y\rangle\sigma_z\rho_a - \gamma_\perp\sigma_y\rho_a\right] \\
&= -\gamma_\perp\langle\sigma_y\rangle + \Delta_a\langle\sigma_x\rangle - 2g\langle y\rangle\langle\sigma_z\rangle
\end{aligned}
\tag{3.20}
$$

With $O = \sigma_z$ I have

$$
\begin{aligned}
&\frac{d}{dt}\langle\sigma_z\rangle = \frac{d}{dt}\mathrm{Tr}_a[\sigma_z\rho_a] = \mathrm{Tr}_a\left[\sigma_z\frac{d}{dt}\rho_a\right] \\
&= \mathrm{Tr}_a\left[\sigma_z[-i\Delta_a\sigma_+\sigma_- - ig\langle x\rangle\sigma_y - ig\langle y\rangle\sigma_x, \rho_a] + 2\gamma_\perp\left(\sigma_z\sigma_-\rho_a\sigma_+ - \frac{1}{2}\sigma_z\sigma_+\sigma_-\rho_a - \frac{1}{2}\sigma_z\rho_a\sigma_+\sigma_-\right)\right] \\
&= \mathrm{Tr}_a\left[-i\Delta_a\sigma_z\sigma_+\sigma_-\rho_a + i\Delta_a\sigma_z\rho_a\sigma_+\sigma_- + \gamma_\perp\left(2\sigma_+\sigma_z\sigma_-\rho_a - \sigma_z\sigma_+\sigma_-\rho_a - \sigma_+\sigma_-\sigma_z\rho_a\right)\right] \\
&+ \mathrm{Tr}_a\left[-g\langle x\rangle\sigma_x\rho_a + g\langle y\rangle\sigma_y\rho_a + ig\langle x\rangle\sigma_z\rho_a\sigma_y + ig\langle y\rangle\sigma_z\rho_a\sigma_x\right] \\
&= \mathrm{Tr}_a\left[-i\Delta_a\sigma_z\sigma_+\sigma_-\rho_a + i\Delta_a\sigma_+\sigma_-\sigma_z\rho_a\right] \\
&+ \mathrm{Tr}_a\left[-g\langle x\rangle\sigma_x\rho_a + g\langle y\rangle\sigma_y\rho_a - g\langle x\rangle\sigma_x\rho_a + g\langle y\rangle\sigma_y\rho_a + \gamma_\perp\left((-\sigma_z - I)\rho_a - (\sigma_z + I)\rho_a\right)\right] \\
&= \mathrm{Tr}_a\left[-2g\langle x\rangle\sigma_x\rho_a + 2g\langle y\rangle\sigma_y\rho_a - 2\gamma_\perp(\sigma_z + I)\rho_a\right] \\
&= -2\gamma_\perp(\langle\sigma_z\rangle + 1) - 2g\langle x\rangle\langle\sigma_x\rangle + 2g\langle y\rangle\langle\sigma_y\rangle
\end{aligned}
$$

Note that the equations of motion for $\langle\sigma_x\rangle, \langle\sigma_y\rangle, \langle\sigma_z\rangle$ are exactly the same as those in the Maxwell-Bloch equations, albeit no approximation is required during the derivation. This is expected as a factorizable density matrix should naturally lead to factorizable expectations of operator products. In addition, this establishes the equivalence between the partially traced master equation for the atom and the equations of motion for $\langle\sigma_x\rangle, \langle\sigma_y\rangle, \langle\sigma_z\rangle$ because the operator expectation triplet together with the unity trace and Hermitian requirement uniquely determine an atomic density matrix. Therefore to solve the partially traced atomic master equation for the time evolution of the atomic density matrix ρ_a I just need to solve the equations of motion for $\langle\sigma_x\rangle, \langle\sigma_y\rangle, \langle\sigma_z\rangle$. We thus have the following factorizable model as a special case of the master equation

field: partially traced master equation

$$\frac{d}{dt}\rho_f = -i[H_f, \rho_f] + 2\kappa\left(a\rho_f a^\dagger - \frac{1}{2}a^\dagger a\rho_f - \frac{1}{2}\rho_f a^\dagger a\right) \tag{3.21}$$

with

$$H_a = \Delta_a\sigma_+\sigma_- + g\langle x\rangle\sigma_y + g\langle y\rangle\sigma_x$$

atom: operator expectation equations of motion

$$\begin{aligned}\frac{d}{dt}\langle\sigma_x\rangle &= -\gamma_\perp\langle\sigma_x\rangle - \Delta_a\langle\sigma_y\rangle + 2g\langle x\rangle\langle\sigma_z\rangle \\ \frac{d}{dt}\langle\sigma_y\rangle &= -\gamma_\perp\langle\sigma_y\rangle + \Delta_a\langle\sigma_x\rangle - 2g\langle y\rangle\langle\sigma_z\rangle \\ \frac{d}{dt}\langle\sigma_z\rangle &= -2\gamma_\perp(\langle\sigma_z\rangle + 1) - 2g\langle x\rangle\langle\sigma_x\rangle + 2g\langle y\rangle\langle\sigma_y\rangle\end{aligned} \tag{3.22}$$

Compared with the Maxwell-Bloch equations based on which the small-signal amplification is established, this model differs in the description of the field. In it the field is represented by a wave function/density matrix, in contrast with the Maxwell-Bloch equations in which the field is treated as a classical field—a single complex value is used to represent the state of the field just as in the classical electrodynamics. We can test whether the amplification is lost in this adoption of quantum description of the field. The computed amplitude gains for this factorizable model at $\mathcal{E}_0 = 15.11808$ for a signal amplitude of $\mathcal{S} = 7.071 \times 10^{-5}$ and $\mathcal{S} = 7.071 \times 10^{-4}$ respectively are compared with those of the master equation and the Maxwell-Bloch equations and plotted in Fig. 3.18 and Fig. 3.19 below.

From the amplitude gain comparison plots one can see that the factorizable model produces nearly the same amount of amplification as that of the Maxwell-Bloch equations. This implies that the quantum description of the field does not destroy the amplification. A closer examination of the steady state solution to the partially traced field master equation reveals that throughout the oscillation the field is close to a coherent state. This again suggests the adequacy of using mean field equation for coherent state dynamics, as I have discovered when attempting to derive a reduced order model for describing the automatic switching in the quantum analog of absorptive bistability. It thus seems that the absence of amplification is probably due to the non-factorizable nature of the atom-field density matrix which implies nonzero correlation between the atomic and field operator expectations invalidating the factorization approximation that I adopted in deriving the Maxwell-Bloch equations[2] (this is also confirmed by the numerical solution to the master equation) as

[2]any state which is not factorizable possesses some kind of correlation because the von Neumann

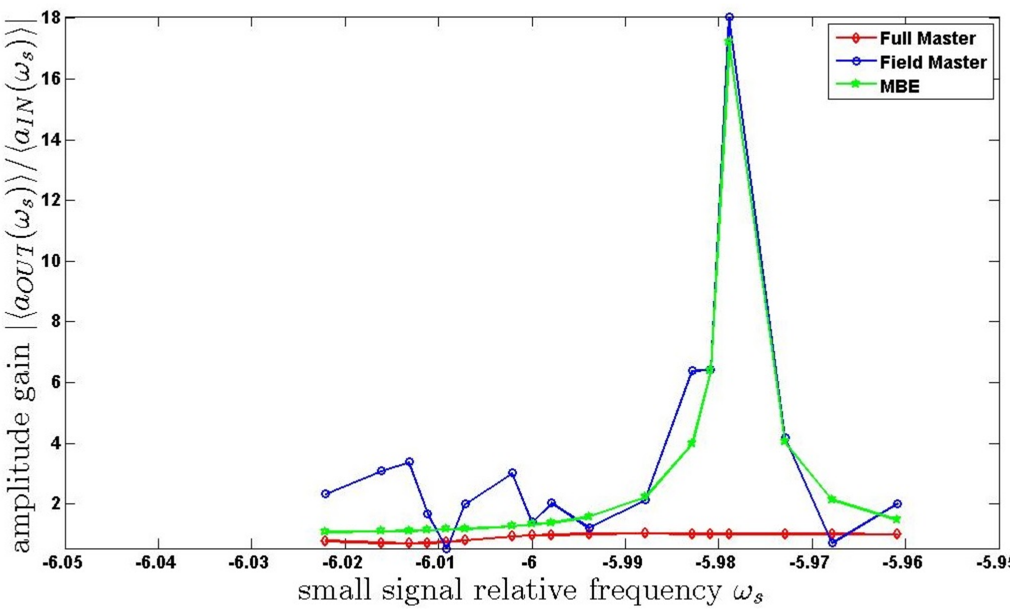

Figure 3.18: Amplitude gain comparison between the factorizable model, the master equation and the Maxwell-Bloch equations for an signal amplitude of $\mathcal{S} = 7.071\times10^{-5}$ at a pumping level of $\mathcal{E}_0 = 15.11808$

well as the feedback control model based on them for explaining the field intensity self-oscillation.

At this point, a natural step to take to address the nonfactorizable expectations of operator products is to expand the repository of variables of the Maxwell-Bloch equations i.e. treat $\langle x\sigma_z\rangle$ etc. as variables and also derive equations of motion for them. After that find some prudent way of closing the resulted operator expectation equations by adopting some approximations for the expectations of higher order operator products. And then one can ask if such an expanded set of equations of motion could fail to yield the amplification predicted by the Maxwell-Bloch equations. With the expectations of higher order operator products approximated by functions of those of lower order operator products suggested by the numerical solution to the master equation, I found the following equations of motion which manage to yield steady state solutions of $\langle x\rangle, \langle y\rangle, \langle\sigma_x\rangle, \langle\sigma_y\rangle, \langle\sigma_z\rangle$ close to those of the master equation

entropy, a measure of mutual information, $I = \mathrm{Tr}[\rho]\ln\rho - \mathrm{Tr}[\rho_a]\ln\rho_a - \mathrm{Tr}[\rho_b]\ln\rho_b$ vanishes if and only if $\rho = \rho_a \otimes \rho_b$ where $\rho_a = \mathrm{Tr}_a[\rho]$ and $\rho_b = \mathrm{Tr}_b[\rho]$ [21]

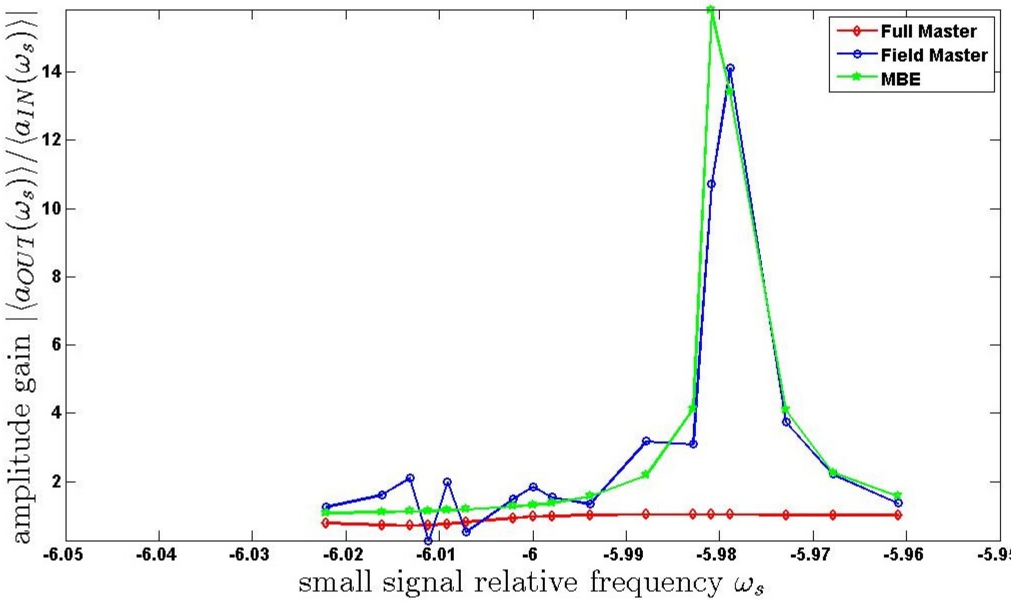

Figure 3.19: Amplitude gain comparison between the factorizable model, the master equation and the Maxwell-Bloch equations for an signal amplitude of $\mathcal{S} = 7.071 \times 10^{-4}$ at a pumping level of $\mathcal{E}_0 = 15.11808$

in the non-Hopf regime (i.e. regime with stationary steady state solutions) yet fail to produce Hopf bifurcation not to mention pre-Hopf small-signal amplification

$$
\begin{aligned}
\frac{d}{dt}\langle x\rangle &= -\kappa\langle x\rangle + \Theta\langle y\rangle + \frac{g}{2}\langle\sigma_x\rangle + \mathrm{Re}[\mathcal{E}] \\
\frac{d}{dt}\langle y\rangle &= -\kappa\langle y\rangle - \Theta\langle x\rangle - \frac{g}{2}\langle\sigma_y\rangle + \mathrm{Im}[\mathcal{E}] \\
\frac{d}{dt}\langle\sigma_x\rangle &= -\gamma\langle\sigma_x\rangle - \Delta\langle\sigma_y\rangle + 2g\langle x\sigma_z\rangle \\
\frac{d}{dt}\langle\sigma_y\rangle &= -\gamma\langle\sigma_y\rangle + \Delta\langle\sigma_x\rangle - 2g\langle y\sigma_z\rangle \\
\frac{d}{dt}\langle\sigma_z\rangle &= -2\gamma(1+\langle\sigma_z\rangle) - 2g\langle x\sigma_x\rangle + 2g\langle y\sigma_y\rangle \\
\frac{d}{dt}\langle x\sigma_z\rangle &= -(\kappa+2\gamma)\langle x\sigma_z\rangle + \Theta\langle y\sigma_z\rangle - 2\gamma\langle x\rangle + \mathrm{Re}[\mathcal{E}]\langle\sigma_z\rangle - 2g\langle xx\rangle\langle\sigma_x\rangle + 2g\langle y\rangle\langle x\sigma_y\rangle \\
\frac{d}{dt}\langle y\sigma_z\rangle &= -(\kappa+2\gamma)\langle y\sigma_z\rangle - \Theta\langle x\sigma_z\rangle - 2\gamma\langle y\rangle + \mathrm{Im}[\mathcal{E}]\langle\sigma_z\rangle + 2g\langle y\rangle\langle y\sigma_y\rangle - 2g\langle y\rangle\langle x\sigma_x\rangle \\
\frac{d}{dt}\langle x\sigma_x\rangle &= -(\gamma+\kappa)\langle x\sigma_x\rangle + \Theta\langle y\sigma_x\rangle - \Delta\langle x\sigma_y\rangle + \mathrm{Re}[\mathcal{E}]\langle\sigma_x\rangle + 2g\left(\langle xx\sigma_z\rangle + \frac{1}{4}\right)
\end{aligned}
$$

$$
\begin{aligned}
\frac{d}{dt}\langle y\sigma_y\rangle &= -(\gamma+\kappa)\langle y\sigma_y\rangle - \Theta\langle x\sigma_y\rangle + \Delta\langle y\sigma_x\rangle + \mathrm{Im}[\mathcal{E}]\langle\sigma_y\rangle - 2g\left(\langle yy\sigma_z\rangle + \frac{1}{4}\right)\\
\frac{d}{dt}\langle x\sigma_y\rangle &= -(\gamma+\kappa)\langle x\sigma_y\rangle + \Theta\langle y\sigma_y\rangle + \Delta\langle x\sigma_x\rangle + \mathrm{Re}[\mathcal{E}]\langle\sigma_y\rangle - g\langle(xy+yx)\sigma_z\rangle\\
\frac{d}{dt}\langle y\sigma_x\rangle &= -(\gamma+\kappa)\langle y\sigma_x\rangle - \Theta\langle x\sigma_x\rangle - \Delta\langle y\sigma_y\rangle + \mathrm{Im}[\mathcal{E}]\langle\sigma_x\rangle + g\langle(xy+yx)\sigma_z\rangle\\
\frac{d}{dt}\langle xy+yx\rangle &= -2\kappa\langle xy+yx\rangle - 2\Theta\langle xx\rangle + 2\Theta\langle yy\rangle + 2\mathrm{Re}[\mathcal{E}]\langle y\rangle + 2\mathrm{Im}[\mathcal{E}]\langle x\rangle - g\langle x\sigma_y\rangle + g\langle y\sigma_x\rangle\\
\frac{d}{dt}\langle xx\rangle &= -2\kappa\left(\langle xx\rangle - \frac{1}{4}\right) + \Theta\langle xy+yx\rangle + g\langle x\sigma_x\rangle + 2\mathrm{Re}[\mathcal{E}]\langle x\rangle\\
\frac{d}{dt}\langle yy\rangle &= -2\kappa\left(\langle yy\rangle - \frac{1}{4}\right) - \Theta\langle xy+yx\rangle - g\langle y\sigma_y\rangle + 2\mathrm{Im}[\mathcal{E}]\langle y\rangle\\
\frac{d}{dt}\langle xx\sigma_z\rangle &= -2(\kappa+\gamma)\langle xx\sigma_z\rangle + \frac{1}{2}\kappa\langle\sigma_z\rangle - 2\gamma\langle xx\rangle + \Theta\langle(xy+yx)\sigma_z\rangle + 2\mathrm{Re}[\mathcal{E}]\langle x\sigma_z\rangle\\
&\quad - 2g\langle xx\rangle\langle x\sigma_x\rangle + 2g\langle xx\rangle\langle y\sigma_y\rangle\\
\frac{d}{dt}\langle yy\sigma_z\rangle &= -2(\kappa+\gamma)\langle yy\sigma_z\rangle + \frac{1}{2}\kappa\langle\sigma_z\rangle - 2\gamma\langle yy\rangle - \Theta\langle(xy+yx)\sigma_z\rangle + 2\mathrm{Im}[\mathcal{E}]\langle y\sigma_z\rangle\\
&\quad + 2g\langle yy\rangle\langle y\sigma_y\rangle - 2g\langle yy\rangle\langle x\sigma_x\rangle\\
\frac{d}{dt}\langle(xy+yx)\sigma_z\rangle &= -2(\kappa+\gamma)\langle(xy+yx)\sigma_z\rangle - 2\gamma\langle xy+yx\rangle - 2\Theta\langle xx\sigma_z\rangle + 2\Theta\langle yy\sigma_z\rangle\\
&\quad + 2\mathrm{Im}[\mathcal{E}]\langle x\sigma_z\rangle + 2\mathrm{Re}[\mathcal{E}]\langle y\sigma_z\rangle - 4g\langle xx\rangle\langle y\sigma_x\rangle + 4g\langle yy\rangle\langle x\sigma_y\rangle \quad (3.23)
\end{aligned}
$$

Note that I am not claiming that the above 17D equations of motion represent a good approximate model for the master equation. These equations of motion simply demonstrate the possibility of the absence of Hopf bifurcation and hence the absence of pre-Hopf amplification as a consequence of adding more operator expectation variables into the Maxwell-Bloch equations for obtaining better approximate mean field equations.

3.6 Conclusion and Discussion

In this chapter I demonstrated that the supercritical Hopf bifurcation produced by the semi-classical Maxwell-Bloch equations is the onset of loop instability for the closed loop feedback system formed by the atom and the cavity field. I also showed that, modeled by the semi-classical Maxwell-Bloch equations a weak coherent light field driving a damped cavity QED system near supercritical Hopf bifurcation can be amplified, in accordance with Wiesenfeld and McNamara's proposal. However the quantum master equation does not exhibit significant amplification and the input-output relation is essentially linear, in contrast with the semi-classical prediction. Currently we do not have a good explanation to this quantum-classical discrepancy. But the success of reproducing the amplification as in the Maxwell-Bloch equations by assuming a factorizable atom-field density matrix, together with the possibility of existing an expanded operator expectation equations of motion which do not produce Hopf bifurcation thus pre-Hopf amplification, suggests the absence of gain be attributed to the atom-field correlation.

The failure of the quantum model in reproducing the semi-classical prediction of small-signal amplification, however, should not be interpreted as a disproof of the amplifier proposal. As has already been pointed out in the chapter of theoretical modeling, the semi-classical Maxwell-Bloch equations are also applicable to non-interacting multi-atom case. Thus by increasing the number of atoms while keeping the overall interaction between the atoms and the field constant, the system dynamics could approach the semi-classical limit for which the factorization approximation is valid. Under this condition the numerical study does suggest ample gain available to signals with the right frequency. In fact this has already been realized experimentally by one of our recent works [1]. Fig.3.20 below is extracted from the reference which plots the power gain calculated from the output oscillation amplitude measurement for three signal powers at an experimentally realizable Hopf bifurcation parameter regime. As one can see the actual maximal power gain, although smaller than the numerical prediction, can still go beyond one hundred and similar gain saturation is also observed. Thus it is confirmed experimentally that indeed this loop instability provides a way of small signal amplification.

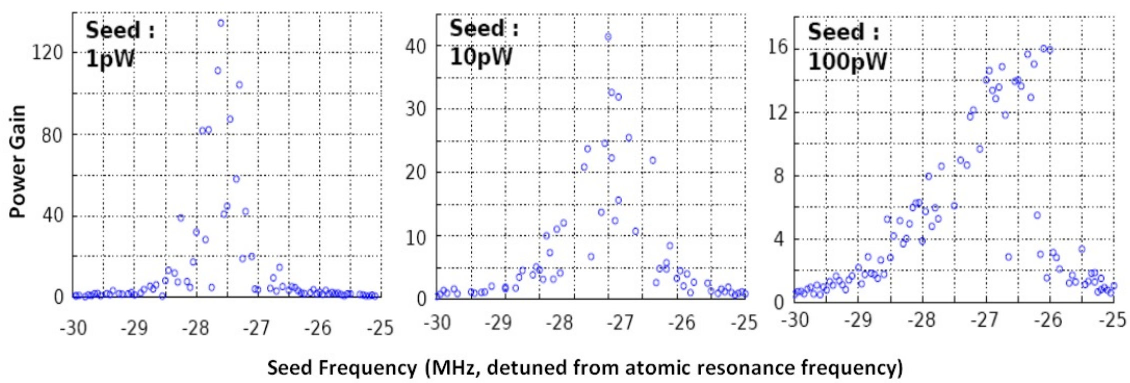

Figure 3.20: Gain curve of the experimentally demonstrated optical amplifier, with 2000 effective number of atoms, cavity detuning = −20MHz, atomic detuning = +5MHz and pump power set at 1400nW [1]

Chapter 4

Multi-atom Cavity Quantum Electrodynamics and Multi-atom Bifurcation

A numerical study on multi-atom cavity quantum electrodynamics is conducted to search for new bifurcation-like phenomenon and the dependence on the number of atoms investigated, which is examined by keeping the collective interaction between the atomic ensemble and the field constant and hence the corresponding semi-classical Maxwell-Bloch equations unchanged. Although due to the limitation of computational power the simulation stopped at a number of atoms $= 8$ it already shows new bifurcation-like phenomenon with clear dependence on the number of atoms. The 2-atom case is examined in more details with the aid of an analytical method called projected equations of motion which are derived by assuming a certain parametrization form of the system density matrix [22]. With this flexible tool an interesting property of the quantum evolution dynamics governed by the master equation is discovered. This same analytical tool is applied to show why the cooperativity, a measure of the strength of the collective interaction between the atomic ensemble and the cavity field, scales with the number of atoms, or equivalently the effective coupling constant between the atomic ensemble and the cavity field scales with the square root of the number of atoms.

4.1 A New Bifurcation-like Phenomenon in Multi-atom Cavity Quantum Electrodynamics and Its Dependence on the Number of Atoms

The cavity quantum electrodynamics (QED) has been a paradigm for theoretical and experimental investigation on quantum-classical correspondence [23] and there is a high volume of studies on the comparison of semi-classical models like the Maxwell-Bloch equations [4] and full quantum models such as the Jaynes-Cummings master equation [2]. The correspondence has been demonstrated in many ways and in particular in predicting bifurcation-like phenomena for the master equation using the semi-classical Maxwell-Bloch equations [3]. The prediction is even good beyond the generally accepted applicable regime of the Maxwell-Bloch equations in which many weakly excited atoms interact with the field [4], into the strong coupling regime in which the semi-classical factorization approximation (refer to the chapter of theoretical modeling) necessarily breaks down due to the atom-field correlation [3].

Previous study on the quantum-classical correspondence manifested in the prediction of bifurcation-like phenomena has focused on single-atom cavity quantum electrodynamics [3]. But as was noted in the chapter of theoretical modeling the semi-classical Maxwell-Bloch equations are applicable to multi-atom cases as well. In fact their dimensionless forms make no distinction between systems with different number of atoms; what counts is only the cooperativity as well as the ratios between the decay rates and detunings. It is therefore interesting to ask the following questions: if a single-atom cavity QED system and a multi-atom cavity QED system could, with properly chosen parameter values, correspond to the same Maxwell-Bloch equations, then what would be the corresponding bifurcation-like phenomenon in the multi-atom cavity QED system? How would it be different from the single-atom case? Based on it can we also propose useful devices for all-optical information processing network just as what I did in the previous two chapters? Whether and if yes how would it depend on the number of atoms? This last question actually suggests a new perspective of studying quantum-classical transition, in addition to the decoherence approach [24, 25].

To answer the above questions I used the following parameter set (where N is the number of atoms)

$$\gamma_\perp = 1, \quad \kappa = 3.5769, \quad \Delta_a = 0.7\kappa, \quad \Delta_c = -1.1\kappa, \quad C = 42.6963, \quad \mathcal{E} = 2.6\kappa \times \sqrt{N}$$

at which the Maxwell-Bloch equations produce absorptive bistability [6]. I then solved the master equation with increasing number of atoms, for which the Wigner function (another quasi-probabilistic representation of the partially traced field density matrix [20]) of the cavity field was evaluated and plotted for comparison.

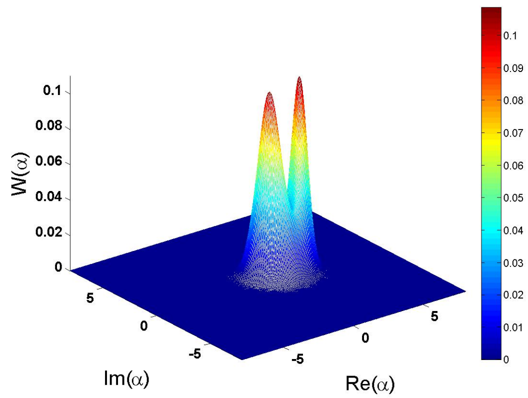

Figure 4.1: 3D plot of the Wigner function of the cavity field for the single-atom master equation

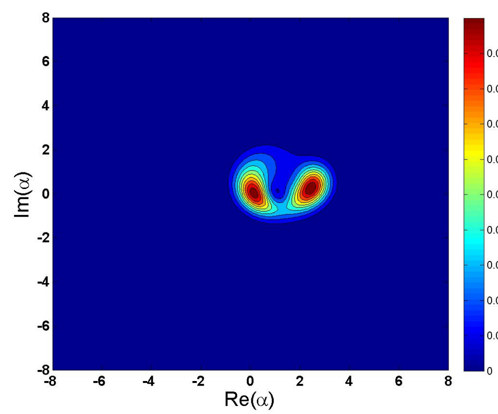

Figure 4.2: Contour plot of the Wigner function of the cavity field for the single-atom master equation

As can be seen from Fig. 4.1 and Fig. 4.2 that the single-atom master equation produces an absorptive bistable field consistent with the prediction of the Maxwell-Bloch equations, manifested by the twin-peak structure of the Wigner function, as is expected. When the number of atoms is increased to 2, there appears one more peak in the Wigner function plot, as is obvious in Fig. 4.3 and Fig. 4.4.

There is one more peak in the Wigner function of the cavity field with one more atom added. This trend continues with the number of atom rising to 4, as is shown in Fig. 4.5 to Fig. 4.8 below.

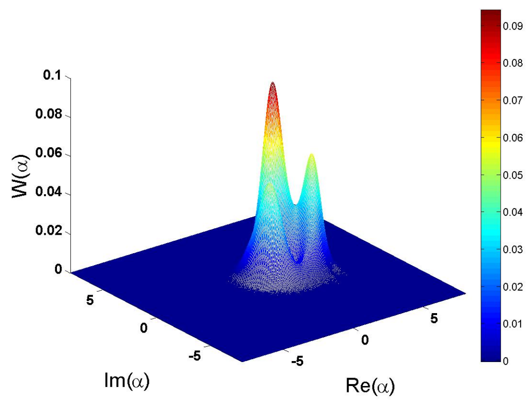

Figure 4.3: 3D plot of the Wigner function of the cavity field for the two-atom master equation

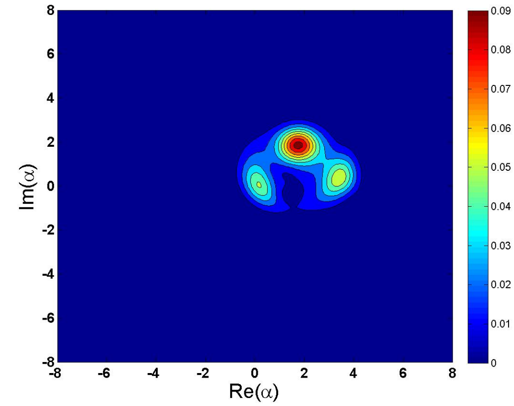

Figure 4.4: Contour plot of the Wigner function of the cavity field for the two-atom master equation

When the number of atoms is increased to 5 and above, the multiple peaks stay too close to each other to become individually discernible (note that for 5 or more atoms due to the constraint of MATLAB memory, instead of using the quantum toolbox to solve directly the steady state solutions to the multi-atom master equations [8] I simulated hundreds of quantum trajectories and took the ensemble averages of the trajectories to approximate the steady state solutions), as can be seen in Fig. 4.9 to Fig. 4.16 below.

This dependence on the number of atoms turns out to be probably due to the detunings. For another parameter set

$$\gamma_\perp = 2.6, \quad \kappa = 0.0542, \quad \Delta_a = 0, \quad \Delta_c = 0, \quad C = 6$$

at which the Maxwell-Bloch equations also produce absorptive bistability, such dependence on the number of atoms is not observed. There are always two peaks no matter how many atoms are added. Although due to the constraint of MATLAB memory the simulation stopped at the number of atoms = 3, the multi-peak structure should be most easily discernible in these cases but is not. This should argue strongly against the appearance of multiple peaks at greater number of atoms, as is

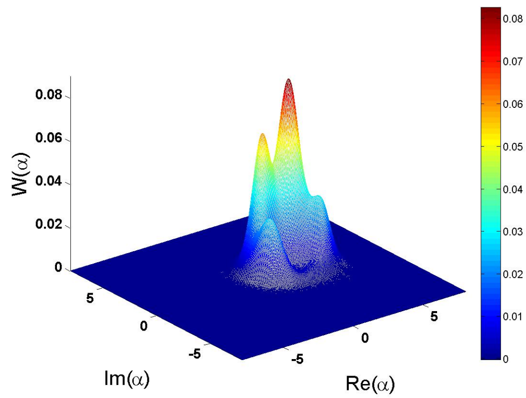

Figure 4.5: 3D plot of the Wigner function of the cavity field for the three-atom master equation

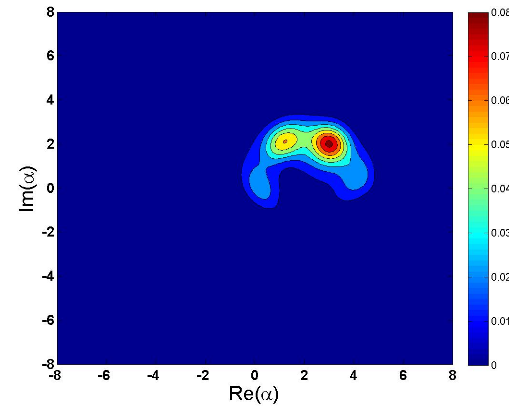

Figure 4.6: Contour plot of the Wigner function of the cavity field for the three-atom master equation

shown in Fig. 4.17 to Fig. 4.20 below[1].

Thus the bifurcation-like phenomena with dependence on the number of atoms seem to be a new-type in that both absorption and dispersion (associated with the detunings) play an important role and the interplay between them produces the observed dependence manifested in the structure of the cavity field Wigner function.

4.2 Stable Submanifold in the Parameter Space of the System Density Matrix in Two-atom Cavity Quantum Electrodynamics

Mabuchi's recipe for deriving projected equations [22] based on Ramon's information geometry formulation of quantum state evolution [26] provides an effective tool for describing not only single-atom but also multi-atom cavity quantum electrodynamics.

[1]the reason why Q function instead of Wigner function is plotted for the three-atom resonant case is that there is some numerical stability problem with the Wigner function evaluation using the quantum optics toolbox, nonetheless both Wigner function and Q function are quasi-probabilistic representations of the field and both are capable of demonstrating the coexistence of multiple states manifested as multi-peak structure albeit Wigner function produces larger separation between the peaks thus is preferred.

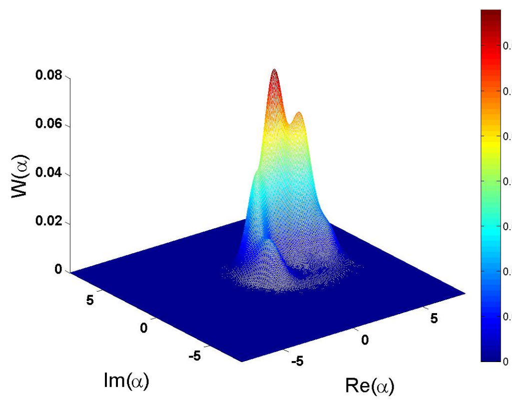

Figure 4.7: 3D plot of the Wigner function of the cavity field for the four-atom master equation

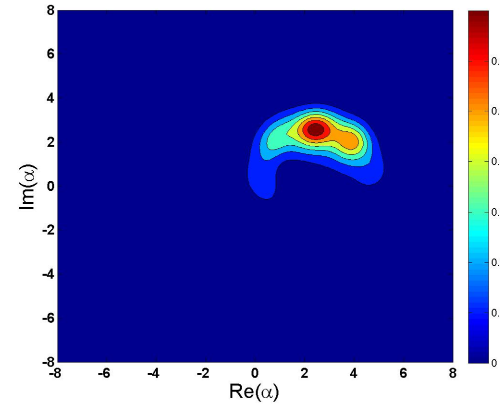

Figure 4.8: Contour plot of the Wigner function of the cavity field for the four-atom master equation

The flexibility of assuming a variety of parametrization forms for the system density matrix allows us to explore the quantum dynamical properties of interest in the most suitable parametrization form, although it might not be so valuable for single-atom quantum electrodynamics because of the relatively fewer parameters and thus parametrization forms. It turns out that two-atom quantum electrodynamics offer an ideal platform for demonstrating the benefit of this flexibility as a result of the tractable number of parameters yet still rich varieties in parametrization. As an example I will show that there exists some unexpected property of the quantum evolution that can only be properly stated in terms of the parametrization form of the system density matrix.

First let's recap Mabuchi's recipe for deriving projected equations. The procedure is as follows

1. start at a point on the prescribed manifold $\rho_t = \rho(\tau_j(t))$ defined by a set of parameters τ_j which also establish a tangent space at every point of the manifold spanned by the partial derivatives w.r.t. the parameters τ_j, $\partial\rho/\partial\tau_j$

2. project the infinitesimal increment in the system density matrix given by the master equation, $d\theta_t = \mathcal{L}[\rho_t]$, onto the tangent space; denoted the projected increment by $d\rho_t$

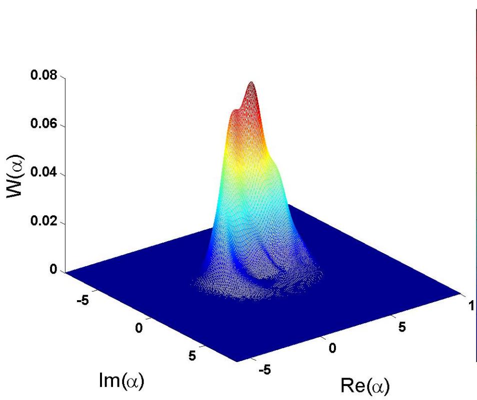

Figure 4.9: 3D plot of the Wigner function of the cavity field for the five-atom master equation

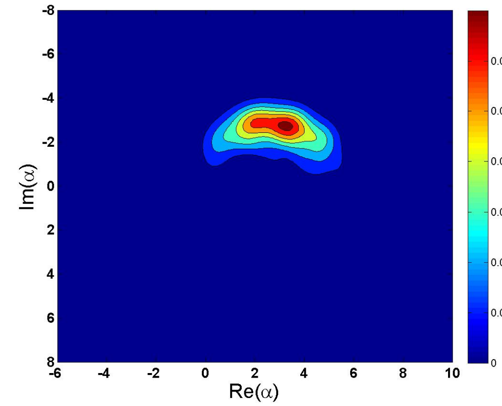

Figure 4.10: Contour plot of the Wigner function of the cavity field for the five-atom master equation

3. as a tangent space is essentially a Euclidean space ($\cong \mathbf{R}^N$) I can write the projected increment $d\rho_t$ as a total differential

$$d\rho_t = \frac{\partial \rho}{\partial \tau_1} d\tau_1 + \frac{\partial \rho}{\partial \tau_2} d\tau_2 + \cdots + \frac{\partial \rho}{\partial \tau_n} d\tau_n \tag{4.1}$$

4. on both sides of the above expression of the total differential, take inner product with every spanning vector

$$\begin{aligned}
\left\langle \frac{\partial \rho}{\partial \tau_1}, d\rho_t \right\rangle &= \left\langle \frac{\partial \rho}{\partial \tau_1}, d\theta_t \right\rangle = \left\langle \frac{\partial \rho}{\partial \tau_1}, \frac{\partial \rho}{\partial \tau_1} \right\rangle d\tau_1 + \left\langle \frac{\partial \rho}{\partial \tau_1}, \frac{\partial \rho}{\partial \tau_2} \right\rangle d\tau_2 + \cdots + \left\langle \frac{\partial \rho}{\partial \tau_1}, \frac{\partial \rho}{\partial \tau_n} \right\rangle d\tau_n \\
\left\langle \frac{\partial \rho}{\partial \tau_2}, d\rho_t \right\rangle &= \left\langle \frac{\partial \rho}{\partial \tau_2}, d\theta_t \right\rangle = \left\langle \frac{\partial \rho}{\partial \tau_2}, \frac{\partial \rho}{\partial \tau_1} \right\rangle d\tau_1 + \left\langle \frac{\partial \rho}{\partial \tau_2}, \frac{\partial \rho}{\partial \tau_2} \right\rangle d\tau_2 + \cdots + \left\langle \frac{\partial \rho}{\partial \tau_2}, \frac{\partial \rho}{\partial \tau_n} \right\rangle d\tau_n \\
&\cdots \\
\left\langle \frac{\partial \rho}{\partial \tau_n}, d\rho_t \right\rangle &= \left\langle \frac{\partial \rho}{\partial \tau_n}, d\theta_t \right\rangle = \left\langle \frac{\partial \rho}{\partial \tau_n}, \frac{\partial \rho}{\partial \tau_1} \right\rangle d\tau_1 + \left\langle \frac{\partial \rho}{\partial \tau_n}, \frac{\partial \rho}{\partial \tau_2} \right\rangle d\tau_2 + \cdots + \left\langle \frac{\partial \rho}{\partial \tau_n}, \frac{\partial \rho}{\partial \tau_n} \right\rangle d\tau_n
\end{aligned} \tag{4.2}$$

where $\langle\, , \rangle$ represents the inner product defined on the manifold, a common choice of which is $\langle X, Y \rangle = \mathrm{Tr}[X^* Y]$; this is also the inner product definition that will be used in the following. The above equations can also be written in

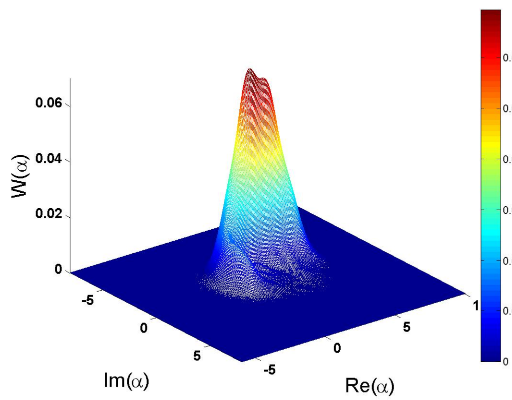

Figure 4.11: 3D plot of the Wigner function of the cavity field for the six-atom master equation

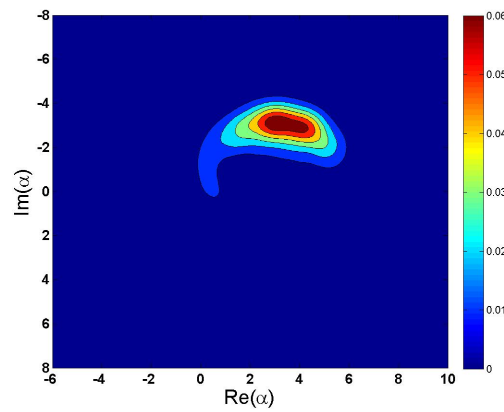

Figure 4.12: Contour plot of the Wigner function of the cavity field for the six-atom master equation

the following matrix form

$$\begin{pmatrix} \left\langle \frac{\partial\rho}{\partial\tau_1}, d\theta_t \right\rangle \\ \left\langle \frac{\partial\rho}{\partial\tau_2}, d\theta_t \right\rangle \\ \cdots \\ \left\langle \frac{\partial\rho}{\partial\tau_n}, d\theta_t \right\rangle \end{pmatrix} = \begin{pmatrix} \left\langle \frac{\partial\rho}{\partial\tau_1}, \frac{\partial\rho}{\partial\tau_1} \right\rangle & \left\langle \frac{\partial\rho}{\partial\tau_1}, \frac{\partial\rho}{\partial\tau_2} \right\rangle & \cdots & \left\langle \frac{\partial\rho}{\partial\tau_1}, \frac{\partial\rho}{\partial\tau_n} \right\rangle \\ \left\langle \frac{\partial\rho}{\partial\tau_2}, \frac{\partial\rho}{\partial\tau_1} \right\rangle & \left\langle \frac{\partial\rho}{\partial\tau_2}, \frac{\partial\rho}{\partial\tau_2} \right\rangle & \cdots & \left\langle \frac{\partial\rho}{\partial\tau_2}, \frac{\partial\rho}{\partial\tau_n} \right\rangle \\ \vdots & \vdots & \ddots & \vdots \\ \left\langle \frac{\partial\rho}{\partial\tau_n}, \frac{\partial\rho}{\partial\tau_1} \right\rangle & \left\langle \frac{\partial\rho}{\partial\tau_n}, \frac{\partial\rho}{\partial\tau_2} \right\rangle & \cdots & \left\langle \frac{\partial\rho}{\partial\tau_n}, \frac{\partial\rho}{\partial\tau_n} \right\rangle \end{pmatrix} \begin{pmatrix} d\tau_1 \\ d\tau_2 \\ \vdots \\ d\tau_n \end{pmatrix} \tag{4.3}$$

from which I can easily write down the solutions to the parameter increments

$$\begin{pmatrix} d\tau_1 \\ d\tau_2 \\ \vdots \\ d\tau_n \end{pmatrix} = \begin{pmatrix} \left\langle \frac{\partial\rho}{\partial\tau_1}, \frac{\partial\rho}{\partial\tau_1} \right\rangle & \left\langle \frac{\partial\rho}{\partial\tau_1}, \frac{\partial\rho}{\partial\tau_2} \right\rangle & \cdots & \left\langle \frac{\partial\rho}{\partial\tau_1}, \frac{\partial\rho}{\partial\tau_n} \right\rangle \\ \left\langle \frac{\partial\rho}{\partial\tau_2}, \frac{\partial\rho}{\partial\tau_1} \right\rangle & \left\langle \frac{\partial\rho}{\partial\tau_2}, \frac{\partial\rho}{\partial\tau_2} \right\rangle & \cdots & \left\langle \frac{\partial\rho}{\partial\tau_2}, \frac{\partial\rho}{\partial\tau_n} \right\rangle \\ \vdots & \vdots & \ddots & \vdots \\ \left\langle \frac{\partial\rho}{\partial\tau_n}, \frac{\partial\rho}{\partial\tau_1} \right\rangle & \left\langle \frac{\partial\rho}{\partial\tau_n}, \frac{\partial\rho}{\partial\tau_2} \right\rangle & \cdots & \left\langle \frac{\partial\rho}{\partial\tau_n}, \frac{\partial\rho}{\partial\tau_n} \right\rangle \end{pmatrix}^{-1} \begin{pmatrix} \left\langle \frac{\partial\rho}{\partial\tau_1}, d\theta_t \right\rangle \\ \left\langle \frac{\partial\rho}{\partial\tau_2}, d\theta_t \right\rangle \\ \cdots \\ \left\langle \frac{\partial\rho}{\partial\tau_n}, d\theta_t \right\rangle \end{pmatrix} \tag{4.4}$$

Therefore once I know the inner products between the spanning vectors of the tangent space—the partial derivatives w.r.t. the various parameters $\partial\rho/\partial\tau_j$—with the quantum evolution increment $d\theta_t$, as well as the inner products among themselves, I then can derive differential equations of motion for τ_j's.

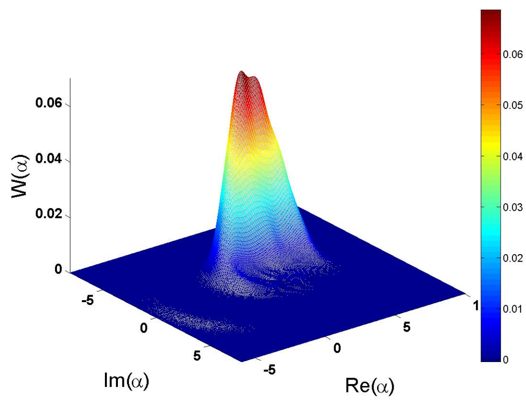

Figure 4.13: 3D plot of the Wigner function of the cavity field for the seven-atom master equation

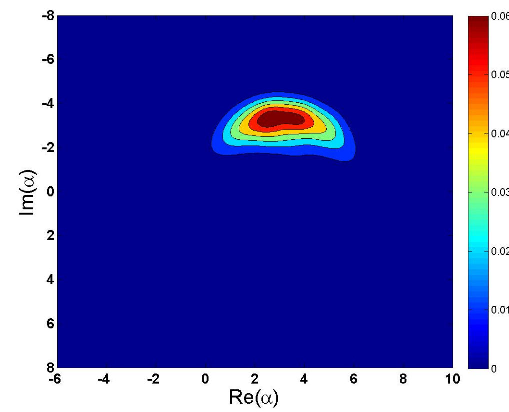

Figure 4.14: Contour plot of the Wigner function of the cavity field for the seven-atom master equation

Although irrelevant to what is going to be discussed (because no comparison with the quantum evolution will be made) some comment on the projection error, which can be quantified by the norm of $d\theta_t - d\rho_t$, is due. For the projected equations to constitute a good approximation of the master equation, in general one needs to show that the projection error is bounded within a reasonable limit or adopt a "pragmatic approach" to justify the assumption i.e. verify by examining the numerical solutions to or analytical properties of the resulted projected equations (in the original paper by Mabuchi, the validity of the assumption is justified by both of these two approaches). From the information geometry perspective, however, the projected increment $d\rho_t$ represents the best possible statistical inference about the evolution of the system state given the constraint that the information about the system state can only be gleaned from the values of the various parameters used to parametrize the system density matrix. Thus the omission of the projection error is not merely an analytical convenience but represents the fundamental restriction of quantum mechanics when only a few physical observables can be measured.

Equipped with the above projected equation derivation procedure one now can explore the power of the manifold projection technique. Start with the two-atom

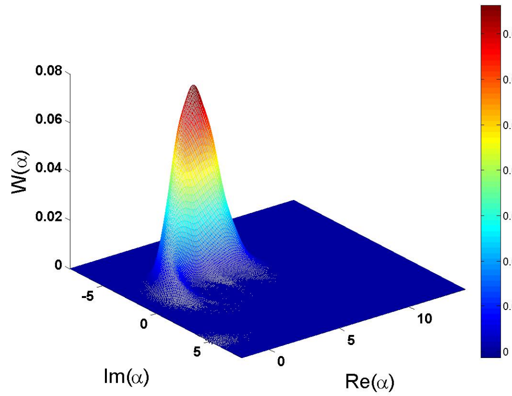

Figure 4.15: 3D plot of the Wigner function of the cavity field for the eight-atom master equation

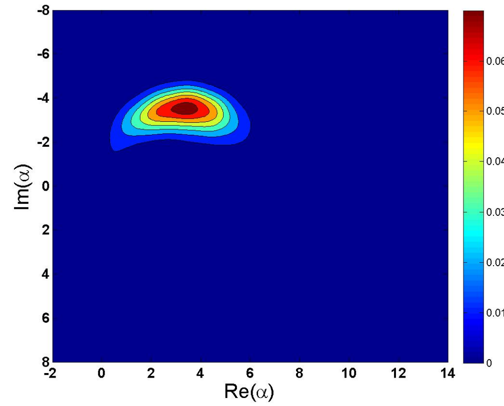

Figure 4.16: Contour plot of the Wigner function of the cavity field for the eight-atom master equation

master equation which reads

$$\begin{aligned}\dot{\rho} &= -i(\mathbf{H}\rho - \rho\mathbf{H}) + \kappa(2\mathbf{a}\rho\mathbf{a}^\dagger - \mathbf{a}^\dagger\mathbf{a}\rho - \rho\mathbf{a}^\dagger\mathbf{a}) \\ &= (\gamma/2)\left(2\boldsymbol{\sigma}_-^1\rho\boldsymbol{\sigma}_+^1 - \boldsymbol{\sigma}_+^1\boldsymbol{\sigma}_-^1\rho - \rho\boldsymbol{\sigma}_+^1\boldsymbol{\sigma}_-^1\right) + (\gamma/2)\left(2\boldsymbol{\sigma}_-^2\rho\boldsymbol{\sigma}_+^2 - \boldsymbol{\sigma}_+^2\boldsymbol{\sigma}_-^2\rho - \rho\boldsymbol{\sigma}_+^2\boldsymbol{\sigma}_-^2\right)\end{aligned} \tag{4.5}$$

where

$$\mathbf{H} = \Delta_c\mathbf{a}^\dagger\mathbf{a} + \Delta_a\boldsymbol{\sigma}_+^1\boldsymbol{\sigma}_-^1 + \Delta_a\boldsymbol{\sigma}_+^2\boldsymbol{\sigma}_-^2 + ig_1(\mathbf{a}^\dagger\boldsymbol{\sigma}_-^1 - \mathbf{a}\boldsymbol{\sigma}_+^1) + ig_2(\mathbf{a}^\dagger\boldsymbol{\sigma}_-^2 - \mathbf{a}\boldsymbol{\sigma}_+^2) + i(\mathcal{E}\mathbf{a}^\dagger - \mathcal{E}^*\mathbf{a}) \tag{4.6}$$

Then assume a factorizable system density matrix and the cavity field always being in a coherent state, i.e. $\rho = \rho_a \otimes |\alpha\rangle\langle\alpha|$. One also needs to parametrize the atomic density matrix ρ_a for which one has at least the following two choices

tensor product basis: i.e. $\sigma_{1i} \otimes \sigma_{2j}$ where $1, 2$ are labels of the atoms and $i, j = 0, 1, 2, 3$ are labels of the Pauli matrices (0 for identity matrix, 1 for σ_x, 2 for σ_y, 3 for σ_z); number the 16 bases and their associated coefficients as follows

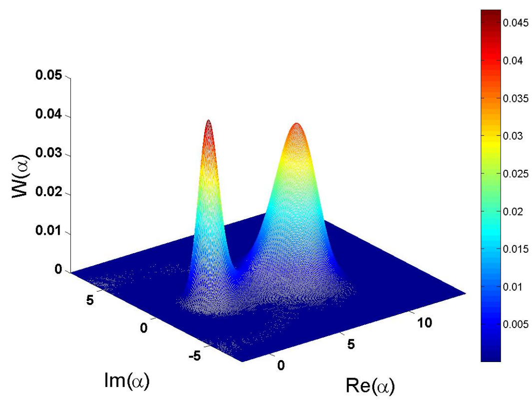

Figure 4.17: 3D plot of the Wigner function of the cavity field for the two-atom master equation at $\mathcal{E} = 0.7495$

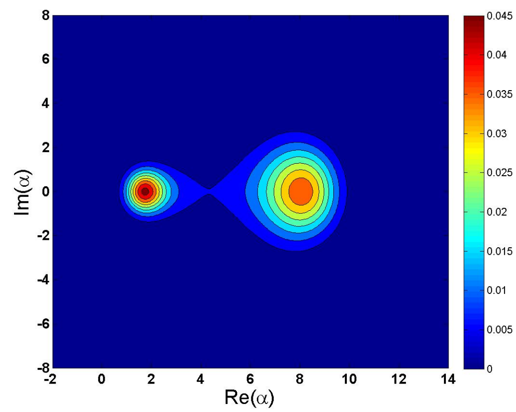

Figure 4.18: Contour plot of the Wigner function of the cavity field for the two-atom master equation at $\mathcal{E} = 0.7495$

label	basis	parameter	physical meaning
P_1	$I^1 \otimes I^2$	$\tilde{\tau}_1$	
P_2	$\sigma_x^1 \otimes I^2$	$\tilde{\tau}_2$	x-spin of Atom #1
P_3	$\sigma_y^1 \otimes I^2$	$\tilde{\tau}_3$	y-spin of Atom #1
P_4	$\sigma_z^1 \otimes I^2$	$\tilde{\tau}_4$	z-spin of Atom #1
P_5	$I^1 \otimes \sigma_x^2$	$\tilde{\tau}_5$	x-spin of Atom #2
P_6	$I^1 \otimes \sigma_y^2$	$\tilde{\tau}_6$	y-spin of Atom #2
P_7	$I^1 \otimes \sigma_z^2$	$\tilde{\tau}_7$	z-spin of Atom #2
P_8	$\sigma_x^1 \otimes \sigma_x^2$	$\tilde{\tau}_8$	
P_9	$\sigma_x^1 \otimes \sigma_y^2$	$\tilde{\tau}_9$	
P_{10}	$\sigma_x^1 \otimes \sigma_z^2$	$\tilde{\tau}_{10}$	
P_{11}	$\sigma_y^1 \otimes \sigma_x^2$	$\tilde{\tau}_{11}$	
P_{12}	$\sigma_y^1 \otimes \sigma_y^2$	$\tilde{\tau}_{12}$	
P_{13}	$\sigma_y^1 \otimes \sigma_z^2$	$\tilde{\tau}_{13}$	
P_{14}	$\sigma_z^1 \otimes \sigma_x^2$	$\tilde{\tau}_{14}$	
P_{15}	$\sigma_z^1 \otimes \sigma_y^2$	$\tilde{\tau}_{15}$	
P_{16}	$\sigma_z^1 \otimes \sigma_z^2$	$\tilde{\tau}_{16}$	

Then parametrize the atomic density matrix as $\rho_a = \sum_{i=1}^{16} \tilde{\tau}_i P_i$ where P_i's are

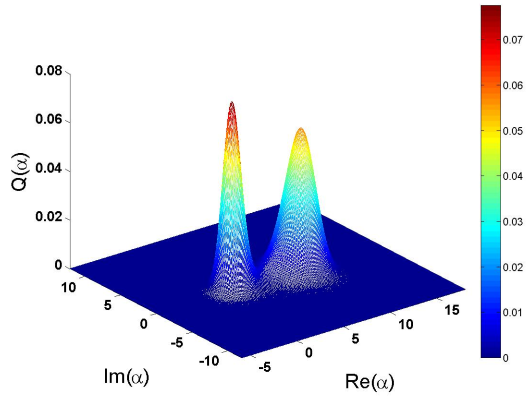

Figure 4.19: 3D plot of the Q function of the cavity field for the three-atom master equation at $\mathcal{E} = 0.9093$

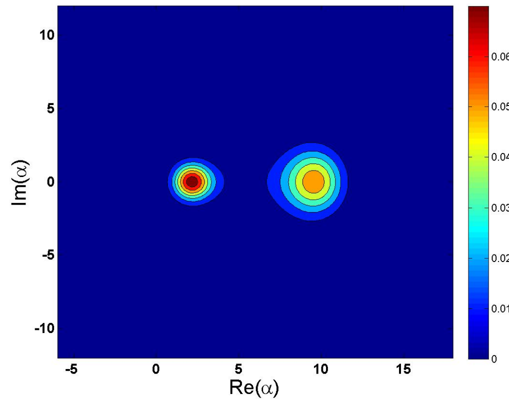

Figure 4.20: Contour plot of the Q function of the cavity field for the three-atom master equation at $\mathcal{E} = 0.9093$

the bases tabulated above; using the above projection procedure I can derive the following equations of motion for the various parameters $\tilde{\tau}_i$

$$
\begin{aligned}
d\tilde{\tau}_1 &= 0 \\
d\tilde{\tau}_2 &= -\gamma_\perp \tilde{\tau}_2 - \Delta_a \tilde{\tau}_3 + 2g_1 x_r \tilde{\tau}_4 \\
d\tilde{\tau}_3 &= -\gamma_\perp \tilde{\tau}_3 + \Delta_a \tilde{\tau}_2 - 2g_1 x_i \tilde{\tau}_4 \\
d\tilde{\tau}_4 &= -2\gamma_\perp \tilde{\tau}_1 - 2\gamma_\perp \tilde{\tau}_4 - 2g_1 x_r \tilde{\tau}_2 + 2g_1 x_i \tilde{\tau}_3 \\
d\tilde{\tau}_5 &= -\gamma_\perp \tilde{\tau}_5 - \Delta_a \tilde{\tau}_6 + 2g_2 x_r \tilde{\tau}_7 \\
d\tilde{\tau}_6 &= -\gamma_\perp \tilde{\tau}_6 + \Delta_a \tilde{\tau}_5 - 2g_2 x_i \tilde{\tau}_7 \\
d\tilde{\tau}_7 &= -2\gamma_\perp \tilde{\tau}_1 - 2\gamma_\perp \tilde{\tau}_7 - 2g_2 x_r \tilde{\tau}_5 + 2g_2 x_i \tilde{\tau}_6 \\
d\tilde{\tau}_8 &= -2\gamma_\perp \tilde{\tau}_8 - \Delta_a (\tilde{\tau}_9 + \tilde{\tau}_{11}) + 2g_2 x_r \tilde{\tau}_{10} + 2g_1 x_r \tilde{\tau}_{14} \\
d\tilde{\tau}_9 &= -2\gamma_\perp \tilde{\tau}_9 + \Delta_a (\tilde{\tau}_8 - \tilde{\tau}_{12}) - 2g_2 x_i \tilde{\tau}_{10} + 2g_1 x_r \tilde{\tau}_{15} \\
d\tilde{\tau}_{10} &= -3\gamma_\perp \tilde{\tau}_{10} - 2\gamma_\perp \tilde{\tau}_2 - \Delta_a \tilde{\tau}_{13} - 2g_2 x_r \tilde{\tau}_8 + 2g_2 x_i \tilde{\tau}_9 + 2g_1 x_r \tilde{\tau}_{16} \\
d\tilde{\tau}_{11} &= -2\gamma_\perp \tilde{\tau}_{11} + \Delta_a (\tilde{\tau}_8 - \tilde{\tau}_{12}) + 2g_2 x_r \tilde{\tau}_{13} - 2g_1 x_i \tilde{\tau}_{14} \\
d\tilde{\tau}_{12} &= -2\gamma_\perp \tilde{\tau}_{12} + \Delta_a (\tilde{\tau}_9 + \tilde{\tau}_{11}) - 2g_2 x_i \tilde{\tau}_{13} - 2g_1 x_i \tilde{\tau}_{15} \\
d\tilde{\tau}_{13} &= -3\gamma_\perp \tilde{\tau}_{13} - 2\gamma_\perp \tilde{\tau}_3 + \Delta_a \tilde{\tau}_{10} - 2g_2 x_r \tilde{\tau}_{11} + 2g_2 x_i \tilde{\tau}_{12} - 2g_1 x_i \tilde{\tau}_{16}
\end{aligned}
$$

$$
\begin{aligned}
d\tilde{\tau}_{14} &= -3\gamma_\perp\tilde{\tau}_{14} - 2\gamma_\perp\tilde{\tau}_5 - \Delta_a\tilde{\tau}_{15} - 2g_1x_r\tilde{\tau}_8 + 2g_1x_i\tilde{\tau}_{11} + 2g_2x_r\tilde{\tau}_{16} \\
d\tilde{\tau}_{15} &= -3\gamma_\perp\tilde{\tau}_{15} - 2\gamma_\perp\tilde{\tau}_6 + \Delta_a\tilde{\tau}_{14} - 2g_1x_r\tilde{\tau}_9 + 2g_1x_i\tilde{\tau}_{12} - 2g_2x_i\tilde{\tau}_{16} \\
d\tilde{\tau}_{16} &= -4\gamma_\perp\tilde{\tau}_{16} - 2\gamma_\perp\tilde{\tau}_4 - 2\gamma_\perp\tilde{\tau}_7 - 2g_1x_r\tilde{\tau}_{10} + 2g_1x_i\tilde{\tau}_{13} - 2g_2x_r\tilde{\tau}_{14} + 2g_2x_i\tilde{\tau}_{15}
\end{aligned}
\tag{4.7}
$$

factorizable basis: assume $\rho_a = \rho_{a1} \otimes \rho_{a2}$ and the standard parametrization of the atomic density matrices using Pauli matrices, i.e.

$$
\begin{aligned}
\rho_a = \rho_{a1} \otimes \rho_{a2} &= (\tau_1 I^1 + \tau_2\sigma_x^1 + \tau_3\sigma_y^1 + \tau_4\sigma_z^1) \otimes (\tau_5 I^2 + \tau_6\sigma_x^2 + \tau_7\sigma_y^2 + \tau_8\sigma_z^2) \\
&= \tau_1\tau_5 I^1 \otimes I^2 + \tau_1\tau_6 I^1 \otimes \sigma_x^2 + \tau_1\tau_7 I^1 \otimes \sigma_y^2 + \tau_1\tau_8 I^1 \otimes \sigma_z^2 \\
&+ \tau_2\tau_5\sigma_x^1 \otimes I^2 + \tau_2\tau_6\sigma_x^1 \otimes \sigma_x^2 + \tau_2\tau_7\sigma_x^1 \otimes \sigma_y^2 + \tau_2\tau_8\sigma_x^1 \otimes \sigma_z^2 \\
&+ \tau_3\tau_5\sigma_y^1 \otimes I^2 + \tau_3\tau_6\sigma_y^1 \otimes \sigma_x^2 + \tau_3\tau_7\sigma_y^1 \otimes \sigma_y^2 + \tau_3\tau_8\sigma_y^1 \otimes \sigma_z^2 \\
&+ \tau_4\tau_5\sigma_z^1 \otimes I^2 + \tau_4\tau_6\sigma_z^1 \otimes \sigma_x^2 + \tau_4\tau_7\sigma_z^1 \otimes \sigma_y^2 + \tau_4\tau_8\sigma_z^1 \otimes \sigma_z^2
\end{aligned}
\tag{4.8}
$$

using the above projection procedure I can derive the following equations of motion for the various parameters τ_j

$$
\begin{aligned}
d\tau_1 &= 0 \\
d\tau_2 &= -\gamma_\perp\tau_2 - \Delta_a\tau_3 + 2g_1\tau_4x_r \\
d\tau_3 &= -\gamma_\perp\tau_3 + \Delta_a\tau_2 - 2g_1\tau_4x_i \\
d\tau_4 &= -2\gamma_\perp\tau_1 - 2\gamma_\perp\tau_4 - 2g_1\tau_2x_r + 2g_1\tau_3x_i \\
d\tau_5 &= 0 \\
d\tau_6 &= -\gamma_\perp\tau_6 - \Delta_a\tau_7 + 2g_2\tau_8x_r \\
d\tau_7 &= -\gamma_\perp\tau_7 + \Delta_a\tau_6 - 2g_2\tau_8x_i \\
d\tau_8 &= -2\gamma_\perp\tau_5 - 2\gamma_\perp\tau_8 - 2g_2\tau_6x_r + 2g_2\tau_7x_i
\end{aligned}
\tag{4.9}
$$

Obviously the parametrization based on the factorizable basis is a special case of the parametrization based on the tensor product basis, in other words the manifold spanned by the factorizable basis (let's denote it by N) is a submanifold of the manifold spanned by the tensor product basis (let's denote it by M) for which one has the following lookup table showing the correspondence between the two bases

tensor product basis	parameter	physical meaning	factorizable basis
$I^1 \otimes I^2$	$\tilde{\tau}_1$		$\tau_1\tau_5$
$\sigma_x^1 \otimes I^2$	$\tilde{\tau}_2$	x-spin of Atom #1	$\tau_2\tau_5$
$\sigma_y^1 \otimes I^2$	$\tilde{\tau}_3$	y-spin of Atom #1	$\tau_3\tau_5$
$\sigma_z^1 \otimes I^2$	$\tilde{\tau}_4$	z-spin of Atom #1	$\tau_4\tau_5$
$I^1 \otimes \sigma_x^2$	$\tilde{\tau}_5$	x-spin of Atom #2	$\tau_1\tau_6$
$I^1 \otimes \sigma_y^2$	$\tilde{\tau}_6$	y-spin of Atom #2	$\tau_1\tau_7$
$I^1 \otimes \sigma_z^2$	$\tilde{\tau}_7$	z-spin of Atom #2	$\tau_1\tau_8$
$\sigma_x^1 \otimes \sigma_x^2$	$\tilde{\tau}_8$		$\tau_2\tau_6$
$\sigma_x^1 \otimes \sigma_y^2$	$\tilde{\tau}_9$		$\tau_2\tau_7$
$\sigma_x^1 \otimes \sigma_z^2$	$\tilde{\tau}_{10}$		$\tau_2\tau_8$
$\sigma_y^1 \otimes \sigma_x^2$	$\tilde{\tau}_{11}$		$\tau_3\tau_6$
$\sigma_y^1 \otimes \sigma_y^2$	$\tilde{\tau}_{12}$		$\tau_3\tau_7$
$\sigma_y^1 \otimes \sigma_z^2$	$\tilde{\tau}_{13}$		$\tau_3\tau_8$
$\sigma_z^1 \otimes \sigma_x^2$	$\tilde{\tau}_{14}$		$\tau_4\tau_6$
$\sigma_z^1 \otimes \sigma_y^2$	$\tilde{\tau}_{15}$		$\tau_4\tau_7$
$\sigma_z^1 \otimes \sigma_z^2$	$\tilde{\tau}_{16}$		$\tau_4\tau_8$

Surprisingly, the submanifold seems to be closed w.r.t. the quantum evolution governed by the master equation, in the sense that the increment $d\theta_t$ projected onto the tangent space T_tM of manifold M would lie within the tangent space T_tN of manifold N which is a subspace of T_tM were the system to start from manifold N i.e. $\rho_t \in N$. Therefore if the system starts from manifold N then the projection of its quantum evolution would always remain within manifold N. This is inferred from the following observation: if I substitute in $\tilde{\tau}_i$'s in terms of τ_j's I then can recover the atomic projected equations under the tensor product basis using those under the factorizable basis, i.e. the projection of $d\theta_t = \mathcal{L}[\rho_t]$, where $\rho_t \in N$, onto the tangent space of manifold M, T_tM, is the same as its projection onto the tangent space of manifold N, T_tN. The detailed proof of the coincidence is as follows

$$d\tilde{\tau}_1 = d(\tau_1\tau_5) = \tau_1 d\tau_5 + \tau_5 d\tau_1 = \tau_1(0) + \tau_5(0) = 0 \tag{4.10}$$

$$\begin{aligned} d\tilde{\tau}_2 &= d(\tau_2\tau_5) = \tau_2 d\tau_5 + \tau_5 d\tau_2 = \tau_2(0) + \tau_5(-\gamma_\perp\tau_2 - \Delta_a\tau_3 + 2g_1\tau_4 x_r) \\ &= -\gamma_\perp\tau_2\tau_5 - \Delta_a\tau_3\tau_5 + 2g_1x_r\tau_4\tau_5 = -\gamma_\perp\tilde{\tau}_2 - \Delta_a\tilde{\tau}_3 + 2g_1x_r\tilde{\tau}_4 \end{aligned} \tag{4.11}$$

$$\begin{aligned} d\tilde{\tau}_3 &= d(\tau_3\tau_5) = \tau_3 d\tau_5 + \tau_5 d\tau_3 = \tau_3(0) + \tau_5(-\gamma_\perp\tau_3 + \Delta_a\tau_2 - 2g_1\tau_4 x_i) \\ &= -\gamma_\perp\tau_3\tau_5 + \Delta_a\tau_2\tau_5 - 2g_1x_i\tau_4\tau_5 = -\gamma_\perp\tilde{\tau}_3 + \Delta_a\tilde{\tau}_2 - 2g_1x_i\tilde{\tau}_4 \end{aligned} \tag{4.12}$$

$$\begin{aligned} d\tilde{\tau}_4 &= d(\tau_4\tau_5) = \tau_4 d\tau_5 + \tau_5 d\tau_4 = \tau_4(0) + \tau_5(-2\gamma_\perp\tau_1 - 2\gamma_\perp\tau_4 - 2g_1\tau_2 x_r + 2g_1\tau_3 x_i) \\ &= -2\gamma_\perp\tau_1\tau_5 - 2\gamma_\perp\tau_4\tau_5 - 2g_1x_r\tau_2\tau_5 + 2g_1x_i\tau_3\tau_5 = -2\gamma_\perp\tilde{\tau}_1 - 2\gamma_\perp\tilde{\tau}_4 - 2g_1x_r\tilde{\tau}_2 + 2g_1x_i\tilde{\tau}_3 \end{aligned} \tag{4.13}$$

$$\begin{aligned} d\tilde{\tau}_5 &= d(\tau_1\tau_6) = \tau_1 d\tau_6 + \tau_6 d\tau_1 = \tau_1(-\gamma_\perp\tau_6 - \Delta_a\tau_7 + 2g_2\tau_8 x_r) + \tau_6(0) \\ &= -\gamma_\perp\tau_1\tau_6 - \Delta_a\tau_1\tau_7 + 2g_2x_r\tau_1\tau_8 = -\gamma_\perp\tilde{\tau}_5 - \Delta_a\tilde{\tau}_6 + 2g_2x_r\tilde{\tau}_7 \end{aligned} \tag{4.14}$$

$$\begin{aligned} d\tilde{\tau}_6 &= d(\tau_1\tau_7) = \tau_1 d\tau_7 + \tau_7 d\tau_1 = \tau_1(-\gamma_\perp\tau_7 + \Delta_a\tau_6 - 2g_2\tau_8 x_i) + \tau_7(0) \\ &= -\gamma_\perp\tau_1\tau_7 + \Delta_a\tau_1\tau_6 - 2g_2x_i\tau_1\tau_8 = -\gamma_\perp\tilde{\tau}_6 + \Delta_a\tilde{\tau}_5 - 2g_2x_i\tilde{\tau}_7 \end{aligned} \tag{4.15}$$

$$\begin{aligned} d\tilde{\tau}_7 &= d(\tau_1\tau_8) = \tau_1 d\tau_8 + \tau_8 d\tau_1 = \tau_1(-2\gamma_\perp\tau_5 - 2\gamma_\perp\tau_8 - 2g_2\tau_6 x_r + 2g_2\tau_7 x_i) + \tau_8(0) \\ &= -2\gamma_\perp\tau_1\tau_5 - 2\gamma_\perp\tau_1\tau_8 - 2g_2x_r\tau_1\tau_6 + 2g_2x_i\tau_1\tau_7 = -2\gamma_\perp\tilde{\tau}_1 - 2\gamma_\perp\tilde{\tau}_7 - 2g_2x_r\tilde{\tau}_5 + 2g_2x_i\tilde{\tau}_6 \end{aligned} \tag{4.16}$$

$$\begin{aligned} d\tilde{\tau}_8 &= d(\tau_2\tau_6) = \tau_2 d\tau_6 + \tau_6 d\tau_2 = \tau_2(-\gamma_\perp\tau_6 - \Delta_a\tau_7 + 2g_2\tau_8 x_r) + \tau_6(-\gamma_\perp\tau_2 - \Delta_a\tau_3 + 2g_1\tau_4 x_r) \\ &= (-\gamma_\perp\tau_2\tau_6 - \Delta_a\tau_2\tau_7 + 2g_2x_r\tau_2\tau_8) + (-\gamma_\perp\tau_2\tau_6 - \Delta_a\tau_3\tau_6 + 2g_1x_r\tau_4\tau_6) \\ &= (-\gamma_\perp\tilde{\tau}_8 - \Delta_a\tilde{\tau}_9 + 2g_2x_r\tilde{\tau}_{10}) + (-\gamma_\perp\tilde{\tau}_8 - \Delta_a\tilde{\tau}_{11} + 2g_1x_r\tilde{\tau}_{14}) \\ &= -2\gamma_\perp\tilde{\tau}_8 - \Delta_a(\tilde{\tau}_9 + \tilde{\tau}_{11}) + 2g_2x_r\tilde{\tau}_{10} + 2g_1x_r\tilde{\tau}_{14} \end{aligned} \tag{4.17}$$

$$\begin{aligned} d\tilde{\tau}_9 &= d(\tau_2\tau_7) = \tau_2 d\tau_7 + \tau_7 d\tau_2 \\ &= \tau_2(-\gamma_\perp\tau_7 + \Delta_a\tau_6 - 2g_2\tau_8 x_i) + \tau_7(-\gamma_\perp\tau_2 - \Delta_a\tau_3 + 2g_1\tau_4 x_r) \\ &= (-\gamma_\perp\tau_2\tau_7 + \Delta_a\tau_2\tau_6 - 2g_2 x_i\tau_2\tau_8) + (-\gamma_\perp\tau_2\tau_7 - \Delta_a\tau_3\tau_7 + 2g_1 x_r\tau_4\tau_7) \\ &= (-\gamma_\perp\tilde{\tau}_9 + \Delta_a\tilde{\tau}_8 - 2g_2 x_i\tilde{\tau}_{10}) + (-\gamma_\perp\tilde{\tau}_9 - \Delta_a\tilde{\tau}_{12} + 2g_1 x_r\tilde{\tau}_{15}) \\ &= -2\gamma_\perp\tilde{\tau}_9 + \Delta_a(\tilde{\tau}_8 - \tilde{\tau}_{12}) - 2g_2 x_i\tilde{\tau}_{10} + 2g_1 x_r\tilde{\tau}_{15} \end{aligned} \tag{4.18}$$

$$\begin{aligned} d\tilde{\tau}_{10} &= d(\tau_2\tau_8) = \tau_2 d\tau_8 + \tau_8 d\tau_2 \\ &= \tau_2(-2\gamma_\perp\tau_5 - 2\gamma_\perp\tau_8 - 2g_2\tau_6 x_r + 2g_2\tau_7 x_i) + \tau_8(-\gamma_\perp\tau_2 - \Delta_a\tau_3 + 2g_1\tau_4 x_r) \\ &= (-2\gamma_\perp\tau_2\tau_5 - 2\gamma_\perp\tau_2\tau_8 - 2g_2 x_r\tau_2\tau_6 + 2g_2 x_i\tau_2\tau_7) + (-\gamma_\perp\tau_2\tau_8 - \Delta_a\tau_3\tau_8 + 2g_1 x_r\tau_4\tau_8) \\ &= (-2\gamma_\perp\tilde{\tau}_2 - 2\gamma_\perp\tilde{\tau}_{10} - 2g_2 x_r\tilde{\tau}_8 + 2g_2 x_i\tilde{\tau}_9) + (-\gamma_\perp\tilde{\tau}_{10} - \Delta_a\tilde{\tau}_{13} + 2g_1 x_r\tilde{\tau}_{16}) \\ &= -3\gamma_\perp\tilde{\tau}_{10} - 2\gamma_\perp\tilde{\tau}_2 - \Delta_a\tilde{\tau}_{13} - 2g_2 x_r\tilde{\tau}_8 + 2g_2 x_i\tilde{\tau}_9 + 2g_1 x_r\tilde{\tau}_{16} \end{aligned} \tag{4.19}$$

$$\begin{aligned} d\tilde{\tau}_{11} &= d(\tau_3\tau_6) = \tau_3 d\tau_6 + \tau_6 d\tau_3 \\ &= \tau_3(-\gamma_\perp\tau_6 - \Delta_a\tau_7 + 2g_2\tau_8 x_r) + \tau_6(-\gamma_\perp\tau_3 + \Delta_a\tau_2 - 2g_1\tau_4 x_i) \\ &= (-\gamma_\perp\tau_3\tau_6 - \Delta_a\tau_3\tau_7 + 2g_2 x_r\tau_3\tau_8) + (-\gamma_\perp\tau_3\tau_6 + \Delta_a\tau_2\tau_6 - 2g_1 x_i\tau_4\tau_6) \\ &= (-\gamma_\perp\tilde{\tau}_{11} - \Delta_a\tilde{\tau}_{12} + 2g_2 x_r\tilde{\tau}_{13}) + (-\gamma_\perp\tilde{\tau}_{11} + \Delta_a\tilde{\tau}_8 - 2g_1 x_i\tilde{\tau}_{14}) \\ &= -2\gamma_\perp\tilde{\tau}_{11} + \Delta_a(\tilde{\tau}_8 - \tilde{\tau}_{12}) + 2g_2 x_r\tilde{\tau}_{13} - 2g_1 x_i\tilde{\tau}_{14} \end{aligned} \tag{4.20}$$

$$\begin{aligned} d\tilde{\tau}_{12} &= d(\tau_3\tau_7) = \tau_3 d\tau_7 + \tau_7 d\tau_3 \\ &= \tau_3(-\gamma_\perp\tau_7 + \Delta_a\tau_6 - 2g_2\tau_8 x_i) + \tau_7(-\gamma_\perp\tau_3 + \Delta_a\tau_2 - 2g_1\tau_4 x_i) \\ &= (-\gamma_\perp\tau_3\tau_7 + \Delta_a\tau_3\tau_6 - 2g_2 x_i\tau_3\tau_8) + (-\gamma_\perp\tau_3\tau_7 + \Delta_a\tau_2\tau_7 - 2g_1 x_i\tau_4\tau_7) \\ &= (-\gamma_\perp\tilde{\tau}_{12} + \Delta_a\tilde{\tau}_{11} - 2g_2 x_i\tilde{\tau}_{13}) + (-\gamma_\perp\tilde{\tau}_{12} + \Delta_a\tilde{\tau}_9 - 2g_1 x_i\tilde{\tau}_{15}) \\ &= -2\gamma_\perp\tilde{\tau}_{12} + \Delta_a(\tilde{\tau}_9 + \tilde{\tau}_{11}) - 2g_2 x_i\tilde{\tau}_{13} - 2g_1 x_i\tilde{\tau}_{15} \end{aligned} \tag{4.21}$$

$$\begin{aligned}
d\tilde{\tau}_{13} &= d(\tau_3\tau_8) = \tau_3 d\tau_8 + \tau_8 d\tau_3 \\
&= \tau_3(-2\gamma_\perp\tau_5 - 2\gamma_\perp\tau_8 - 2g_2\tau_6 x_r + 2g_2\tau_7 x_i) + \tau_8(-\gamma_\perp\tau_3 + \Delta_a\tau_2 - 2g_1\tau_4 x_i) \\
&= (-2\gamma_\perp\tau_3\tau_5 - 2\gamma_\perp\tau_3\tau_8 - 2g_2 x_r\tau_3\tau_6 + 2g_2 x_i\tau_3\tau_7) + (-\gamma_\perp\tau_3\tau_8 + \Delta_a\tau_2\tau_8 - 2g_1 x_i\tau_4\tau_8) \\
&= (-2\gamma_\perp\tilde{\tau}_3 - 2\gamma_\perp\tilde{13} - 2g_2 x_r\tilde{\tau}_{11} + 2g_2 x_i\tilde{\tau}_{12}) + (-\gamma_\perp\tilde{\tau}_{13} + \Delta_a\tilde{\tau}_{10} - 2g_1 x_i\tilde{\tau}_{16}) \\
&= -3\gamma_\perp\tilde{13} - 2\gamma_\perp\tilde{\tau}_3 + \Delta_a\tilde{\tau}_{10} - 2g_2 x_r\tilde{\tau}_{11} + 2g_2 x_i\tilde{\tau}_{12} - 2g_1 x_i\tilde{\tau}_{16}
\end{aligned} \tag{4.22}$$

$$\begin{aligned}
d\tilde{\tau}_{14} &= d(\tau_4\tau_6) = \tau_4 d\tau_6 + \tau_6 d\tau_4 \\
&= \tau_4(-\gamma_\perp\tau_6 - \Delta_a\tau_7 + 2g_2\tau_8 x_r) + \tau_6(-2\gamma_\perp\tau_1 - 2\gamma_\perp\tau_4 - 2g_1\tau_2 x_r + 2g_1\tau_3 x_i) \\
&= (-\gamma_\perp\tau_4\tau_6 - \Delta_a\tau_4\tau_7 + 2g_2 x_r\tau_4\tau_8) + (-2\gamma_\perp\tau_1\tau_6 - 2\gamma_\perp\tau_4\tau_6 - 2g_1 x_r\tau_2\tau_6 + 2g_1 x_i\tau_3\tau_6) \\
&= (-\gamma_\perp\tilde{\tau}_{14} - \Delta_a\tilde{\tau}_{15} + 2g_2 x_r\tilde{\tau}_{16}) + (-2\gamma_\perp\tilde{\tau}_5 - 2\gamma_\perp\tilde{\tau}_{14} - 2g_1 x_r\tilde{\tau}_8 + 2g_1 x_i\tilde{\tau}_{11}) \\
&= -3\gamma_\perp\tilde{\tau}_{14} - 2\gamma_\perp\tilde{\tau}_5 - \Delta_a\tilde{\tau}_{15} - 2g_1 x_r\tilde{\tau}_8 + 2g_1 x_i\tilde{\tau}_{11} + 2g_2 x_r\tilde{\tau}_{16}
\end{aligned} \tag{4.23}$$

$$\begin{aligned}
d\tilde{\tau}_{15} &= d(\tau_4\tau_7) = \tau_4 d\tau_7 + \tau_7 d\tau_4 \\
&= \tau_4(-\gamma_\perp\tau_7 + \Delta_a\tau_6 - 2g_2\tau_8 x_i) + \tau_7(-2\gamma_\perp\tau_1 - 2\gamma_\perp\tau_4 - 2g_1\tau_2 x_r + 2g_1\tau_3 x_i) \\
&= (-\gamma_\perp\tau_4\tau_7 + \Delta_a\tau_4\tau_6 - 2g_2 x_i\tau_4\tau_8) + (-2\gamma_\perp\tau_1\tau_7 - 2\gamma_\perp\tau_4\tau_7 - 2g_1 x_r\tau_2\tau_7 + 2g_1 x_i\tau_3\tau_7) \\
&= (-\gamma_\perp\tilde{\tau}_{15} + \Delta_a\tilde{\tau}_{14} - 2g_2 x_i\tilde{\tau}_{16}) + (-2\gamma_\perp\tilde{\tau}_6 - 2\gamma_\perp\tilde{\tau}_{15} - 2g_1 x_r\tilde{\tau}_9 + 2g_1 x_i\tilde{\tau}_{12}) \\
&= -3\gamma_\perp\tilde{\tau}_{15} - 2\gamma_\perp\tilde{\tau}_6 + \Delta_a\tilde{\tau}_{14} - 2g_1 x_r\tilde{\tau}_9 + 2g_1 x_i\tilde{\tau}_{12} - 2g_2 x_i\tilde{\tau}_{16}
\end{aligned} \tag{4.24}$$

$$\begin{aligned}
d\tilde{\tau}_{16} &= d(\tau_4\tau_8) = \tau_4 d\tau_8 + \tau_8 d\tau_4 \\
&= \tau_4(-2\gamma_\perp\tau_5 - 2\gamma_\perp\tau_8 - 2g_2\tau_6 x_r + 2g_2\tau_7 x_i) + \tau_8(-2\gamma_\perp\tau_1 - 2\gamma_\perp\tau_4 - 2g_1\tau_2 x_r + 2g_1\tau_3 x_i) \\
&= (-2\gamma_\perp\tilde{\tau}_4 - 2\gamma_\perp\tilde{\tau}_{16} - 2g_2 x_r\tilde{\tau}_{14} + 2g_2 x_i\tilde{\tau}_{15}) + (-2\gamma_\perp\tilde{\tau}_7 - 2\gamma_\perp\tilde{\tau}_{16} - 2g_1 x_r\tilde{\tau}_{10} + 2g_1 x_i\tilde{\tau}_{13}) \\
&= -4\gamma_\perp\tilde{\tau}_{16} - 2\gamma_\perp\tilde{\tau}_4 - 2\gamma_\perp\tilde{\tau}_7 - 2g_1 x_r\tilde{\tau}_{10} + 2g_1 x_i\tilde{\tau}_{13} - 2g_2 x_r\tilde{\tau}_{14} + 2g_2 x_i\tilde{\tau}_{15}
\end{aligned} \tag{4.25}$$

The recovery of the atomic projected equations under the tensor product basis can be interpreted as follows. Obviously N, the factorized basis projection manifold, is a submanifold of M, the tensor product basis projection manifold. If I start from a point $\rho_t \in N \subsetneq M$, I will have two projections of $d\theta_t$, one $\Pi_{T_tM} d\theta_t$ associated with the projected equations under the tensor product basis, and the other $\Pi_{T_tN} d\theta_t$ associated with the projected equations under the factorizable basis. Note that since $N \subsetneq M$, $T_tN \subsetneq T_tM$ thus both $\Pi_{T_tM} d\theta_t$ and $\Pi_{T_tN} d\theta_t$ lie in T_tM therefore I can make a comparison. The above derivation demonstrates that $\Pi_{T_tM} d\theta_t = \Pi_{T_tN} d\theta_t \in T_tN \subsetneq T_tM$ and this holds $\forall \rho_t \in N \subsetneq M$. The implication is that, once the system starts from a factorizable initial condition ($\rho = \rho_{a1} \otimes \rho_{a2} \otimes \rho_f$), the quantum evolution projected onto manifold M is confined to its submanifold N. Graphically what I have done is the following

$$\begin{tikzcd} d\tilde{\tau}_j \arrow[d] & = & \tau_k d\tau_l + \tau_l d\tau_k \arrow[d] \\ \Pi_{T_tM} d\theta_t & \overset{?}{=} & \Pi_{T_tN} d\theta_t \end{tikzcd}$$

I showed that the question mark is void and the equality is indeed true.

Note that the field tangential vectors of T_tM and T_tN are the same for any $\rho_t \in N \subsetneq M$ as the differentiations involve no atomic parameters thus do not distinguish between different parametrizations of ρ_a.

In fact one can prove directly (albeit tediously) the claim of the projected quantum evolution confined to the submanifold N. The detailed proof through term-by-term examination is given in the appendix.

4.3 Proof of the Scaling Law of the Cooperativity with the Number of Atoms

Here is another example demonstrating the power of assuming a proper parametrization form of the system density matrix for showing certain properties of the quantum dynamics. In this section I will extend the manifold projection technique to cavity

QED systems with arbitrary number of atoms (denoted by N) and show why the co-operativity, a measure of the strength of the collective interaction between the atoms and the cavity field, scales linearly with the number of atoms N or equivalently the effective coupling constant scales linearly with the square root of the number of atoms under weak excitation condition, the same condition as that at which the factorization approximation necessary for deriving the Maxwell-Bloch equations is valid.

Under weak excitation assumption, there is at most one out of the N atoms that can be excited, which suggests the following manifold for projecting the master equation: again let the system density matrix be in a factorizable form and assume the cavity field is always in a coherent state i.e. $\rho = \rho_a \otimes \rho_f = \rho_a \otimes |\alpha\rangle\langle\alpha|$ where $\alpha = x_r + ix_i$ is a complex number representing the amplitude of the coherent state, and let the atomic density matrix ρ_a be spanned by the following 4 bases ($\mathfrak{s}_{1i}$ stands for transposition $(1i)$ in symmetric group S_N)

$$\begin{aligned}
P_1 &= |g\rangle\langle g| = |\downarrow\downarrow\cdots\downarrow\rangle\langle\downarrow\downarrow\cdots\downarrow| \\
P_2 &= |g\rangle\langle e| = |\downarrow\downarrow\cdots\downarrow\rangle\left(\frac{1}{\sqrt{N}}\sum_{k=1}^{N}\langle\uparrow\downarrow\cdots\downarrow|\mathfrak{s}_{1k}^{\dagger}\right) \\
P_3 &= |e\rangle\langle g| = \left(\frac{1}{\sqrt{N}}\sum_{k=1}^{N}\mathfrak{s}_{1k}|\uparrow\downarrow\cdots\downarrow\rangle\right)\langle\downarrow\downarrow\cdots\downarrow| \\
P_4 &= |e\rangle\langle e| = \left(\frac{1}{\sqrt{N}}\sum_{k=1}^{N}\mathfrak{s}_{1k}|\uparrow\downarrow\cdots\downarrow\rangle\right)\left(\frac{1}{\sqrt{N}}\sum_{l=1}^{N}\langle\uparrow\downarrow\cdots\downarrow|\mathfrak{s}_{1l}^{\dagger}\right)
\end{aligned}$$

i.e. $\rho_a = \sum_{i=1}^{4} t_i P_i$. More specifically,

$$\begin{aligned}
\rho_a = {} & \tau_1|\downarrow\downarrow\cdots\downarrow\rangle\langle\downarrow\downarrow\cdots\downarrow| + \tau_2|\downarrow\downarrow\cdots\downarrow\rangle\left(\frac{1}{\sqrt{N}}\sum_{k=1}^{N}\langle\uparrow\downarrow\cdots\downarrow|\mathfrak{s}_{1k}^{\dagger}\right) \\
& + \tau_3\left(\frac{1}{\sqrt{N}}\sum_{k=1}^{N}\mathfrak{s}_{1k}|\uparrow\downarrow\cdots\downarrow\rangle\right)\langle\downarrow\downarrow\cdots\downarrow| \\
& + \tau_4\left(\frac{1}{\sqrt{N}}\sum_{k=1}^{N}\mathfrak{s}_{1k}|\uparrow\downarrow\cdots\downarrow\rangle\right)\left(\frac{1}{\sqrt{N}}\sum_{l=1}^{N}\langle\uparrow\downarrow\cdots\downarrow|\mathfrak{s}_{1l}^{\dagger}\right)
\end{aligned} \tag{4.26}$$

Choose τ_1, τ_4 to be real numbers and τ_2, τ_3 complex conjugates thus the Hermiticity $(\rho_a)^\dagger = \rho_a$ is preserved.

Using the following multi-atom master equation

$$\frac{d}{dt}\rho = -i(\mathbf{H}\rho - \rho\mathbf{H}) + \kappa(2\mathbf{a}\rho\mathbf{a}^\dagger - \mathbf{a}^\dagger\mathbf{a}\rho - \rho\mathbf{a}^\dagger\mathbf{a}) + (\gamma/2)\sum_{i=1}^{N}\left(2\boldsymbol{\sigma}_-^i\rho\boldsymbol{\sigma}_+^i - \boldsymbol{\sigma}_+^i\boldsymbol{\sigma}_-^i\rho - \rho\boldsymbol{\sigma}_+^i\boldsymbol{\sigma}_-^i\right) \tag{4.27}$$

where

$$\mathbf{H} = \Delta_c\mathbf{a}^\dagger\mathbf{a} + \Delta_a\sum_{i=1}^{N}\boldsymbol{\sigma}_+^i\boldsymbol{\sigma}_-^i + i\sum_{i=1}^{N} g_i(\mathbf{a}^\dagger\boldsymbol{\sigma}_-^i - \mathbf{a}\boldsymbol{\sigma}_+^i) + i(\mathcal{E}\mathbf{a}^\dagger - \mathcal{E}^*\mathbf{a}) \tag{4.28}$$

with the parametrization form $\rho = \sum \tau_j P_j \otimes |\alpha\rangle\langle\alpha|$ for the system density matrix and the associated partial derivatives

$$\begin{aligned}
\frac{\partial\rho}{\partial\tau_j} &= P_j \otimes |\alpha\rangle\langle\alpha| \\
\frac{\partial\rho}{\partial x_r} &= \rho_a \otimes \left[(\mathbf{a}^\dagger - \alpha^*)|\alpha\rangle\langle\alpha| + |\alpha\rangle\langle\alpha|(\mathbf{a} - \alpha)\right] \\
\frac{\partial\rho}{\partial x_i} &= \rho_a \otimes \left[i(\mathbf{a}^\dagger - \alpha^*)|\alpha\rangle\langle\alpha| - i|\alpha\rangle\langle\alpha|(\mathbf{a} - \alpha)\right]
\end{aligned} \tag{4.29}$$

following the recipe for deriving projected equations I have the following differential equations for the atomic parameters τ_j

$$\begin{aligned}
d\tau_j &= M^{-1}\langle\frac{\partial\rho}{\partial\tau_j}, d\rho\rangle = M^{-1}\,\mathrm{Tr}\left[(P_j)^\dagger \otimes |\alpha\rangle\langle\alpha| d\rho\right] = \mathrm{Tr}_a\left[\mathrm{Tr}_f\left[(P_j)^\dagger \otimes |\alpha\rangle\langle\alpha| d\rho\right]\right] \\
&= M^{-1}\,\mathrm{Tr}_a\Bigg\{-i\Delta_a(P_j)^\dagger\sum_{i=1}^{N}\left(\boldsymbol{\sigma}_+^i\boldsymbol{\sigma}_-^i\rho_a - \rho_a\boldsymbol{\sigma}_+^i\boldsymbol{\sigma}_-^i\right) \\
&+ \frac{\gamma}{2}(P_j)^\dagger\sum_{i=1}^{N}\left(2\boldsymbol{\sigma}_-^i\rho_a\boldsymbol{\sigma}_+^i - \boldsymbol{\sigma}_+^i\boldsymbol{\sigma}_-^i\rho_a - \rho_a\boldsymbol{\sigma}_+^i\boldsymbol{\sigma}_-^i\right) \\
&+ (P_j)^\dagger\left[\alpha^*\left(\sum_{i=1}^{N} g_i\boldsymbol{\sigma}_-^i\rho_a - \rho_a\sum_{i=1}^{N} g_i\boldsymbol{\sigma}_-^i\right) - \alpha\left(\sum_{i=1}^{N} g_i\boldsymbol{\sigma}_+^i\rho_a - \rho_a\sum_{i=1}^{N} g_i\boldsymbol{\sigma}_+^i\right)\right]\Bigg\}
\end{aligned} \tag{4.30}$$

where the coefficient matrix $M_{kl} = \langle\frac{\partial\rho}{\partial\tau_k}, \frac{\partial\rho}{\partial\tau_l}\rangle$, and the following differential equations concerning the field parameters x_r and x_i

$$\begin{aligned} dx_r &= N_r^{-1}\langle \frac{\partial \rho}{\partial x_r}, d\rho \rangle = N_r^{-1}\langle \rho_a \otimes [(\mathbf{a}^\dagger - \alpha^*)|\alpha\rangle\langle\alpha| + |\alpha\rangle\langle\alpha|(\mathbf{a}-\alpha)], d\rho\rangle \\ &= N_r^{-1}\mathrm{Tr}\left[(\rho_a)^\dagger \otimes [|\alpha\rangle\langle\alpha|(\mathbf{a}-\alpha) + (\mathbf{a}^\dagger - \alpha^*)|\alpha\rangle\langle\alpha|]d\rho\right] \\ &= -\kappa x_r + \Delta_c x_i + N_r^{-1}\mathrm{Tr}_a\left[(\rho_a)^\dagger\left(\sum_{i=1}^N g_i \boldsymbol{\sigma}_-^i \rho_a + \rho_a \sum_{i=1}^N g_i \boldsymbol{\sigma}_+^i\right)\right] + \Re(\mathcal{E}) \end{aligned} \tag{4.31}$$

where $N_r = 2\mathrm{Tr}[(\rho_a)^\dagger \rho_a]$, and

$$\begin{aligned} dx_i &= N_i^{-1}\langle \frac{\partial \rho}{\partial x_i}, d\rho \rangle = N_i^{-1}\langle \rho_a \otimes [i(\mathbf{a}^\dagger - \alpha^*)|\alpha\rangle\langle\alpha| - i|\alpha\rangle\langle\alpha|(\mathbf{a}-\alpha)], d\rho\rangle \\ &= N_i^{-1}\mathrm{Tr}\left[(\rho_a)^\dagger \otimes [-i|\alpha\rangle\langle\alpha|(\mathbf{a}-\alpha) + i(\mathbf{a}^\dagger - \alpha^*)|\alpha\rangle\langle\alpha|]d\rho\right] \\ &= -\kappa x_i - \Delta_c x_r - N_i^{-1} i\mathrm{Tr}_a\left[(\rho_a)^\dagger\left(\sum_{i=1}^N g_i \boldsymbol{\sigma}_-^i \rho_a - \rho_a \sum_{i=1}^N g_i \boldsymbol{\sigma}_+^i\right)\right] + \Im(\mathcal{E}) \end{aligned} \tag{4.32}$$

where $N_i = 2\mathrm{Tr}[(\rho_a)^\dagger \rho_a]$.

Substitute in the 4 bases and evaluate the various traces onewould then have the following projected equations for the atomic parameters τ_j

$$\begin{aligned} d\tau_1 &= +2\gamma_\perp \tau_4 + \sqrt{N} g \tau_2 \alpha + \sqrt{N} g \tau_3 \alpha^* \\ d\tau_2 &= (-\gamma_\perp + i\Delta_a)\tau_2 - \sqrt{N} g \tau_1 \alpha^* + \sqrt{N} g \tau_4 \alpha^* \\ d\tau_3 &= (-\gamma_\perp - i\Delta_a)\tau_3 - \sqrt{N} g \tau_1 \alpha + \sqrt{N} g \tau_4 \alpha \\ d\tau_4 &= -2\gamma_\perp \tau_4 - \sqrt{N} g \tau_2 \alpha - \sqrt{N} g \tau_3 \alpha^* \end{aligned} \tag{4.33}$$

and those for the field parameter x_r and x_i

$$\begin{aligned} dx_r &= -\kappa x_r + \Delta_c x_i + N_r^{-1}\,\mathrm{Tr}_a\left[(\rho_a)^\dagger\left(\sum_{i=1}^N g_i \boldsymbol{\sigma}_-^i \rho_a + \rho_a \sum_{i=1}^N g_i \boldsymbol{\sigma}_+^i\right)\right] + \Re(\mathcal{E}) \\ &= -\kappa x_r + \Delta_c x_i + \frac{\sqrt{N} g(\tau_2+\tau_3)(\tau_1+\tau_4)}{2(\tau_1 t_1 + \tau_2\tau_3 + \tau_3\tau_2 + \tau_4 t_4)} + \Re(\mathcal{E}) \end{aligned} \tag{4.34}$$

$$
\begin{aligned}
dx_i &= -\kappa x_i - \Delta_c x_r - N_i^{-1} i \operatorname{Tr}_a \left[(\rho_a)^\dagger \left(\sum_{i=1}^{N} g_i \boldsymbol{\sigma}_-^i \rho_a - \rho_a \sum_{i=1}^{N} g_i \boldsymbol{\sigma}_+^i \right) \right] + \Im(\mathcal{E}) \\
&= -\kappa x_i - \Delta_c x_r + \frac{\sqrt{N} g i (\tau_2 - \tau_3)(\tau_1 + \tau_4)}{2(\tau_1 t_1 + \tau_2 \tau_3 + \tau_3 \tau_2 + \tau_4 t_4)} + \Im(\mathcal{E})
\end{aligned}
\tag{4.35}
$$

The explicit dependence of the effective coupling constant on the number of atoms—the effective coupling constant $\sqrt{N}g$ scales with the square root of the number of atoms—can then been easily seen from the above differential equations.

4.4 Conclusion and Discussion

In this chapter I presented some initial effort in exploring the multi-atom cavity QED. The number of atoms as an extra degree of freedom complicates the model yet produces new bifurcation-like phenomenon that invites further investigation. In addition despite the extra variables introduced with the addition of atoms there is still chance of deriving useful algebraic properties to facilitate the examination of the dynamics. Two of such, the closed submanifold and the scaling law of the effective coupling constant, were presented in this chapter. Future work in this direction is worthy as the properties would be able to provide insights that cannot be gained via simulation.

Chapter 5

Summary and Discussion

In this dissertation I have presented two device proposals based on the understanding of bifurcation-like phenomena in the quantum model as well as its semi-classical limit. They demonstrate the potential of cavity quantum electrodynamics to serve as an ideal theoretical platform for designing ultra-low energy all-optical information processing devices. The study on multi-atom cavity quantum electrodynamics also suggests the possibility of existing new bifurcation-like phenomenon that can provide new physical basis for device applications.

In terms of the physics, there seems to be a great difference between the quantum analog of absorptive bistability and that of Hopf bifurcation. In the former case the system density matrix is very close to a factorizable form $\rho = \rho_a \otimes \rho_f$ throughout the dynamics thus permits the factorization of the expectations of operator products. This is confirmed by the goodness of approximation of the reduced order model derived. In contrast the system density matrix is far from being factorizable in the latter case, manifested in the difference in the small-signal amplification prediction of the quantum model and that of the semi-classical model. However it is intuitive why the atom-field correlation is so important in the latter case—the self-oscillation mechanism is based on a certain phase relation between the atom and the field and a definite phase relation requires coherent interaction between them prevailing over the incoherent dissipation which necessarily gives rise to strong correlation. Nonetheless in the path of discovering this factorizable/non-factorizable property of the system density matrix there seems to emerge three common themes. 1) the cavity field being in a non-coherent state is closely associated with the system density matrix being non-factorizable. 2) for coherent state dynamics the quantum description of the field (i.e. representing the field state by a wave function or a density matrix) is not necessary and mean field equation is adequate for describing the dynamics. 3) both investigations rely upon the spin precession picture (spontaneous emission interrupting precession for explaining the automatic switching in absorptive bistability, and phase lag resulted from finite speed of precession explaining the self-oscillation in Hopf bifurcation). This suggests spin precession be a not only intuitive but also useful perspective to take for deciphering new dynamics arisen from the atom-field interaction.

In addition to the semi-classical Maxwell-Bloch equations and the multi-atom quantum master equation, the manifold projection technique provides a powerful analytical tool to explore new bifurcation-like phenomenon in multi-atom quantum electrodynamics. However this technique is found to be not easily adaptable to address the atom-field correlation. This is due to the fact that there are infinitely many possible quantum states that can yield the same set of operator expectations e.g. the $(\langle x\rangle, \langle\sigma_z\rangle, \langle x\sigma_z\rangle)$ triplet. In fact close examination of the parametrization reveals that, although there is much flexibility in assuming a parametrization form for the system density matrix, the parameters are all the eigenvalues/expectations of physical observables, which can be regarded as the "rigidity" of the technique. Nevertheless this is a rather general challenge for deriving a reduced order model. That is, besides the expectations of operators, what other variables/parameters we can use to describe the quantum state. This remains an open question and invites further investigation.

There are other open questions that need to be answered by future work, such as whether and how a reduced order model can help elucidate the underlying physics, how to explain the quantum-classical discrepancy in the pre-Hopf amplification proposal, what is the origin of the new bifurcation-like phenomenon that exhibits explicit dependence on the number of atoms. Although the discussions in the respective chapters provide some clues, there is a lot more work to be done in order to reach a satisfactory answer.

Appendix A

Proof of the Submanifold Closed under the Projected Quantum Evolution

Substitute in the two-atom master equation the parametrization under the factorizable basis

$$\rho = (\tau_1 I^1 + \tau_2\sigma_x^1 + \tau_3\sigma_y^1 + \tau_4\sigma_z^1) \otimes (\tau_5 I^2 + \tau_6\sigma_x^2 + \tau_7\sigma_y^2 + \tau_8\sigma_z^2) \otimes |\alpha\rangle\langle\alpha|$$

I have

$$\begin{aligned}
& d\theta_t = -i\Delta_c(\tau_1 I^1 + \tau_2\sigma_x^1 + \tau_3\sigma_y^1 + \tau_4\sigma_z^1) \otimes (\tau_5 I^2 + \tau_6\sigma_x^2 + \tau_7\sigma_y^2 + \tau_8\sigma_z^2) \otimes \mathbf{a}^\dagger\mathbf{a}|\alpha\rangle\langle\alpha| \\
- \; & i\Delta_a\boldsymbol{\sigma}_+^1\boldsymbol{\sigma}_-^1(\tau_1 I^1 + \tau_2\sigma_x^1 + \tau_3\sigma_y^1 + \tau_4\sigma_z^1) \otimes (\tau_5 I^2 + \tau_6\sigma_x^2 + \tau_7\sigma_y^2 + \tau_8\sigma_z^2) \otimes |\alpha\rangle\langle\alpha| \\
- \; & i\Delta_a\boldsymbol{\sigma}_+^2\boldsymbol{\sigma}_-^2(\tau_1 I^1 + \tau_2\sigma_x^1 + \tau_3\sigma_y^1 + \tau_4\sigma_z^1) \otimes (\tau_5 I^2 + \tau_6\sigma_x^2 + \tau_7\sigma_y^2 + \tau_8\sigma_z^2) \otimes |\alpha\rangle\langle\alpha| \\
+ \; & (g_1\boldsymbol{\sigma}_-^1 + g_2\boldsymbol{\sigma}_-^2)(\tau_1 I^1 + \tau_2\sigma_x^1 + \tau_3\sigma_y^1 + \tau_4\sigma_z^1) \otimes (\tau_5 I^2 + \tau_6\sigma_x^2 + \tau_7\sigma_y^2 + \tau_8\sigma_z^2) \otimes \mathbf{a}^\dagger|\alpha\rangle\langle\alpha| \\
- \; & (g_1\boldsymbol{\sigma}_+^1 + g_2\boldsymbol{\sigma}_+^2)(\tau_1 I^1 + \tau_2\sigma_x^1 + \tau_3\sigma_y^1 + \tau_4\sigma_z^1) \otimes (\tau_5 I^2 + \tau_6\sigma_x^2 + \tau_7\sigma_y^2 + \tau_8\sigma_z^2) \otimes \mathbf{a}|\alpha\rangle\langle\alpha| \\
+ \; & (\tau_1 I^1 + \tau_2\sigma_x^1 + \tau_3\sigma_y^1 + \tau_4\sigma_z^1) \otimes (\tau_5 I^2 + \tau_6\sigma_x^2 + \tau_7\sigma_y^2 + \tau_8\sigma_z^2) \otimes (\mathcal{E}\mathbf{a}^\dagger|\alpha\rangle\langle\alpha| - \mathcal{E}^*\mathbf{a}|\alpha\rangle\langle\alpha|) \\
+ \; & i\Delta_c(\tau_1 I^1 + \tau_2\sigma_x^1 + \tau_3\sigma_y^1 + \tau_4\sigma_z^1) \otimes (\tau_5 I^2 + \tau_6\sigma_x^2 + \tau_7\sigma_y^2 + \tau_8\sigma_z^2) \otimes |\alpha\rangle\langle\alpha|\mathbf{a}^\dagger\mathbf{a} \\
+ \; & i\Delta_a(\tau_1 I^1 + \tau_2\sigma_x^1 + \tau_3\sigma_y^1 + \tau_4\sigma_z^1) \otimes (\tau_5 I^2 + \tau_6\sigma_x^2 + \tau_7\sigma_y^2 + \tau_8\sigma_z^2)\boldsymbol{\sigma}_+^1\boldsymbol{\sigma}_-^1 \otimes |\alpha\rangle\langle\alpha|
\end{aligned}$$

$$
\begin{aligned}
+ &\quad i\Delta_a(\tau_1 I^1 + \tau_2\sigma_x^1 + \tau_3\sigma_y^1 + \tau_4\sigma_z^1) \otimes (\tau_5 I^2 + \tau_6\sigma_x^2 + \tau_7\sigma_y^2 + \tau_8\sigma_z^2)\boldsymbol{\sigma}_+^2\boldsymbol{\sigma}_-^2 \otimes |\alpha\rangle\langle\alpha| \\
- &\quad (\tau_1 I^1 + \tau_2\sigma_x^1 + \tau_3\sigma_y^1 + \tau_4\sigma_z^1) \otimes (\tau_5 I^2 + \tau_6\sigma_x^2 + \tau_7\sigma_y^2 + \tau_8\sigma_z^2)(g_1\boldsymbol{\sigma}_-^1 + g_2\boldsymbol{\sigma}_-^2) \otimes |\alpha\rangle\langle\alpha|\mathbf{a}^\dagger \\
+ &\quad (\tau_1 I^1 + \tau_2\sigma_x^1 + \tau_3\sigma_y^1 + \tau_4\sigma_z^1) \otimes (\tau_5 I^2 + \tau_6\sigma_x^2 + \tau_7\sigma_y^2 + \tau_8\sigma_z^2)(g_1\boldsymbol{\sigma}_+^1 + g_2\boldsymbol{\sigma}_+^2) \otimes |\alpha\rangle\langle\alpha|\mathbf{a} \\
- &\quad (\tau_1 I^1 + \tau_2\sigma_x^1 + \tau_3\sigma_y^1 + \tau_4\sigma_z^1) \otimes (\tau_5 I^2 + \tau_6\sigma_x^2 + \tau_7\sigma_y^2 + \tau_8\sigma_z^2) \otimes (|\alpha\rangle\langle\alpha|\mathcal{E}\mathbf{a}^\dagger - |\alpha\rangle\langle\alpha|\mathcal{E}^*\mathbf{a}) \\
+ &\quad 2\kappa(\tau_1 I^1 + \tau_2\sigma_x^1 + \tau_3\sigma_y^1 + \tau_4\sigma_z^1) \otimes (\tau_5 I^2 + \tau_6\sigma_x^2 + \tau_7\sigma_y^2 + \tau_8\sigma_z^2) \otimes \mathbf{a}|\alpha\rangle\langle\alpha|\mathbf{a}^\dagger \\
- &\quad \kappa(\tau_1 I^1 + \tau_2\sigma_x^1 + \tau_3\sigma_y^1 + \tau_4\sigma_z^1) \otimes (\tau_5 I^2 + \tau_6\sigma_x^2 + \tau_7\sigma_y^2 + \tau_8\sigma_z^2) \otimes \mathbf{a}^\dagger\mathbf{a}|\alpha\rangle\langle\alpha| \\
- &\quad \kappa(\tau_1 I^1 + \tau_2\sigma_x^1 + \tau_3\sigma_y^1 + \tau_4\sigma_z^1) \otimes (\tau_5 I^2 + \tau_6\sigma_x^2 + \tau_7\sigma_y^2 + \tau_8\sigma_z^2) \otimes |\alpha\rangle\langle\alpha|\mathbf{a}^\dagger\mathbf{a} \\
+ &\quad 2\gamma_\perp\boldsymbol{\sigma}_-^1(\tau_1 I^1 + \tau_2\sigma_x^1 + \tau_3\sigma_y^1 + \tau_4\sigma_z^1) \otimes (\tau_5 I^2 + \tau_6\sigma_x^2 + \tau_7\sigma_y^2 + \tau_8\sigma_z^2)\boldsymbol{\sigma}_+^1 \otimes |\alpha\rangle\langle\alpha| \\
- &\quad \gamma_\perp\boldsymbol{\sigma}_+^1\boldsymbol{\sigma}_-^1(\tau_1 I^1 + \tau_2\sigma_x^1 + \tau_3\sigma_y^1 + \tau_4\sigma_z^1) \otimes (\tau_5 I^2 + \tau_6\sigma_x^2 + \tau_7\sigma_y^2 + \tau_8\sigma_z^2) \otimes |\alpha\rangle\langle\alpha| \\
- &\quad \gamma_\perp(\tau_1 I^1 + \tau_2\sigma_x^1 + \tau_3\sigma_y^1 + \tau_4\sigma_z^1) \otimes (\tau_5 I^2 + \tau_6\sigma_x^2 + \tau_7\sigma_y^2 + \tau_8\sigma_z^2)\boldsymbol{\sigma}_+^1\boldsymbol{\sigma}_-^1 \otimes |\alpha\rangle\langle\alpha| \\
+ &\quad 2\gamma_\perp\boldsymbol{\sigma}_-^2(\tau_1 I^1 + \tau_2\sigma_x^1 + \tau_3\sigma_y^1 + \tau_4\sigma_z^1) \otimes (\tau_5 I^2 + \tau_6\sigma_x^2 + \tau_7\sigma_y^2 + \tau_8\sigma_z^2)\boldsymbol{\sigma}_+^2 \otimes |\alpha\rangle\langle\alpha| \\
- &\quad \gamma_\perp\boldsymbol{\sigma}_+^2\boldsymbol{\sigma}_-^2(\tau_1 I^1 + \tau_2\sigma_x^1 + \tau_3\sigma_y^1 + \tau_4\sigma_z^1) \otimes (\tau_5 I^2 + \tau_6\sigma_x^2 + \tau_7\sigma_y^2 + \tau_8\sigma_z^2) \otimes |\alpha\rangle\langle\alpha| \\
- &\quad \gamma_\perp(\tau_1 I^1 + \tau_2\sigma_x^1 + \tau_3\sigma_y^1 + \tau_4\sigma_z^1) \otimes (\tau_5 I^2 + \tau_6\sigma_x^2 + \tau_7\sigma_y^2 + \tau_8\sigma_z^2)\boldsymbol{\sigma}_+^2\boldsymbol{\sigma}_-^2 \otimes |\alpha\rangle\langle\alpha|
\end{aligned}
$$

Using the algebraic properties of Pauli matrices as well as those of coherent state vectors $\mathbf{a}|\alpha\rangle = \alpha|\alpha\rangle$ and $\langle\alpha|\mathbf{a}^\dagger = \langle\alpha|\alpha^*$, I can simplify $d\theta_t$ to

$$
\begin{aligned}
&\quad d\theta_t = -i\Delta_c(\tau_1 I^1 + \tau_2\sigma_x^1 + \tau_3\sigma_y^1 + \tau_4\sigma_z^1) \otimes (\tau_5 I^2 + \tau_6\sigma_x^2 + \tau_7\sigma_y^2 + \tau_8\sigma_z^2) \otimes \mathbf{a}^\dagger\alpha|\alpha\rangle\langle\alpha| \\
- &\quad i\Delta_a(\frac{\tau_1}{2}I^1 + \frac{\tau_1}{2}\sigma_z^1 + \tau_2\sigma_+^1 - i\tau_3\sigma_+^1 + \frac{\tau_4}{2}I^1 + \frac{\tau_4}{2}\sigma_z^1) \otimes (\tau_5 I^2 + \tau_6\sigma_x^2 + \tau_7\sigma_y^2 + \tau_8\sigma_z^2) \otimes |\alpha\rangle\langle\alpha| \\
- &\quad i\Delta_a(\tau_1 I^1 + \tau_2\sigma_x^1 + \tau_3\sigma_y^1 + \tau_4\sigma_z^1) \otimes (\frac{\tau_5}{2}I^2 + \frac{\tau_5}{2}\sigma_z^2 + \tau_6\sigma_+^2 - i\tau_7\sigma_+^2 + \frac{\tau_8}{2}I^2 + \frac{\tau_8}{2}\sigma_z^2) \otimes |\alpha\rangle\langle\alpha| \\
+ &\quad \frac{g_1}{2}(2\tau_1\sigma_-^1 + \tau_2 I^1 - \tau_2\sigma_z^1 - i\tau_3 I^1 + i\tau_3\sigma_z^1 + 2\tau_4\sigma_-^1) \otimes (\tau_5 I^2 + \tau_6\sigma_x^2 + \tau_7\sigma_y^2 + \tau_8\sigma_z^2) \otimes \mathbf{a}^\dagger|\alpha\rangle\langle\alpha| \\
+ &\quad \frac{g_2}{2}(\tau_1 I^1 + \tau_2\sigma_x^1 + \tau_3\sigma_y^1 + \tau_4\sigma_z^1) \otimes (2\tau_5\sigma_-^2 + \tau_6 I^2 - \tau_6\sigma_z^2 - i\tau_7 I^2 + i\tau_7\sigma_z^2 + 2\tau_8\sigma_-^2) \otimes \mathbf{a}^\dagger|\alpha\rangle\langle\alpha| \\
- &\quad \frac{g_1}{2}(2\tau_1\sigma_+^1 + \tau_2 I^1 + \tau_2\sigma_z^1 + i\tau_3 I^1 + i\tau_3\sigma_z^1 - 2\tau_4\sigma_+^1) \otimes (\tau_5 I^2 + \tau_6\sigma_x^2 + \tau_7\sigma_y^2 + \tau_8\sigma_z^2) \otimes \alpha|\alpha\rangle\langle\alpha| \\
- &\quad \frac{g_2}{2}(\tau_1 I^1 + \tau_2\sigma_x^1 + \tau_3\sigma_y^1 + \tau_4\sigma_z^1) \otimes (2\tau_5\sigma_+^2 + \tau_6 I^2 + \tau_6\sigma_z^2 + i\tau_7 I^2 + i\tau_7\sigma_z^2 - 2\tau_8\sigma_+^2) \otimes \alpha|\alpha\rangle\langle\alpha| \\
+ &\quad (\tau_1 I^1 + \tau_2\sigma_x^1 + \tau_3\sigma_y^1 + \tau_4\sigma_z^1) \otimes (\tau_5 I^2 + \tau_6\sigma_x^2 + \tau_7\sigma_y^2 + \tau_8\sigma_z^2) \otimes (\mathcal{E}\mathbf{a}^\dagger|\alpha\rangle\langle\alpha| - \mathcal{E}^*\alpha|\alpha\rangle\langle\alpha|) \\
+ &\quad i\Delta_c(\tau_1 I^1 + \tau_2\sigma_x^1 + \tau_3\sigma_y^1 + \tau_4\sigma_z^1) \otimes (\tau_5 I^2 + \tau_6\sigma_x^2 + \tau_7\sigma_y^2 + \tau_8\sigma_z^2) \otimes |\alpha\rangle\langle\alpha|\alpha^*\mathbf{a}
\end{aligned}
$$

$$
\begin{aligned}
&+ \quad i\Delta_a(\frac{\tau_1}{2}I^1 + \frac{\tau_1}{2}\sigma_z^1 + \tau_2\sigma_-^1 + i\tau_3\sigma_-^1 + \frac{\tau_4}{2}I^1 + \frac{\tau_4}{2}\sigma_z^1) \otimes (\tau_5 I^2 + \tau_6\sigma_x^2 + \tau_7\sigma_y^2 + \tau_8\sigma_z^2) \otimes |\alpha\rangle\langle\alpha| \\
&+ \quad i\Delta_a(\tau_1 I^1 + \tau_2\sigma_x^1 + \tau_3\sigma_y^1 + \tau_4\sigma_z^1) \otimes (\frac{\tau_5}{2}I^2 + \frac{\tau_5}{2}\sigma_z^2 + \tau_6\sigma_-^2 + i\tau_7\sigma_-^2 + \frac{\tau_8}{2}I^2 + \frac{\tau_8}{2}\sigma_z^2) \otimes |\alpha\rangle\langle\alpha| \\
&- \quad \frac{g_1}{2}(2\tau_1\sigma_-^1 + \tau_2 I^1 + \tau_2\sigma_z^1 - i\tau_3 I^1 - i\tau_3\sigma_z^1 - 2\tau_4\sigma_-^1) \otimes (\tau_5 I^2 + \tau_6\sigma_x^2 + \tau_7\sigma_y^2 + \tau_8\sigma_z^2) \otimes |\alpha\rangle\langle\alpha|\alpha^* \\
&- \quad \frac{g_2}{2}(\tau_1 I^1 + \tau_2\sigma_x^1 + \tau_3\sigma_y^1 + \tau_4\sigma_z^1) \otimes (2\tau_5\sigma_-^2 + \tau_6 I^2 + \tau_6\sigma_z^2 - i\tau_7 I^2 - i\tau_7\sigma_z^2 - 2\tau_8\sigma_-^2) \otimes |\alpha\rangle\langle\alpha|\alpha^* \\
&+ \quad \frac{g_1}{2}(2\tau_1\sigma_+^1 + \tau_2 I^1 - \tau_2\sigma_z^1 + i\tau_3 I^1 - i\tau_3\sigma_z^1 + 2\tau_4\sigma_+^1) \otimes (\tau_5 I^2 + \tau_6\sigma_x^2 + \tau_7\sigma_y^2 + \tau_8\sigma_z^2) \otimes |\alpha\rangle\langle\alpha|\mathbf{a} \\
&+ \quad \frac{g_2}{2}(\tau_1 I^1 + \tau_2\sigma_x^1 + \tau_3\sigma_y^1 + \tau_4\sigma_z^1) \otimes (2\tau_5\sigma_+^2 + \tau_6 I^2 - \tau_6\sigma_z^2 + i\tau_7 I^2 - i\tau_7\sigma_z^2 + 2\tau_8\sigma_+^2) \otimes |\alpha\rangle\langle\alpha|\mathbf{a} \\
&- \quad (\tau_1 I^1 + \tau_2\sigma_x^1 + \tau_3\sigma_y^1 + \tau_4\sigma_z^1) \otimes (\tau_5 I^2 + \tau_6\sigma_x^2 + \tau_7\sigma_y^2 + \tau_8\sigma_z^2) \otimes (|\alpha\rangle\langle\alpha|\mathcal{E}\alpha^* - |\alpha\rangle\langle\alpha|\mathcal{E}^*\mathbf{a}) \\
&+ \quad 2\kappa(\tau_1 I^1 + \tau_2\sigma_x^1 + \tau_3\sigma_y^1 + \tau_4\sigma_z^1) \otimes (\tau_5 I^2 + \tau_6\sigma_x^2 + \tau_7\sigma_y^2 + \tau_8\sigma_z^2) \otimes \alpha|\alpha\rangle\langle\alpha|\alpha^* \\
&- \quad \kappa(\tau_1 I^1 + \tau_2\sigma_x^1 + \tau_3\sigma_y^1 + \tau_4\sigma_z^1) \otimes (\tau_5 I^2 + \tau_6\sigma_x^2 + \tau_7\sigma_y^2 + \tau_8\sigma_z^2) \otimes \mathbf{a}^\dagger\alpha|\alpha\rangle\langle\alpha| \\
&- \quad \kappa(\tau_1 I^1 + \tau_2\sigma_x^1 + \tau_3\sigma_y^1 + \tau_4\sigma_z^1) \otimes (\tau_5 I^2 + \tau_6\sigma_x^2 + \tau_7\sigma_y^2 + \tau_8\sigma_z^2) \otimes |\alpha\rangle\langle\alpha|\alpha^*\mathbf{a} \\
&+ \quad \gamma_\perp(\tau_1 I^1 - \tau_1\sigma_z^1 + \tau_4 I^1 - \tau_4\sigma_z^1) \otimes (\tau_5 I^2 + \tau_6\sigma_x^2 + \tau_7\sigma_y^2 + \tau_8\sigma_z^2) \otimes |\alpha\rangle\langle\alpha| \\
&- \quad \gamma_\perp(\frac{\tau_1}{2}I^1 + \frac{\tau_1}{2}\sigma_z^1 + \tau_2\sigma_+^1 - i\tau_3\sigma_+^1 + \frac{\tau_4}{2}I^1 + \frac{\tau_4}{2}\sigma_z^1) \otimes (\tau_5 I^2 + \tau_6\sigma_x^2 + \tau_7\sigma_y^2 + \tau_8\sigma_z^2) \otimes |\alpha\rangle\langle\alpha| \\
&- \quad \gamma_\perp(\frac{\tau_1}{2}I^1 + \frac{\tau_1}{2}\sigma_z^1 + \tau_2\sigma_-^1 + i\tau_3\sigma_-^1 + \frac{\tau_4}{2}I^1 + \frac{\tau_4}{2}\sigma_z^1) \otimes (\tau_5 I^2 + \tau_6\sigma_x^2 + \tau_7\sigma_y^2 + \tau_8\sigma_z^2) \otimes |\alpha\rangle\langle\alpha| \\
&+ \quad \gamma_\perp(\tau_1 I^1 + \tau_2\sigma_x^1 + \tau_3\sigma_y^1 + \tau_4\sigma_z^1) \otimes (\tau_5 I^2 - \tau_5\sigma_z^2 + \tau_8 I^2 - \tau_8\sigma_z^2) \otimes |\alpha\rangle\langle\alpha| \\
&- \quad \gamma_\perp(\tau_1 I^1 + \tau_2\sigma_x^1 + \tau_3\sigma_y^1 + \tau_4\sigma_z^1) \otimes (\frac{\tau_5}{2}I^2 + \frac{\tau_5}{2}\sigma_z^2 + \tau_6\sigma_+^2 - i\tau_7\sigma_+^2 + \frac{\tau_8}{2}I^2 + \frac{\tau_8}{2}\sigma_z^2) \otimes |\alpha\rangle\langle\alpha| \\
&- \quad \gamma_\perp(\tau_1 I^1 + \tau_2\sigma_x^1 + \tau_3\sigma_y^1 + \tau_4\sigma_z^1) \otimes (\frac{\tau_5}{2}I^2 + \frac{\tau_5}{2}\sigma_z^2 + \tau_6\sigma_-^2 + i\tau_7\sigma_-^2 + \frac{\tau_8}{2}I^2 + \frac{\tau_8}{2}\sigma_z^2) \otimes |\alpha\rangle\langle\alpha|
\end{aligned}
$$

Notice that every term in the expression of $d\rho$ above has an atomic density matrix component being a linear combination of either $\sigma_i^1 \otimes (\tau_5 I^2 + \tau_6\sigma_x^2 + \tau_7\sigma_y^2 + \tau_8\sigma_z^2)$ or $(\tau_1 I^1 + \tau_2\sigma_x^1 + \tau_3\sigma_y^1 + \tau_4\sigma_z^1) \otimes \sigma_j^2$ where the subscripts $i, j \in \{0, 1, 2, 3\}$ and $0, 1, 2, 3$ denote the Pauli matrices $\{I, \sigma_x, \sigma_y, \sigma_z\}$ respectively. On the other hand the tangent space $T_t N$ is spanned by the following vectors

$$\sigma_i^1 \otimes (\tau_5 I^2 + \tau_6\sigma_x^2 + \tau_7\sigma_y^2 + \tau_8\sigma_z^2) \otimes |\alpha\rangle\langle\alpha|, \quad (\tau_1 I^1 + \tau_2\sigma_x^1 + \tau_3\sigma_y^1 + \tau_4\sigma_z^1) \otimes \sigma_j^2 \otimes |\alpha\rangle\langle\alpha|, \quad i, j \in \{0, 1, 2, 3\}$$

$$(\tau_1 I^1 + \tau_2\sigma_x^1 + \tau_3\sigma_y^1 + \tau_4\sigma_z^1) \otimes (\tau_5 I^2 + \tau_6\sigma_x^2 + \tau_7\sigma_y^2 + \tau_8\sigma_z^2) \otimes [(\mathbf{a}^\dagger - \alpha^*)|\alpha\rangle\langle\alpha| + |\alpha\rangle\langle\alpha|(\mathbf{a} - \alpha)]$$

$$(\tau_1 I^1+\tau_2\sigma_x^1+\tau_3\sigma_y^1+\tau_4\sigma_z^1)\otimes(\tau_5 I^2+\tau_6\sigma_x^2+\tau_7\sigma_y^2+\tau_8\sigma_z^2)\otimes[i(\mathbf{a}^\dagger-\alpha^*)|\alpha\rangle\langle\alpha|-i|\alpha\rangle\langle\alpha|(\mathbf{a}-\alpha)]$$

Thus it is plausible that, $\forall\rho_t\in N$ the projection of $d\theta_t=\mathcal{L}[\rho_t]$ on the tangent space T_tM, $\Pi_{T_tM}d\theta_t\in T_tN$. The rigorous proof is as follows

Examine term by term. The following terms (the first category) obviously lie in T_tN as they can readily be written as a linear combination of $\sigma_i^1\otimes(\tau_5 I^2+\tau_6\sigma_x^2+\tau_7\sigma_y^2+\tau_8\sigma_z^2)\otimes|\alpha\rangle\langle\alpha|$ and $(\tau_1 I^1+\tau_2\sigma_x^1+\tau_3\sigma_y^1+\tau_4\sigma_z^1)\otimes\sigma_j^2\otimes|\alpha\rangle\langle\alpha|$

$$\begin{aligned}
-\quad & i\Delta_a(\frac{\tau_1}{2}I^1+\frac{\tau_1}{2}\sigma_z^1+\tau_2\sigma_+^1-i\tau_3\sigma_+^1+\frac{\tau_4}{2}I^1+\frac{\tau_4}{2}\sigma_z^1)\otimes(\tau_5 I^2+\tau_6\sigma_x^2+\tau_7\sigma_y^2+\tau_8\sigma_z^2)\otimes|\alpha\rangle\langle\alpha|\\
-\quad & i\Delta_a(\tau_1 I^1+\tau_2\sigma_x^1+\tau_3\sigma_y^1+\tau_4\sigma_z^1)\otimes(\frac{\tau_5}{2}I^2+\frac{\tau_5}{2}\sigma_z^2+\tau_6\sigma_+^2-i\tau_7\sigma_+^2+\frac{\tau_8}{2}I^2+\frac{\tau_8}{2}\sigma_z^2)\otimes|\alpha\rangle\langle\alpha|\\
-\quad & \frac{g_1}{2}(2\tau_1\sigma_+^1+\tau_2 I^1+\tau_2\sigma_z^1+i\tau_3 I^1+i\tau_3\sigma_z^1-2\tau_4\sigma_+^1)\otimes(\tau_5 I^2+\tau_6\sigma_x^2+\tau_7\sigma_y^2+\tau_8\sigma_z^2)\otimes\alpha|\alpha\rangle\langle\alpha|\\
-\quad & \frac{g_2}{2}(\tau_1 I^1+\tau_2\sigma_x^1+\tau_3\sigma_y^1+\tau_4\sigma_z^1)\otimes(2\tau_5\sigma_+^2+\tau_6 I^2+\tau_6\sigma_z^2+i\tau_7 I^2+i\tau_7\sigma_z^2-2\tau_8\sigma_+^2)\otimes\alpha|\alpha\rangle\langle\alpha|\\
-\quad & (\tau_1 I^1+\tau_2\sigma_x^1+\tau_3\sigma_y^1+\tau_4\sigma_z^1)\otimes(\tau_5 I^2+\tau_6\sigma_x^2+\tau_7\sigma_y^2+\tau_8\sigma_z^2)\otimes(-\mathcal{E}^*\alpha|\alpha\rangle\langle\alpha|)\\
+\quad & i\Delta_a(\frac{\tau_1}{2}I^1+\frac{\tau_1}{2}\sigma_z^1+\tau_2\sigma_-^1+i\tau_3\sigma_-^1+\frac{\tau_4}{2}I^1+\frac{\tau_4}{2}\sigma_z^1)\otimes(\tau_5 I^2+\tau_6\sigma_x^2+\tau_7\sigma_y^2+\tau_8\sigma_z^2)\otimes|\alpha\rangle\langle\alpha|\\
+\quad & i\Delta_a(\tau_1 I^1+\tau_2\sigma_x^1+\tau_3\sigma_y^1+\tau_4\sigma_z^1)\otimes(\frac{\tau_5}{2}I^2+\frac{\tau_5}{2}\sigma_z^2+\tau_6\sigma_-^2+i\tau_7\sigma_-^2+\frac{\tau_8}{2}I^2+\frac{\tau_8}{2}\sigma_z^2)\otimes|\alpha\rangle\langle\alpha|\\
-\quad & \frac{g_1}{2}(2\tau_1\sigma_-^1+\tau_2 I^1+\tau_2\sigma_z^1-i\tau_3 I^1-i\tau_3\sigma_z^1-2\tau_4\sigma_-^1)\otimes(\tau_5 I^2+\tau_6\sigma_x^2+\tau_7\sigma_y^2+\tau_8\sigma_z^2)\otimes|\alpha\rangle\langle\alpha|\alpha^*\\
-\quad & \frac{g_2}{2}(\tau_1 I^1+\tau_2\sigma_x^1+\tau_3\sigma_y^1+\tau_4\sigma_z^1)\otimes(2\tau_5\sigma_-^2+\tau_6 I^2+\tau_6\sigma_z^2-i\tau_7 I^2-i\tau_7\sigma_z^2-2\tau_8\sigma_-^2)\otimes|\alpha\rangle\langle\alpha|\alpha^*\\
-\quad & (\tau_1 I^1+\tau_2\sigma_x^1+\tau_3\sigma_y^1+\tau_4\sigma_z^1)\otimes(\tau_5 I^2+\tau_6\sigma_x^2+\tau_7\sigma_y^2+\tau_8\sigma_z^2)\otimes|\alpha\rangle\langle\alpha|\mathcal{E}\alpha^*\\
+\quad & 2\kappa(\tau_1 I^1+\tau_2\sigma_x^1+\tau_3\sigma_y^1+\tau_4\sigma_z^1)\otimes(\tau_5 I^2+\tau_6\sigma_x^2+\tau_7\sigma_y^2+\tau_8\sigma_z^2)\otimes\alpha|\alpha\rangle\langle\alpha|\alpha^*\\
+\quad & \gamma_\perp(\tau_1 I^1-\tau_1\sigma_z^1+\tau_4 I^1-\tau_4\sigma_z^1)\otimes(\tau_5 I^2+\tau_6\sigma_x^2+\tau_7\sigma_y^2+\tau_8\sigma_z^2)\otimes|\alpha\rangle\langle\alpha|\\
-\quad & \gamma_\perp(\frac{\tau_1}{2}I^1+\frac{\tau_1}{2}\sigma_z^1+\tau_2\sigma_+^1-i\tau_3\sigma_+^1+\frac{\tau_4}{2}I^1+\frac{\tau_4}{2}\sigma_z^1)\otimes(\tau_5 I^2+\tau_6\sigma_x^2+\tau_7\sigma_y^2+\tau_8\sigma_z^2)\otimes|\alpha\rangle\langle\alpha|\\
-\quad & \gamma_\perp(\frac{\tau_1}{2}I^1+\frac{\tau_1}{2}\sigma_z^1+\tau_2\sigma_-^1+i\tau_3\sigma_-^1+\frac{\tau_4}{2}I^1+\frac{\tau_4}{2}\sigma_z^1)\otimes(\tau_5 I^2+\tau_6\sigma_x^2+\tau_7\sigma_y^2+\tau_8\sigma_z^2)\otimes|\alpha\rangle\langle\alpha|\\
+\quad & \gamma_\perp(\tau_1 I^1+\tau_2\sigma_x^1+\tau_3\sigma_y^1+\tau_4\sigma_z^1)\otimes(\tau_5 I^2-\tau_5\sigma_z^2+\tau_8 I^2-\tau_8\sigma_z^2)\otimes|\alpha\rangle\langle\alpha|\\
-\quad & \gamma_\perp(\tau_1 I^1+\tau_2\sigma_x^1+\tau_3\sigma_y^1+\tau_4\sigma_z^1)\otimes(\frac{\tau_5}{2}I^2+\frac{\tau_5}{2}\sigma_z^2+\tau_6\sigma_+^2-i\tau_7\sigma_+^2+\frac{\tau_8}{2}I^2+\frac{\tau_8}{2}\sigma_z^2)\otimes|\alpha\rangle\langle\alpha|\\
-\quad & \gamma_\perp(\tau_1 I^1+\tau_2\sigma_x^1+\tau_3\sigma_y^1+\tau_4\sigma_z^1)\otimes(\frac{\tau_5}{2}I^2+\frac{\tau_5}{2}\sigma_z^2+\tau_6\sigma_-^2+i\tau_7\sigma_-^2+\frac{\tau_8}{2}I^2+\frac{\tau_8}{2}\sigma_z^2)\otimes|\alpha\rangle\langle\alpha|
\end{aligned}$$

The following terms (the second category) require a bit of manipulation to prove to be in T_tN

$$\begin{aligned}
&- i\Delta_c(\tau_1 I^1 + \tau_2\sigma_x^1 + \tau_3\sigma_y^1 + \tau_4\sigma_z^1)\otimes(\tau_5 I^2 + \tau_6\sigma_x^2 + \tau_7\sigma_y^2 + \tau_8\sigma_z^2)\otimes \mathbf{a}^\dagger\alpha|\alpha\rangle\langle\alpha| \\
&+ (\tau_1 I^1 + \tau_2\sigma_x^1 + \tau_3\sigma_y^1 + \tau_4\sigma_z^1)\otimes(\tau_5 I^2 + \tau_6\sigma_x^2 + \tau_7\sigma_y^2 + \tau_8\sigma_z^2)\otimes \mathcal{E}\mathbf{a}^\dagger|\alpha\rangle\langle\alpha| \\
&+ i\Delta_c(\tau_1 I^1 + \tau_2\sigma_x^1 + \tau_3\sigma_y^1 + \tau_4\sigma_z^1)\otimes(\tau_5 I^2 + \tau_6\sigma_x^2 + \tau_7\sigma_y^2 + \tau_8\sigma_z^2)\otimes |\alpha\rangle\langle\alpha|\alpha^*\mathbf{a} \\
&+ (\tau_1 I^1 + \tau_2\sigma_x^1 + \tau_3\sigma_y^1 + \tau_4\sigma_z^1)\otimes(\tau_5 I^2 + \tau_6\sigma_x^2 + \tau_7\sigma_y^2 + \tau_8\sigma_z^2)\otimes |\alpha\rangle\langle\alpha|\mathcal{E}^*\mathbf{a} \\
&- \kappa(\tau_1 I^1 + \tau_2\sigma_x^1 + \tau_3\sigma_y^1 + \tau_4\sigma_z^1)\otimes(\tau_5 I^2 + \tau_6\sigma_x^2 + \tau_7\sigma_y^2 + \tau_8\sigma_z^2)\otimes \mathbf{a}^\dagger\alpha|\alpha\rangle\langle\alpha| \\
&- \kappa(\tau_1 I^1 + \tau_2\sigma_x^1 + \tau_3\sigma_y^1 + \tau_4\sigma_z^1)\otimes(\tau_5 I^2 + \tau_6\sigma_x^2 + \tau_7\sigma_y^2 + \tau_8\sigma_z^2)\otimes |\alpha\rangle\langle\alpha|\alpha^*\mathbf{a}
\end{aligned}$$

which are proportional to either $\rho_a\otimes\mathbf{a}^\dagger|\alpha\rangle\langle\alpha|$ or $\rho_a\otimes|\alpha\rangle\langle\alpha|\mathbf{a}$, where $\rho_a = (\tau_1 I^1 + \tau_2\sigma_x^1 + \tau_3\sigma_y^1 + \tau_4\sigma_z^1)\otimes(\tau_5 I^2 + \tau_6\sigma_x^2 + \tau_7\sigma_y^2 + \tau_8\sigma_z^2)$. Thus to show that they lie in T_tN it suffices to show $\rho_a\otimes\mathbf{a}^\dagger|\alpha\rangle\langle\alpha| \in T_tN$ and $\rho_a\otimes|\alpha\rangle\langle\alpha|\mathbf{a}\in T_tN$, which is not hard to prove by manipulating the following two spanning vectors of T_tN

$$P_r = \rho_a\otimes[(\mathbf{a}^\dagger-\alpha^*)|\alpha\rangle\langle\alpha| + |\alpha\rangle\langle\alpha|(\mathbf{a}-\alpha)],\quad P_i = \rho_a\otimes[i(\mathbf{a}^\dagger-\alpha^*)|\alpha\rangle\langle\alpha| - i|\alpha\rangle\langle\alpha|(\mathbf{a}-\alpha)]$$

From the above expression I have

$$\begin{aligned}
iP_r + P_i &= \rho_a\otimes[2i(\mathbf{a}^\dagger-\alpha^*)|\alpha\rangle\langle\alpha|] = 2i\rho_a\otimes\mathbf{a}^\dagger|\alpha\rangle\langle\alpha| - 2i\rho_a\otimes\alpha^*|\alpha\rangle\langle\alpha| \Rightarrow \\
2i\rho_a\otimes\mathbf{a}^\dagger|\alpha\rangle\langle\alpha| &= iP_r + P_i + 2i\rho_a\otimes\alpha^*|\alpha\rangle\langle\alpha| \Rightarrow \\
\rho_a\otimes\mathbf{a}^\dagger|\alpha\rangle\langle\alpha| &= \frac{1}{2}(P_r - iP_i) + \rho_a\otimes\alpha^*|\alpha\rangle\langle\alpha| \\
&= \frac{1}{2}(P_r - iP_i) + \alpha^*\tau_1[I^1\otimes(\tau_5 I^2 + \tau_6\sigma_x^2 + \tau_7\sigma_y^2 + \tau_8\sigma_z^2)\otimes|\alpha\rangle\langle\alpha|] \\
&+ \alpha^*\tau_2[\sigma_x^1\otimes(\tau_5 I^2 + \tau_6\sigma_x^2 + \tau_7\sigma_y^2 + \tau_8\sigma_z^2)\otimes|\alpha\rangle\langle\alpha|] \\
&+ \alpha^*\tau_3[\sigma_y^1\otimes(\tau_5 I^2 + \tau_6\sigma_x^2 + \tau_7\sigma_y^2 + \tau_8\sigma_z^2)\otimes|\alpha\rangle\langle\alpha|] \\
&+ \alpha^*\tau_4[\sigma_z^1\otimes(\tau_5 I^2 + \tau_6\sigma_x^2 + \tau_7\sigma_y^2 + \tau_8\sigma_z^2)\otimes|\alpha\rangle\langle\alpha|] \in T_tN
\end{aligned}$$

similarly

$$\begin{aligned}
iP_r - P_i &= \rho_a\otimes[2i|\alpha\rangle\langle\alpha|(\mathbf{a}-\alpha)] = 2i\rho_a\otimes|\alpha\rangle\langle\alpha|\mathbf{a} - 2i\rho_a\otimes\alpha|\alpha\rangle\langle\alpha| \Rightarrow \\
2i\rho_a\otimes|\alpha\rangle\langle\alpha|\mathbf{a} &= iP_r - P_i + 2i\rho_a\otimes\alpha|\alpha\rangle\langle\alpha| \Rightarrow
\end{aligned}$$

$$
\begin{aligned}
\rho_a \otimes |\alpha\rangle\langle\alpha|\mathbf{a} &= \frac{1}{2}(P_r + iP_i) + \rho_a \otimes \alpha|\alpha\rangle\langle\alpha| \\
&= \frac{1}{2}(P_r - iP_i) + \alpha\tau_1[I^1 \otimes (\tau_5 I^2 + \tau_6\sigma_x^2 + \tau_7\sigma_y^2 + \tau_8\sigma_z^2) \otimes |\alpha\rangle\langle\alpha|] \\
&+ \alpha\tau_2[\sigma_x^1 \otimes (\tau_5 I^2 + \tau_6\sigma_x^2 + \tau_7\sigma_y^2 + \tau_8\sigma_z^2) \otimes |\alpha\rangle\langle\alpha|] \\
&+ \alpha\tau_3[\sigma_y^1 \otimes (\tau_5 I^2 + \tau_6\sigma_x^2 + \tau_7\sigma_y^2 + \tau_8\sigma_z^2) \otimes |\alpha\rangle\langle\alpha|] \\
&+ \alpha\tau_4[\sigma_z^1 \otimes (\tau_5 I^2 + \tau_6\sigma_x^2 + \tau_7\sigma_y^2 + \tau_8\sigma_z^2) \otimes |\alpha\rangle\langle\alpha|] \in T_tN
\end{aligned}
$$

thus indeed $\rho_a \otimes \mathbf{a}^\dagger|\alpha\rangle\langle\alpha| \in T_tN$ and $\rho_a \otimes |\alpha\rangle\langle\alpha|\mathbf{a} \in T_tN$.

The following terms (the third category) require explicit evaluation of the tangent component in T_tM i.e. need to be projected onto T_tM

$$
\begin{aligned}
&+ \frac{g_1}{2}(2\tau_1\sigma_-^1 + \tau_2 I^1 - \tau_2\sigma_z^1 - i\tau_3 I^1 + i\tau_3\sigma_z^1 + 2\tau_4\sigma_-^1) \otimes (\tau_5 I^2 + \tau_6\sigma_x^2 + \tau_7\sigma_y^2 + \tau_8\sigma_z^2) \otimes \mathbf{a}^\dagger|\alpha\rangle\langle\alpha| \\
&+ \frac{g_2}{2}(\tau_1 I^1 + \tau_2\sigma_x^1 + \tau_3\sigma_y^1 + \tau_4\sigma_z^1) \otimes (2\tau_5\sigma_-^2 + \tau_6 I^2 - \tau_6\sigma_z^2 - i\tau_7 I^2 + i\tau_7\sigma_z^2 + 2\tau_8\sigma_-^2) \otimes \mathbf{a}^\dagger|\alpha\rangle\langle\alpha| \\
&+ \frac{g_1}{2}(2\tau_1\sigma_+^1 + \tau_2 I^1 - \tau_2\sigma_z^1 + i\tau_3 I^1 - i\tau_3\sigma_z^1 + 2\tau_4\sigma_+^1) \otimes (\tau_5 I^2 + \tau_6\sigma_x^2 + \tau_7\sigma_y^2 + \tau_8\sigma_z^2) \otimes |\alpha\rangle\langle\alpha|\mathbf{a} \\
&+ \frac{g_2}{2}(\tau_1 I^1 + \tau_2\sigma_x^1 + \tau_3\sigma_y^1 + \tau_4\sigma_z^1) \otimes (2\tau_5\sigma_+^2 + \tau_6 I^2 - \tau_6\sigma_z^2 + i\tau_7 I^2 - i\tau_7\sigma_z^2 + 2\tau_8\sigma_+^2) \otimes |\alpha\rangle\langle\alpha|\mathbf{a}
\end{aligned}
$$

Notice that these terms are linear combinations of

$$\sigma_i^1 \otimes (\tau_5 I^2 + \tau_6\sigma_x^2 + \tau_7\sigma_y^2 + \tau_8\sigma_z^2) \otimes \mathbf{a}^\dagger|\alpha\rangle\langle\alpha|, \quad (\tau_1 I^1 + \tau_2\sigma_x^1 + \tau_3\sigma_y^1 + \tau_4\sigma_z^1) \otimes \sigma_j^2 \otimes \mathbf{a}^\dagger|\alpha\rangle\langle\alpha|$$

$$\sigma_i^1 \otimes (\tau_5 I^2 + \tau_6\sigma_x^2 + \tau_7\sigma_y^2 + \tau_8\sigma_z^2) \otimes |\alpha\rangle\langle\alpha|\mathbf{a}, \quad (\tau_1 I^1 + \tau_2\sigma_x^1 + \tau_3\sigma_y^1 + \tau_4\sigma_z^1) \otimes \sigma_j^2 \otimes |\alpha\rangle\langle\alpha|\mathbf{a}$$

where $i, j \in \{0, 1, 2, 3\}$. Therefore to show that their projected components lie in T_tN it suffices to show that

$$\Pi_{T_tM}[\sigma_i^1 \otimes (\tau_5 I^2 + \tau_6\sigma_x^2 + \tau_7\sigma_y^2 + \tau_8\sigma_z^2) \otimes \mathbf{a}^\dagger|\alpha\rangle\langle\alpha|] \in T_tN$$

$$\Pi_{T_tM}[(\tau_1 I^1 + \tau_2\sigma_x^1 + \tau_3\sigma_y^1 + \tau_4\sigma_z^1) \otimes \sigma_j^2 \otimes \mathbf{a}^\dagger|\alpha\rangle\langle\alpha|] \in T_tN$$

$$\Pi_{T_tM}[\sigma_i^1 \otimes (\tau_5 I^2 + \tau_6\sigma_x^2 + \tau_7\sigma_y^2 + \tau_8\sigma_z^2) \otimes |\alpha\rangle\langle\alpha|\mathbf{a}] \in T_tN$$

$$\Pi_{T_tM}[(\tau_1 I^1 + \tau_2\sigma_x^1 + \tau_3\sigma_y^1 + \tau_4\sigma_z^1) \otimes \sigma_j^2 \otimes |\alpha\rangle\langle\alpha|\mathbf{a}] \in T_tN$$

To show for example $\Pi_{T_tM}[\sigma_i^1\otimes(\tau_5 I^2+\tau_6\sigma_x^2+\tau_7\sigma_y^2+\tau_8\sigma_z^2)\otimes\mathbf{a}^\dagger|\alpha\rangle\langle\alpha|]\in T_tN$ it suffices to check its projection onto the 16 spanning vectors $P_{kl}=\sigma_k^1\otimes\sigma_l^2\otimes|\alpha\rangle\langle\alpha|$ since the spanning vectors

$$P_r=\rho_a\otimes[(\mathbf{a}^\dagger-\alpha^*)|\alpha\rangle\langle\alpha|+|\alpha\rangle\langle\alpha|(\mathbf{a}-\alpha)],\quad P_i=\rho_a\otimes[i(\mathbf{a}^\dagger-\alpha^*)|\alpha\rangle\langle\alpha|-i|\alpha\rangle\langle\alpha|(\mathbf{a}-\alpha)]$$

are common to T_tM and T_tN. By the trace property of Pauli matrices, among the 16 spanning vectors, only 4 have nonzero projected components

$$\begin{aligned}
& \mathrm{Tr}\left\{(P_{kl})^\dagger[\sigma_i^1\otimes(\tau_5 I^2+\tau_6\sigma_x^2+\tau_7\sigma_y^2+\tau_8\sigma_z^2)\otimes\mathbf{a}^\dagger|\alpha\rangle\langle\alpha|]\right\}\\
= {} & \mathrm{Tr}\left\{(\sigma_k^1\otimes\sigma_l^2\otimes|\alpha\rangle\langle\alpha|)[\sigma_i^1\otimes(\tau_5 I^2+\tau_6\sigma_x^2+\tau_7\sigma_y^2+\tau_8\sigma_z^2)\otimes\mathbf{a}^\dagger|\alpha\rangle\langle\alpha|]\right\}\\
= {} & \mathrm{Tr}\left\{\sigma_k^1\sigma_i^1\otimes\sigma_l^2(\tau_5 I^2+\tau_6\sigma_x^2+\tau_7\sigma_y^2+\tau_8\sigma_z^2)\otimes|\alpha\rangle\langle\alpha|\mathbf{a}^\dagger|\alpha\rangle\langle\alpha|\right\}\\
= {} & \mathrm{Tr}\left\{\sigma_k^1\sigma_i^1\otimes\sigma_l^2(\tau_5 I^2+\tau_6\sigma_x^2+\tau_7\sigma_y^2+\tau_8\sigma_z^2)\otimes\alpha^*|\alpha\rangle\langle\alpha|\right\}\\
= {} & \mathrm{Tr}_1[\sigma_k^1\sigma_i^1]\cdot\mathrm{Tr}_2[\sigma_l^2(\tau_5 I^2+\tau_6\sigma_x^2+\tau_7\sigma_y^2+\tau_8\sigma_z^2)]\cdot\mathrm{Tr}_f[\alpha^*|\alpha\rangle\langle\alpha|]\\
= {} & 2\alpha^*\delta_{ki}\,\mathrm{Tr}_2[\sigma_l^2(\tau_5 I^2+\tau_6\sigma_x^2+\tau_7\sigma_y^2+\tau_8\sigma_z^2)]
\end{aligned}$$

therefore

$$\begin{aligned}
& \Pi_{T_tM}[\sigma_i^1\otimes(\tau_5 I^2+\tau_6\sigma_x^2+\tau_7\sigma_y^2+\tau_8\sigma_z^2)\otimes\mathbf{a}^\dagger|\alpha\rangle\langle\alpha|]\\
= {} & \sum_{l=0}^{3}\left\{\sum_{k=0}^{3}\langle P_{kl},(\tau_5 I^2+\tau_6\sigma_x^2+\tau_7\sigma_y^2+\tau_8\sigma_z^2)\otimes\mathbf{a}^\dagger|\alpha\rangle\langle\alpha|\rangle P_{kl}\right\}+P_r,P_i\text{ components}\\
= {} & \sum_{l=0}^{3}\left\{2\alpha^*\,\mathrm{Tr}_2[\sigma_l^2(\tau_5 I^2+\tau_6\sigma_x^2+\tau_7\sigma_y^2+\tau_8\sigma_z^2)]P_{il}\right\}+P_r,P_i\text{ components}\\
= {} & 2\alpha^*2\tau_5(\sigma_i^1\otimes I^2\otimes|\alpha\rangle\langle\alpha|)+2\alpha^*2\tau_6(\sigma_i^1\otimes\sigma_x^2\otimes|\alpha\rangle\langle\alpha|)\\
+ {} & 2\alpha^*2\tau_7(\sigma_i^1\otimes\sigma_y^2\otimes|\alpha\rangle\langle\alpha|)+2\alpha^*2\tau_8(\sigma_i^1\otimes\sigma_z^2\otimes|\alpha\rangle\langle\alpha|)+P_r,P_i\text{ components}\\
= {} & 4\alpha^*[\sigma_i^1\otimes(\tau_5 I^2+\tau_6\sigma_x^2+\tau_7\sigma_y^2+\tau_8\sigma_z^2)\otimes|\alpha\rangle\langle\alpha|]+P_r,P_i\text{ components}\in T_tN
\end{aligned}$$

Similarly

$$\begin{aligned}
& \mathrm{Tr}\left\{(P_{kl})^\dagger[\sigma_i^1\otimes(\tau_5 I^2+\tau_6\sigma_x^2+\tau_7\sigma_y^2+\tau_8\sigma_z^2)\otimes|\alpha\rangle\langle\alpha|\mathbf{a}]\right\}\\
= {} & \mathrm{Tr}\left\{(\sigma_k^1\otimes\sigma_l^2\otimes|\alpha\rangle\langle\alpha|)[\sigma_i^1\otimes(\tau_5 I^2+\tau_6\sigma_x^2+\tau_7\sigma_y^2+\tau_8\sigma_z^2)\otimes|\alpha\rangle\langle\alpha|\mathbf{a}]\right\}
\end{aligned}$$

$$
\begin{aligned}
&= \mathrm{Tr}\left\{\sigma_k^1\sigma_i^1 \otimes \sigma_l^2(\tau_5 I^2 + \tau_6\sigma_x^2 + \tau_7\sigma_y^2 + \tau_8\sigma_z^2) \otimes |\alpha\rangle\langle\alpha|\mathbf{a}\right\} \\
&= \mathrm{Tr}_1[\sigma_k^1\sigma_i^1] \cdot \mathrm{Tr}_2[\sigma_l^2(\tau_5 I^2 + \tau_6\sigma_x^2 + \tau_7\sigma_y^2 + \tau_8\sigma_z^2)] \cdot \mathrm{Tr}_f[|\alpha\rangle\langle\alpha|\mathbf{a}] \\
&= 2\alpha\delta_{ki}\,\mathrm{Tr}_2[\sigma_l^2(\tau_5 I^2 + \tau_6\sigma_x^2 + \tau_7\sigma_y^2 + \tau_8\sigma_z^2)]
\end{aligned}
$$

therefore

$$
\begin{aligned}
& \Pi_{T_tM}[\sigma_i^1 \otimes (\tau_5 I^2 + \tau_6\sigma_x^2 + \tau_7\sigma_y^2 + \tau_8\sigma_z^2) \otimes |\alpha\rangle\langle\alpha|\mathbf{a}] \\
= & \sum_{l=0}^{3}\left\{\sum_{k=0}^{3}\langle P_{kl}, (\tau_5 I^2 + \tau_6\sigma_x^2 + \tau_7\sigma_y^2 + \tau_8\sigma_z^2) \otimes |\alpha\rangle\langle\alpha|\mathbf{a}\rangle P_{kl}\right\} + P_r, P_i \text{ components} \\
= & \sum_{l=0}^{3}\left\{2\alpha\,\mathrm{Tr}_2[\sigma_l^2(\tau_5 I^2 + \tau_6\sigma_x^2 + \tau_7\sigma_y^2 + \tau_8\sigma_z^2)]P_{il}\right\} + P_r, P_i \text{ components} \\
= & 2\alpha 2\tau_5(\sigma_i^1 \otimes I^2 \otimes |\alpha\rangle\langle\alpha|) + 2\alpha 2\tau_6(\sigma_i^1 \otimes \sigma_x^2 \otimes |\alpha\rangle\langle\alpha|) \\
+ & 2\alpha 2\tau_7(\sigma_i^1 \otimes \sigma_y^2 \otimes |\alpha\rangle\langle\alpha|) + 2\alpha 2\tau_8(\sigma_i^1 \otimes \sigma_z^2 \otimes |\alpha\rangle\langle\alpha|) + P_r, P_i \text{ components} \\
= & 4\alpha[\sigma_i^1 \otimes (\tau_5 I^2 + \tau_6\sigma_x^2 + \tau_7\sigma_y^2 + \tau_8\sigma_z^2) \otimes |\alpha\rangle\langle\alpha|] + P_r, P_i \text{ components} \in T_tN
\end{aligned}
$$

Also to show $\Pi_{T_tM}[(\tau_1 I^1 + \tau_2\sigma_x^1 + \tau_3\sigma_y^1 + \tau_4\sigma_z^1) \otimes \sigma_j^2 \otimes \mathbf{a}^\dagger|\alpha\rangle\langle\alpha|] \in T_tN$ it suffices to check its projection onto the 16 spanning vectors $P_{kl} = \sigma_k^1 \otimes \sigma_l^2 \otimes |\alpha\rangle\langle\alpha|$ since the spanning vectors

$$P_r = \rho_a \otimes [(\mathbf{a}^\dagger - \alpha^*)|\alpha\rangle\langle\alpha| + |\alpha\rangle\langle\alpha|(\mathbf{a} - \alpha)], \quad P_i = \rho_a \otimes [i(\mathbf{a}^\dagger - \alpha^*)|\alpha\rangle\langle\alpha| - i|\alpha\rangle\langle\alpha|(\mathbf{a} - \alpha)]$$

are common to T_tM and T_tN. By the trace property of Pauli matrices, among the 16 spanning vectors, only 4 have nonzero projected components

$$
\begin{aligned}
& \mathrm{Tr}\left\{(P_{kl})^\dagger[(\tau_1 I^1 + \tau_2\sigma_x^1 + \tau_3\sigma_y^1 + \tau_4\sigma_z^1) \otimes \sigma_j^2 \otimes \mathbf{a}^\dagger|\alpha\rangle\langle\alpha|]\right\} \\
= & \mathrm{Tr}\left\{(\sigma_k^1 \otimes \sigma_l^2 \otimes |\alpha\rangle\langle\alpha|)[(\tau_1 I^1 + \tau_2\sigma_x^1 + \tau_3\sigma_y^1 + \tau_4\sigma_z^1) \otimes \sigma_j^2 \otimes \mathbf{a}^\dagger|\alpha\rangle\langle\alpha|]\right\} \\
= & \mathrm{Tr}\left\{\sigma_k^1(\tau_1 I^1 + \tau_2\sigma_x^1 + \tau_3\sigma_y^1 + \tau_4\sigma_z^1) \otimes \sigma_l^2\sigma_j^2 \otimes |\alpha\rangle\langle\alpha|\mathbf{a}^\dagger|\alpha\rangle\langle\alpha|\right\} \\
= & \mathrm{Tr}\left\{\sigma_k^1(\tau_1 I^1 + \tau_2\sigma_x^1 + \tau_3\sigma_y^1 + \tau_4\sigma_z^1) \otimes \sigma_l^2\sigma_j^2 \otimes \alpha^*|\alpha\rangle\langle\alpha|\right\} \\
= & \mathrm{Tr}_1[\sigma_k^1(\tau_1 I^1 + \tau_2\sigma_x^1 + \tau_3\sigma_y^1 + \tau_4\sigma_z^1)] \cdot \mathrm{Tr}_2[\sigma_l^2\sigma_j^2] \cdot \mathrm{Tr}_f[\alpha^*|\alpha\rangle\langle\alpha|] \\
= & 2\alpha^*\delta_{lj}\,\mathrm{Tr}_1[\sigma_k^1(\tau_1 I^1 + \tau_2\sigma_x^1 + \tau_3\sigma_y^1 + \tau_4\sigma_z^1)]
\end{aligned}
$$

therefore

$$
\begin{aligned}
& \Pi_{T_tM}[(\tau_1 I^1 + \tau_2\sigma_x^1 + \tau_3\sigma_y^1 + \tau_4\sigma_z^1) \otimes \sigma_j^2 \otimes \mathbf{a}^\dagger|\alpha\rangle\langle\alpha|] \\
= & \sum_{k=0}^{3}\left\{\sum_{l=0}^{3}\langle P_{kl}, (\tau_1 I^1 + \tau_2\sigma_x^1 + \tau_3\sigma_y^1 + \tau_4\sigma_z^1) \otimes \sigma_j^2 \otimes \mathbf{a}^\dagger|\alpha\rangle\langle\alpha|\rangle P_{kl}\right\} + P_r, P_i \text{ components} \\
= & \sum_{k=0}^{3}\left\{2\alpha^* \operatorname{Tr}_1[\sigma_k^1(\tau_1 I^1 + \tau_2\sigma_x^1 + \tau_3\sigma_y^1 + \tau_4\sigma_z^1)]P_{kj}\right\} + P_r, P_i \text{ components} \\
= & 2\alpha^* 2\tau_1(I^1 \otimes \sigma_j^2 \otimes |\alpha\rangle\langle\alpha|) + 2\alpha^* 2\tau_2(\sigma_x^1 \otimes \sigma_j^2 \otimes |\alpha\rangle\langle\alpha|) \\
+ & 2\alpha^* 2\tau_3(\sigma_y^1 \otimes \sigma_j^2 \otimes |\alpha\rangle\langle\alpha|) + 2\alpha^* 2\tau_4(\sigma_z^1 \otimes \sigma_j^2 \otimes |\alpha\rangle\langle\alpha|) + P_r, P_i \text{ components} \\
= & 4\alpha^*[(\tau_1 I^1 + \tau_2\sigma_x^1 + \tau_3\sigma_y^1 + \tau_4\sigma_z^1) \otimes \sigma_j^2 \otimes |\alpha\rangle\langle\alpha|] + P_r, P_i \text{ components} \in T_tN
\end{aligned}
$$

Similarly

$$
\begin{aligned}
& \operatorname{Tr}\left\{(P_{kl})^\dagger[(\tau_1 I^1 + \tau_2\sigma_x^1 + \tau_3\sigma_y^1 + \tau_4\sigma_z^1) \otimes \sigma_j^2 \otimes |\alpha\rangle\langle\alpha|\mathbf{a}]\right\} \\
= & \operatorname{Tr}\left\{(\sigma_k^1 \otimes \sigma_l^2 \otimes |\alpha\rangle\langle\alpha|)[(\tau_1 I^1 + \tau_2\sigma_x^1 + \tau_3\sigma_y^1 + \tau_4\sigma_z^1) \otimes \sigma_j^2 \otimes |\alpha\rangle\langle\alpha|\mathbf{a}]\right\} \\
= & \operatorname{Tr}\left\{\sigma_k^1(\tau_1 I^1 + \tau_2\sigma_x^1 + \tau_3\sigma_y^1 + \tau_4\sigma_z^1) \otimes \sigma_l^2\sigma_j^2 \otimes |\alpha\rangle\langle\alpha|\mathbf{a}\right\} \\
= & \operatorname{Tr}_1[\sigma_k^1(\tau_1 I^1 + \tau_2\sigma_x^1 + \tau_3\sigma_y^1 + \tau_4\sigma_z^1)] \cdot \operatorname{Tr}_2[\sigma_l^2\sigma_j^2] \cdot \operatorname{Tr}_f[|\alpha\rangle\langle\alpha|\mathbf{a}] \\
= & 2\alpha\delta_{lj} \operatorname{Tr}_1[\sigma_k^1(\tau_1 I^1 + \tau_2\sigma_x^1 + \tau_3\sigma_y^1 + \tau_4\sigma_z^1)]
\end{aligned}
$$

therefore

$$
\begin{aligned}
& \Pi_{T_tM}[(\tau_1 I^1 + \tau_2\sigma_x^1 + \tau_3\sigma_y^1 + \tau_4\sigma_z^1) \otimes \sigma_j^2 \otimes |\alpha\rangle\langle\alpha|\mathbf{a}] \\
= & \sum_{k=0}^{3}\left\{\sum_{l=0}^{3}\langle P_{kl}, (\tau_1 I^1 + \tau_2\sigma_x^1 + \tau_3\sigma_y^1 + \tau_4\sigma_z^1) \otimes \sigma_j^2 \otimes |\alpha\rangle\langle\alpha|\mathbf{a}\rangle P_{kl}\right\} + P_r, P_i \text{ components} \\
= & \sum_{k=0}^{3}\left\{2\alpha \operatorname{Tr}_1[\sigma_k^1(\tau_1 I^1 + \tau_2\sigma_x^1 + \tau_3\sigma_y^1 + \tau_4\sigma_z^1)]P_{kj}\right\} + P_r, P_i \text{ components} \\
= & 2\alpha 2\tau_1(I^1 \otimes \sigma_j^2 \otimes |\alpha\rangle\langle\alpha|) + 2\alpha 2\tau_2(\sigma_x^1 \otimes \sigma_j^2 \otimes |\alpha\rangle\langle\alpha|) \\
+ & 2\alpha 2\tau_3(\sigma_y^1 \otimes \sigma_j^2 \otimes |\alpha\rangle\langle\alpha|) + 2\alpha 2\tau_4(\sigma_z^1 \otimes \sigma_j^2 \otimes |\alpha\rangle\langle\alpha|) + P_r, P_i \text{ components} \\
= & 4\alpha[(\tau_1 I^1 + \tau_2\sigma_x^1 + \tau_3\sigma_y^1 + \tau_4\sigma_z^1) \otimes \sigma_j^2 \otimes |\alpha\rangle\langle\alpha|] + P_r, P_i \text{ components} \in T_tN
\end{aligned}
$$

Hence by examining the master equation term by term (which were grouped into three categories for using different methods to prove) after the substitution of the parametrization under the factorizable basis, one sees that indeed the M-manifold projected component of the quantum evolution increment $\Pi_{T_tM}d\theta_t$ does lie within the sub-tangent space T_tN whenever the system state lies in N.

Bibliography

[1] Yeong-Dae Kwon. *Cavity Nonlinear Optics with a Cold Atom Ensemble on an Atom Chip*. PhD thesis, Stanford University, 2013.

[2] H. J. Carmichael. *An Open Systems Approach to Quantum Optics*. Springer-Verlag, 1993.

[3] M. A. Armen and H. Mabuchi. Low-lying bifurcations in cavity quantum electrodynamics. *Phys. Rev. A*, 73:063801, Jun 2006.

[4] Luigi Lugiato. Theory of optical bistability. *Progress in Optics*, 21:69–216, 1984.

[5] Hideo Mabuchi. Cavity-qed models of switches for attojoule-scale nanophotonic logic. *Phys. Rev. A*, 80:045802, Oct 2009.

[6] J. Kerckhoff, M. A. Armen, and H. Mabuchi. Resonance behaviour near hopf bifurcations in the electrical conductivity of bsn crystals. *Opt. Express*, 19:24468–24482, 2011.

[7] Hideo Mabuchi. Coherent-feedback control strategy to suppress spontaneous switching in ultralow power optical bistability. *Appl. Phys. Lett.*, 98:193109, Oct 2011.

[8] Tan M. Sze. A computational toolbox for quantum and atomic optics. *J. Opt. B: Quantum and Semiclasscal Optics*, 1:424, 1999.

[9] E. M. Purcell. Proceedings of the american physical society. *Phys. Rev.*, 69:674–674, Jun 1946.

[10] H. M. Wiseman and G. J. Milburn. Quantum theory of field-quadrature measurements. *Phys. Rev. A*, 47:642–662, Jan 1993.

[11] P Alsing and HJ Carmichael. Spontaneous dressed-state polarization of a coupled atom and cavity mode. *Quantum Optics: Journal of the European Optical Society Part B*, 3(1):13, 1991.

[12] S. H. Strogatz. *Nonlinear Dynamics and Chaos: With Applications to Physics, Biology, Chemistry and Engineering*. Westview Press, 2001.

[13] L. Perko. *Differential Equations and Dynamical Systems*. Springer-Verlag, 2006.

[14] Kurt Wiesenfeld and Bruce McNamara. Small-signal amplification in bifurcating dynamical systems. *Phys. Rev. A*, 33:629–642, Jan 1986.

[15] R. B. Karabalin, Ron Lifshitz, M. C. Cross, M. H. Matheny, S. C. Masmanidis, and M. L. Roukes. Signal amplification by sensitive control of bifurcation topology. *Phys. Rev. Lett.*, 106:094102, Feb 2011.

[16] C. H. Tseng, D. Enzer, G. Gabrielse, and F. L. Walls. 1-bit memory using one electron: Parametric oscillations in a penning trap. *Phys. Rev. A*, 59:2094–2104, Mar 1999.

[17] I. Siddiqi, R. Vijay, F. Pierre, C. M. Wilson, M. Metcalfe, C. Rigetti, L. Frunzio, and M. H. Devoret. Rf-driven josephson bifurcation amplifier for quantum measurement. *Phys. Rev. Lett.*, 93:207002, Nov 2004.

[18] Martin S. and Martienssen W. Resonance behaviour near hopf bifurcations in the electrical conductivity of bsn crystals. *Z. Phys. B-Condensed Matter*, 68:299–304, Oct 1986.

[19] Karl Johan Aström and Richard M. Murray. *Feedback Systems: An Introduction for Scientists and Engineers*. Princeton University Press, 2008.

[20] D. F. Walls and G. J. Milburn. *Quantum Optics*. Springer, 1995.

[21] Anna Sanpera, Rolf Tarrach, and Guifré Vidal. Local description of quantum inseparability. *Phys. Rev. A*, 58:826–830, Aug 1998.

[22] Hideo Mabuchi. Derivation of maxwell-bloch-type equations by projection of quantum models. *Phys. Rev. A*, 78:015801, Jul 2008.

[23] H. Mabuchi and A. C. Doherty. Cavity quantum electrodynamics: Coherence in context. *Science*, 298:1372–1377, November 2006.

[24] Wojciech Hubert Zurek. Decoherence, einselection, and the quantum origins of the classical. *Rev. Mod. Phys.*, 75:715–775, May 2003.

[25] Salman Habib, Kurt Jacobs, Hideo Mabuchi, Robert Ryne, Kosuke Shizume, and Bala Sundaram. Quantum-classical transition in nonlinear dynamical systems. *Phys. Rev. Lett.*, 88:040402, Jan 2002.

[26] Ramon van Handel and Hideo Mabuchi. Quantum projection filter for a highly nonlinear model in cavity qed. *J. Opt. B: Quantum Semiclass. Opt.*, 7:S226, Sep 2005.